Geological storage of carbon dioxide in the coal seams : from material to the reservoir

Saeid Nikoosokhan

École des Ponts
ParisTech

UNIVERSITÉ PARIS-EST

ÉCOLE DOCTORALE SCIENCE INGÉNIERIE ET ENVIRONNEMENT

THÈSE

présentée pour l'obtention du diplome de

DOCTEUR

DE

L'UNIVERSITÉ PARIS-EST

Spécialité : *Sciences de l'ingénieur*

par

Saeid NIKOOSOKHAN

Sujet de la thèse

Stockage géologique du dioxyde de carbone dans les veines de charbon : du matériau au réservoir

Mémoire provisoire

Président :	**Pr. Yves BERTHAUD**
Rapporteurs :	**Pr. Behrouz GATMIRI**
	Dr. Annie GROSMAN
Examinateurs :	**Pr. Guy BONNET**
	Dr. Matthieu VANDAMME
Directeur de thèse :	**Dr. Patrick DANGLA**

À ma famille,
À mon frère que je n'ai jamais eu,
Un an après moi tu es né et un an avant ma soutenance tu m'as quitté,
Farzad

Acknowledgment

Je tiens tout d'abord à remercier Matthieu Vandamme, qui m'a encadré au quotidien durant ces trois années. J'ai eu la chance de travailler non seulement aux côtés d'un grand scientifique, mais aussi auprès d'une personne chaleureuse, dont j'aimerais saluer ici les qualités humaines. Matthieu, je te remercie pour tout le temps que tu m'a accordé, pour tes conseils, ton soutien sans faille et ta gentillesse. Un grand merci à toi.

Je souhaite exprimer toute ma gratitude à Patrick Dangla qui a dirigé ma thèse après le décès d'Olivier Coussy, mon première directeur de thèse, dont la disparition tragique en janvier 2010 a laissé un vide pour sa famille, ses amis, ses collègues, ses étudiants, ainsi que moi-même. Patrick, j'ai pu apprécier non seulement tes qualités scientifiques?, mais aussi tes non moins importante qualités humaines. Je t'exprime ici ma plus profonde gratitude.

Je remercie l'ensemble des membres de mon jury pour leurs critiques et suggestions constructives : Behrouz Gatmiri et Annie Grosman qui ont accepté d'être mes rapporteurs, ainsi que Yves Berthaud et Guy Bonnet qui ont bien voulu compléter ce jury.

Je remercie chaleureusement Laurent Brochard, qui m'a apporté son aide scientifique. Merci de m'avoir informé, écouté et soutenu.

Un grand merci à l'équipe de la Direction de la Recherche, en particulier à Marie-Françoise Kaspi pour m'avoir encouragé lorsque j'étais représentant des doctorants, et pour avoir soutenu et reconnu mes initiatives.

Durant ces trois années de thèse, j'ai eu la chance de côtoyer à Siavash Ghabezloo qui m'a conseillé durant des périodes où j'avais des choix difficiles à faire. Merci à toi, Siavash. Je pense notamment (pardon à ceux que j'oublie) à Laurent, Thibault, Reza, Saeed, Behzad, Jiyun et Yangwei qui ont su me supporter au quotidien et avec qui j'ai passé des moments inoubliables, ainsi que tous ceux que je n'ai pas cités mais avec qui j'ai pu partager un déjeuner, recevoir un enseignement ou discuter autour d'un café.

Enfin, je remercie du fond du cœur mes parents ainsi que l'ensemble de mes amis pour leur soutien, leurs encouragements et leur affection. Il m'est impossible de trouver des mots pour dire à quel point je suis fier d'eux, et à quel point je les aime.

Saeid

Abstract

CO_2 emissions into the atmosphere are recognized to have a significant effect on global warming. Geological storage of CO_2 is widely regarded as an essential approach to reduce the impact of such emissions on the environment. Moreover, injecting carbon dioxide in coal bed methane reservoirs facilitates the recovery of the methane naturally present, a process known as enhanced coal bed methane recovery (ECBM). But the swelling of the coal matrix induced by the preferential adsorption by coal of carbon dioxide over the methane in place leads to a closure of the cleat system (a set of small natural fractures) of the reservoir and therefore to a loss of injectivity. This PhD thesis is dedicated to a study of how this injectivity evolves in presence of fluids.

We derive two poromechanical dual-porosity models for a coal bed reservoir saturated by a pure fluid. The resulting constitutive equations enable to better understand and model the link between the injectivity of a coal seam and the adsorption-induced swelling of coal. For both models, the pore space of the reservoir is considered to be divided into the macroporous cleats and the pores of the coal matrix. The two models differ by how adsorption of fluid is taken into account: the first model is restricted to surface adsorption, while the second model can be applied for adsorption in a medium with a generic pore size distribution and thus in a microporous medium such as coal, in which adsorption mostly occurs by micropore filling.

The latter model is calibrated on two coals with different sorption and swelling properties. We then perform simulations at various scales (Representative Elementary Volume, coal sample, coal seam). In particular, we validate our model on experimental data of adsorption-induced variations of permeability of coal. We also perform simulations of seams from which methane would be produced (CBM) or of methane-free seams into which CO_2 would be injected. We study the effect of various parameters such as boundary conditions, compressibility of the coal matrix, or kinetics of transfer of fluid between cleats and coal matrix.

In a final part, the derived model is extended to cases for which coal is in presence of fluid binary mixtures such as mixtures of methane and carbon dioxide. We fully calibrate this extended model on available data obtained experimentally and by molecular simulations. Calculations are then performed at the scale of a Representative Elementary Volume in order to predict how its porosity and its permeability vary in presence of fluid mixtures of methane and carbon dioxide.

Keywords: poromechanics, adsorption, coal swelling, reservoir simulation, CO_2 storage, coal bed methane (CBM), enhanced coal bed methane (ECBM).

Résumé

Les émissions de CO_2 dans l'atmosphère sont reconnues comme ayant un effet significatif sur le réchauffement climatique. Le stockage géologique de CO_2 est largement considéré comme une approche essentielle pour réduire l'impact de telles émissions sur l'environnement. De plus, injecter du dioxyde de carbone dans les veines de charbon remplies de méthane présent naturellement facilite la récupération de ce méthane, un processus connu sous le nom de récupération assistée du méthane des veines de charbon (ECBM en anglais). Mais le gonflement de la matrice de charbon induite par l'adsorption préférentielle de dioxyde de carbone par rapport au méthane conduit à la fermeture du système de cleats (un ensemble de petites fractures naturelles) du réservoir et donc à une perte d'injectivité. Cette thèse de doctorat est consacrée à l'étude de comment cette injectivité évolue en présence de fluides.

Nous dérivons deux modèles poromécaniques à double porosité pour une veine de charbon saturée par un liquide pur. Les équations constitutives obtenues permettent de de mieux comprendre et modéliser le lien entre injectivité de la veine de charbon et gonflement du charbon induit par l'adsorption. Pour les deux modèles, on considère l'espace poreux du réservoir comme divisé en les cleats macroporeuses et les pores de la matrice de charbon. Les deux modèles diffèrent dans la manière dont l'adsorption de fluide est prise en compte : le premier modèle est limité à une adsorption surfacique, tandis que le deuxième modèle peut être appliqué à l'adsorption dans un milieu possédant un réseau poreux générique, et donc dans un milieu microporeux comme le charbon, pour lequel l'adsorption se déroule principalement par remplissage de micropores.

Le second modèle est calibré sur deux charbons avec des propriétés de sorption et de gonflement différentes. Nous effectuons ensuite des simulations à différentes échelles (du Volume Élémentaire Représentatif, de l'échantillon de charbon, de la veine de charbon). En particulier, nous validons notre modèle sur des données expérimentales de variations de perméabilité de charbon induites par l'adsorption. Nous effectuons aussi des simulations de veines dont le méthane serait produit (un processus connu sous le nom de CBM en anglais) ou de veines sans méthane dans lesquelles du CO_2 serait injecté. Nous étudions l'effet de différents paramètres tels que les conditions aux limites, la compressibilité de la matrice de charbon, ou la cinétique de transfert de liquide entre les cleats et la matrice de charbon.

Dans une dernière partie, le modèle dérivé est étendu aux cas pour lesquels le charbon est en présence de mélanges fluides binaires tels que les mélanges de méthane et de dioxyde de carbone. Nous calibrons entièrement ce modèle étendu sur des données disponibles obtenues expérimentalement et par simulations moléculaires. Des calculs sont alors effectués à l'échelle d'un Volume Élémentaire Représentatif pour prévoir comment sa porosité et sa perméabilité varient en présence de mélanges fluides de méthane et de

dioxyde de carbone.

Mots clefs: poromécanique, adsorption, gonflement du charbon, simulation de réservoir, stockage de CO_2, récupération de méthane (CBM), récupération assistée de méthane (ECBM).

Contents

List of Figures **13**

List of Tables **19**

1 Introduction **21**
1.1 Overview . . . 24
1.2 Carbon capture and storage . . . 25
1.2.1 The three steps of carbon capture and storage . . . 26
1.2.2 Options for geological storage . . . 26
1.2.3 Trapping mechanisms . . . 29
1.3 Geological storage of CO_2 in coal seams . . . 30
1.3.1 Criteria for coal seam to be unmineable . . . 31
1.3.2 Coal seams for CBM, ECBM, and CCS . . . 32
1.4 Motivation and incentives through research . . . 35
1.5 Outline of the thesis . . . 38

2 Poromechanical model of coal bed reservoir saturated by pure fluid **41**
2.1 Introduction . . . 44
2.1.1 Models governing adsorption-induced strain . . . 44
2.1.2 Coal permeability models . . . 45
2.2 Dual-porosity model in absence of adsorption . . . 47
2.3 Dual-porosity model considering surface adsorption . . . 49
2.3.1 Physics of swelling induced by surface adsorption . . . 49
2.3.2 Derivation of constitutive equations . . . 51
2.4 Dual-porosity model considering generic adsorption . . . 53
2.4.1 Derivation of constitutive equations . . . 54
2.4.2 Simplification of the adsorption isotherm . . . 58
2.5 Comparison of model for surface adsorption with the model for generic adsorption: meaning of a simplification of the adsorption isotherm . . . 59
2.6 Concluding remarks . . . 61

3 Calibration of constitutive equations **63**
3.1 Introduction . . . 66
3.2 Calibration of adsorption isotherm . . . 66
3.3 Calibration of adsorption-induced swelling . . . 71
3.4 Effect of matrix compressibility on calibration . . . 76
3.5 Conclusions . . . 78

4 Simulations **81**
4.1 Introduction 84
4.2 Coal sample: comparison with experiment 84
4.3 Representative Elementary Volume 88
4.3.1 Effect of boundary conditions 89
4.3.2 Effect of compressibility of coal matrix 91
4.3.3 Effect of kinetics of transfer of fluid between cleats and coal matrix 92
4.4 Primary recovery of coal bed methane (CBM) 97
4.4.1 Effect of compressibility of coal matrix 99
4.4.2 Effect of temperature 100
4.5 Injection of carbon dioxide in methane-free coal bed 102
4.5.1 Effect of boundary conditions 106
4.5.2 Effect of compressibility of coal matrix 108
4.5.3 Effect of kinetics of transfer of fluid between cleats and coal matrix 111
4.6 Conclusion 114

5 Toward enhanced coal bed methane recovery: extension of model to binary mixtures **117**
5.1 Introduction 120
5.2 Assumptions of the model extended to binary mixtures 120
5.3 Derivation of constitutive equations 121
5.4 Simplification and calibration for coal 128
5.5 Simulation of a Representative Elementary Volume 134
5.6 Concluding remarks 134

6 Conclusion and perspectives **137**
6.1 Conclusion 138
6.2 Perspectives 140

List of Notations **143**

Bibliography **147**

List of Figures

1.1 World savings in energy-related CO_2 emissions made possible by the *450 Scenario* with respect to the *Current Policies Scenario*. (Courtesy Sarah M. Forbes). 24
1.2 Schematic diagram of possible CCS systems displaying the sources for which CCS might be relevant. (Courtesy CO2CRC). 25
1.3 Density of CO_2 at various depths of geological formations. The blue numbers indicate the volume of a given mass of CO_2, in percent of the volume occupied by the same mass at ground level. (Courtesy CO2CRC). 27
1.4 Overview of geological storage options. (Courtesy CO2CRC). 27
1.5 Trapping mechanisms: in stratigraphic trapping (left), CO_2 is trapped by an overlying layer of cap rock coupled with impermeable rock within a narrowing of the storage formation. In structural trapping, CO_2 is trapped by a fold in the rock formations (middle) or by impermeable rock layers shifted along a sealing fault (right) to contain the CO_2. (Courtesy CO2CRC). 30
1.6 Classifications and rank of coal. (Credit: Wikimedia Commons). 32
1.7 Coal bed methane recovery enhanced by carbon dioxide injection. (Courtesy L. Brochard). The temperature and pressure conditions are obtained by considering a geothermal gradient of 25 °C/km with a surface temperature of 15 °C and a hydrostatic pressure gradient with the water density (1000 kg/m^3), the Earth gravitation field g = 9.81 m.s^2 and a surface pressure of 101325 Pa. 33
1.8 Decrease of injectivity at the Allison Unit injection pilot. (adapted from Reeves [2004]). 36
1.9 Schematic representation of a coal seam (adapted from Harpalani and Schraufnagel [1990]). Coal matrix is responsible for the differential swelling. The cleats network governs the transport properties of the seam. 37
1.10 Volumetric strain of coal sample immersed in a pure fluid. The results are adapted from Pini et al. [2009]. The experiments are performed on dry coal samples from the Sulcis coal province (Italy). 37
1.11 Adsorption amount of coal sample immersed in a pure fluid. (adapted from Pini et al. [2009]). The experiments are performed on dry coal samples from the Sulcis coal province (Italy). 38

2.1 Different scales considered for a coal bed reservoir in absence of any adsorption. 47
2.2 Different scales considered for a coal bed reservoir considering surface adsorption. 49

2.3 Schematic multi-scale model for a coal bed reservoir with a microporous matrix. 54

3.1 Equation of state for CO_2 and for CH_4 at a temperature $T = 318$ K. The data is from NIST Chemistry WebBook (http://webbook.nist.gov/chemistry/). 67

3.2 Rubotherm magnetic suspension balance (Source: www.rubotherm.de/magnet/). 68

3.3 Total adsorbed amount of CO_2 and CH_4 at zero strain in Sulcis and Ribolla coals at $T = 318$ K. Symbols are experimental data adapted from Pini [2009], whereas lines are fitted Langmuir isotherms. 70

3.4 Schematic of the high pressure view cell used for the swelling experiments, adapted from Pini [2009]. 71

3.5 Swelling of Ribolla and Sulcis coal samples immersed in carbon dioxide and methane (experimental data adapted from Pini [2009]). Symbols are experimental data, whereas lines are the calibrated poromechanical model. 72

3.6 Coupling coefficient $C(p)$ for Ribolla and Sulcis coals in presence of pure carbon dioxide or pure methane. 74

3.7 Adsorption-induced pressure p^a for Ribolla and Sulcis coals immersed in pure carbon dioxide and pure methane. 74

3.8 Tangent Biot coefficient b_m^{tan} associated to coal matrix for Sulcis and Ribolla coals in presence of pure carbon dioxide and pure methane. 75

3.9 Apparent porosity $n_0^{ads}(p)\overline{V}_b(p)$ for Sulcis and Ribolla coals in presence of pure carbon dioxide and pure methane. 76

3.10 Effect of matrix compressibility on the calibrated adsorption - induced pressure p^a for Sulcis coal in presence of pure carbon dioxide. K and K_m are the bulk moduli of the fractured coal and of the coal matrix, respectively. 77

3.11 Effect of matrix compressibility on the calibrated tangent Biot coefficient b_m^{tan} of the coal matrix for Sulcis coal in presence of pure carbon dioxide. K and K_m are the bulk moduli of the fractured coal and of the coal matrix, respectively. 77

3.12 Effect of matrix compressibility on the apparent porosity of the Sulcis coal matrix in presence of pure carbon dioxide. K and K_m are the bulk moduli of the fractured coal and of the coal matrix, respectively. 78

4.1 Experimental setup used by Mazzotti et al. [2009] to measure the permeability of a Sulcis coal sample at different levels of confining stress and of pore fluid pressure (adapted from Mazzotti et al. [2009]). 85

4.2 Numerical model for the experiment performed by Mazzotti et al. [2009] to measure permeabilities of coal samples to carbon dioxide. 87

4.3 Simulation of transient steps experiment performed at 318.15 K with CO_2 at various levels of confining stresses. Symbols correspond to experimental data by Mazzotti et al. [2009] and lines correspond to model results. Both the pressures in the upstream reservoir ($\circ$) and in the downstream reservoir ($\square$) are represented. 88

4.4 Simulation of transient steps experiment performed at 318.15 K with CO_2 at a constant level of confining stress. Symbols correspond to experimental data by Mazzotti et al. [2009] and lines correspond to model results. Both the pressures in the upstream reservoir (○) and in the downstream reservoir (□) are represented. 89

4.5 Variations of the cleat porosity of the coal sample at 318.15 K with the CO_2 pressure at constant level of confining stress. 89

4.6 Schematic diagram of applied boundary conditions: (a) constant volume case, for which the volume of the REV is kept constant throughout the process, and (b) constant stress case, for which the confining stress is kept constant throughout the process. 90

4.7 Effect of boundary conditions on dimensionless permeability for Ribolla and Sulcis coal samples. For both Sulcis and Ribolla coals, imposing a confining stress of 4 MPa, 8 MPa, or 12 MPa yields identical results. . . . 90

4.8 Dimensionless permeability of a Representative Elementary Volume of Sulcis coal kept at constant volume and injected with carbon dioxide, for various ratios K/K_m of the bulk modulus K of the reservoir to the bulk modulus K_m of the coal matrix. 92

4.9 Dimensionless permeability of a Representative Elementary Volume of Sulcis coal injected with carbon dioxide and submitted to a given confining stress, for various ratios K/K_m of bulk modulus K of the reservoir to the bulk modulus K_m of the coal matrix. 93

4.10 Schematic diagram of applied boundary conditions: (a) immersion, for which the loading stress is governed by the pressure of the fluid, (b) constant volume case, for which the volume of the Representative Elementary Volume is kept constant throughout the process, and (c) constant stress case, for which the confining stress is kept constant throughout the process. 95

4.11 Variation of cleat porosity of a Representative Elementary Volume of Sulcis coal immersed in a fluid with a pressure that increases linearly with time, for various ratios $\alpha = \tau_d/\tau_l$ of the characteristic time τ_d of diffusion to the characteristic time τ_l of loading. 96

4.12 Variation of cleat porosity of a Representative Elementary Volume of Sulcis coal the deformation ϵ of which is set to zero and subjected to a pore pressure in the cleats that increases linearly with time, for various ratios $\alpha = \tau_d/\tau_l$ of the characteristic time τ_d of diffusion to the characteristic time τ_l of loading. 96

4.13 Variation of cleat porosity of a Representative Elementary Volume of Sulcis coal subjected to a constant confining stress σ and to a pressure of fluid in the cleats that increases linearly with time, for various ratios $\alpha = \tau_d/\tau_l$ of the characteristic time τ_d of diffusion to the characteristic time τ_l of loading. 97

4.14 CH_4 pressure in reservoir made of Sulcis coal at different times of the production process. 98

4.15 CH_4 production rate of reservoirs made of Ribolla coal and of Sulcis coal. 99

4.16 Variations of production rate of CH_4 over a year for the reservoir made of Sulcis coal at various ratios K/K_m of the bulk modulus K of the reservoir to the bulk modulus K_m of the coal matrix. 100
4.17 Dimensionless permeability in the reservoir made of Sulcis coal during production of methane at different ratios K/K_m of the bulk modulus K of the reservoir to the bulk modulus K_m of the coal matrix. 101
4.18 Equation of state for CH_4 at various temperatures. The data is from NIST Chemistry WebBook (http://webbook.nist.gov/chemistry/). 102
4.19 Production rate of methane for coal bed reservoirs at various temperatures during a year of production. 103
4.20 Pressures of methane in coal bed reservoirs at various temperatures, after a year of production. 103
4.21 Injectivity of reservoirs made of Ribolla coal and of Sulcis coal with pure CO_2 injected at three different pressures of injection. 105
4.22 Volumetric strains at various times over the injection process in reservoirs made of Sulcis and Ribolla coals. 105
4.23 Various types of boundary conditions used for simulating an injection of carbon dioxide into a methane-free coal bed reservoir: (a) coal seam located between sandstone layers, (b) coal seam with constant thickness, (c) coal seam under constant vertical confining stress. 107
4.24 Distribution of CO_2 pressure in a coal seam and in surrounding sandstone layers at various times of the injection process. 108
4.25 (a) Rate of injection in the coal seam and (b) Average amount of CO_2 per unit volume of the seam for various boundary conditions: seam between two sandstone layers, seam to which a constant vertical confining stress is applied, and seam with a constant thickness. 109
4.26 Dimensionless permeability along the reservoir made of Sulcis coal for various ratios K/K_m of the bulk modulus K of the reservoir to the bulk modulus K_m of the coal matrix. 110
4.27 Injection rates of CO_2 into the reservoir made of Sulcis coal for various ratios K/K_m of the bulk modulus K of the reservoir to the bulk modulus K_m of the coal matrix. 110
4.28 Pressure of fluid in cleats after a month of injection for various characteristic times τ_d of diffusion. 112
4.29 Pressure of fluid in coal matrix after a month of injection for various characteristic times τ_d of diffusion. 112
4.30 Molar concentration n_m of fluid in coal matrix per unit volume of reservoir after a month of injection for various characteristic times τ_d of diffusion. 113
4.31 Dimensionless permeability in the reservoir after a month of injection for various characteristic times τ_d of diffusion. 113
4.32 Variations of injectivity of carbon dioxide over a year for various characteristic times τ_d of diffusion. 114

5.1 Different scales considered for a coal bed reservoir which contains two fluids. 120

5.2 Fugacity of CH_4 and CO_2 as a function of the mixture composition, adapted from Brochard et al. [2012a]. Open symbols are for CO_2 while filled symbols are for CH_4. 121
5.3 (a) Adsorbed amounts of pure fluids in Ribolla coal, adapted from Pini et al. [2010a] and (b) coupling coefficients $C(p)$ for pure fluids and Ribolla coal. 129
5.4 Total amounts of CO_2 and CH_4 adsorbed in a coal sample exposed to a mixture of CO_2 and CH_4 for, adapted from Brochard et al. [2012a]. Open symbols are for CO_2 while filled symbols are for CH_4. The CO_2 mole fraction is that in a reservoir in thermodynamic equilibrium with the sample (i.e., in our case, of the fluid in the cleats). 130
5.5 Fugacity $f_*^{CO_2}(p)$ of pure carbon dioxide and $f_*^{CH_4}(p)$ of pure methane at $T = 318.15$ K, adapted from Span and Wagner [2003a, b]. 131
5.6 Adsorption-induced pressure $p^a(p, x^{CO_2})$ versus the pressure p of the fluid and the CO_2 mole fraction x^{CO_2} of the fluid in the cleats for Ribolla coal sample exposed to a mixture of CO_2 and CH_4 at $T = 318.15$ K. 133
5.7 (a) Cleat porosity ϕ_c and (b) permeability of a Representative Elementary Volume versus the pressure p of fluid for various values of CO_2 mole fraction x^{CO_2} of the fluid in the cleats for Ribolla coal sample kept at constant volume. 135
5.8 (a) Cleat porosity ϕ_c and (b) permeability of a Representative Elementary Volume versus the CO_2 mole fraction x^{CO_2} of the fluid in the cleats for various pressures p of the fluid for Ribolla coal sample kept at constant volume. 136

List of Tables

1.1 ECBM pilots. Well configuration: sw (single-well), 2w (two-well) and mw (multi-well) 35

3.1 Properties of the Ribolla and Sulcis coal samples tested by Pini and used for the calibration of the constitutive equations Pini et al. [2010b]. All percentages are mass fractions. *Volatile matter* refers to the components of coal, except for moisture, which are liberated at high temperature in the absence of air. *Fixed carbon content* of the coal is the carbon found in the material which is left after volatile materials are driven off. *Ash* represents the bulk mineral matter after carbon, oxygen, sulfur and water has been driven off during combustion. R_0 is the term reactivity which is used to describe a critical property or behavior during reaction or conversion in a chemical or a metallurgical process of coal [Raaness, 1990]. 67

3.2 Parameters of Langmuir isotherms fitted on adsorption data of CO_2 and CH_4 on Ribolla and Sulcis samples at $T = 318$ K, adapted from Pini [2009]. The meaning of n^{max} and b_p is provided in the text. 70

3.3 Parameters obtained for the fit of Eq. (3.7) to the swelling of Ribolla and Sulcis samples for CO_2 and CH_4 at a temperature $T = 318.15$ K, adapted from Pini [2009]. The meaning of ϵ^u_{max} and b_s is provided in the text. . . . 72

3.4 Mechanical properties of the Ribolla and Sulcis coals 73

4.1 Input parameters of the model for the permeability experiments performed on Sulcis coal (adapted from Mazzotti et al. [2009] 85

4.2 Model input parameters of the coal seam for simulation of CBM production 98

4.3 Geothermal temperature at various depths of the coal bed reservoir. 101

4.4 Langmuir model parameters for CH_4 adsorption on Ribolla coal at three temperatures (33 °C, 45 °C, 60 °C). Data is from [Pini et al., 2010a]. The langmuir isotherm is given in Eq. (3.6). 101

4.5 Model input parameters for simulation of methane-free coal seam injected with carbon dioxide. 104

4.6 Model input parameters of 2D simulations of a coal seam under various boundary conditions. 106

Chapter 1

Introduction

This chapter presents a general overview of this thesis. Over the last decade the storage of carbon dioxide in deep geological formations has been considered with increasing attention as one of the major solutions to contribute to the struggle against anthropogenic climate change. The main geological storage options (i.e., in oil and gas reservoirs, in deep saline aquifers, and in deep coal bed reservoirs) are at various stages of technological development. The know-how related to the exploration and production of hydrocarbons is of extreme importance, because these techniques are directly applicable to CO_2 storage. In this thesis, we aim at studying the injectivity of carbon dioxide in coal bed reservoirs. An extra benefit of the storage of carbon dioxide in this type of reservoirs is the capability to enhance the recovery of the naturally present methane. However, one of the main issues encountered with this type of storage is the loss of permeability of the reservoir during the injection of carbon dioxide. Such a decrease of permeability originates from the closure of the cleat system in these reservoirs, which itself is a consequence of the swelling of the coal matrix during injection. Previous studies such as Brochard et al. [2012b] focused on how the adsorption in a coal matrix can induce strain. The objective of this thesis is to upscale such a phenomenon up to the scale of a reservoir, a scale at which cleats can play major role in the permeability and injectivity of coal seam.

Ce chapitre présente une vue générale de cette thèse. Au cours de la dernière décennie, le stockage de dioxyde de carbone dans des formations géologiques profondes a été considéré avec une attention croissante comme une des solutions majeures pour contribuer à la lutte contre le changement climatique d'origine anthropique. Les principales options de stockage géologique (réservoirs déplétés de pétrole et de gaz, aquifères salins profonds et veines profondes de charbon) sont à des niveaux variés de développement technologique. Le savoir-faire lié à l'exploration et à la production d'hydrocarbures a une importance extrême, parce que ces techniques sont directement applicables au stockage du CO_2. Dans cette thèse, nous visons à étudier l'injectivité du dioxyde de carbone dans les veines de charbon. Un avantage supplémentaire du stockage de dioxyde de carbone dans ce type de réservoirs est qu'il permet d'augmenter la récupération du méthane en place. Cependant, une des principaux problèmes rencontrés avec ce type de stockage est la perte de perméabilité du réservoir pendant l'injection de dioxyde de carbone. Une telle perte de perméabilité observée in-situ est due à la fermeture du système de fractures de la veine, qui lui-même est une conséquence du gonflement de la matrice de charbon durant l'injection. Des études précédentes comme celle de Brochard et al. [2012b] se sont focalisées sur comment l'adsorption dans une matrice de charbon peut conduire à une déformation. L'objectif de cette thèse est de faire remonter ce phénomène à l'échelle de la veine, une échelle à laquelle les fractures peuvent jouer un rôle majeur dans la perméabilité et l'injectivité d'une veine de charbon.

Contents

1.1 Overview 24

1.2 Carbon capture and storage 25

1.2.1 The three steps of carbon capture and storage 26

1.2.2 Options for geological storage 26

1.2.3 Trapping mechanisms 29

1.3 Geological storage of CO_2 in coal seams 30

1.3.1 Criteria for coal seam to be unmineable 31

1.3.2 Coal seams for CBM, ECBM, and CCS 32

1.4 Motivation and incentives through research 35

1.5 Outline of the thesis 38

1.1 Overview

Currently 81% of the world's energy demand is met by fossil fuels, of which oil accounts for 34.4%, coal for 26% and natural gas for 20.5%, while geothermal, solar and wind energy cover only 0.6% of the total energy demand: the fossil fuels are a predominant source of energy and will continue to be at least for several years [IEA, 2010]. However, the use of fossil fuels has led to a significant increase of the amount of carbon dioxide in the atmosphere. Consequently, the development of greenhouse gas mitigation technologies could play a role in a response to global warming [Loeser and Treede, 2008]. The world energy outlook to 2035 hinges critically on government policy action, and on how that action affects technology, the price of energy services, and end-user behavior [Karaeusel et al., 2010]. In september 2009, G20 leaders presented a New Policies Scenario called *450 Scenario*, which sets out an energy pathway aiming at limiting global warming to 2°C by 2050 [Meinshausen et al., 2009] by restricting the concentration of greenhouse gases in the atmosphere to around 450 parts per million of CO_2 equivalent (ppm CO_2-eq) [Karaeusel et al., 2010]. Fig. 1.1 displays world savings in energy-related CO_2 emissions made possible by the *450 Scenario* with respect to the current policies scenario. In the *450 Scenario*, world primary energy demand increases by 36% between

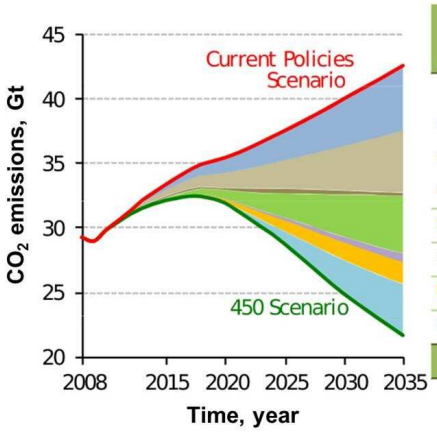

	Abatement		
	2020	2030	2035
Efficiency	71%	49%	48%
– End-use (direct)	*34%*	*24%*	*24%*
– End-use (indirect)	*33%*	*23%*	*23%*
– Power plants	*3%*	*2%*	*1%*
Renewables	18%	21%	21%
Biofuels	1%	3%	3%
Nuclear	7%	9%	8%
CCS	2%	17%	19%
Total (Gt CO_2)	3.5	15.1	20.9

Figure 1.1 – World savings in energy-related CO_2 emissions made possible by the *450 Scenario* with respect to the *Current Policies Scenario*. (Courtesy Sarah M. Forbes).

2008 and 2035, from around 12,300 million tonnes of oil equivalent (Mtoe) to over 16,700 Mtoe, i.e., 1.2% per year on average. Over the last 27 years, this demand increased by about 2% per year. In the *450 Scenario*, fossil fuel, oil, coal and natural gas remain the predominant sources of energy in 2035, though their share of the overall primary fuel mix varies markedly from one scenario to the other. The uncertainty with respect to future energy use is largest for coal, nuclear power and non-hydro renewable energy sources [Karaeusel et al., 2010]. Fig. 1.1 also shows that, until 2020, the reductions in CO_2 emissions will mostly be due to an improvement of efficiency. From 2020, further reductions should be made possible by a significant use of renewables, nuclear power, and CO_2 capture and storage (CCS). Our work will focus on CO_2 storage.

1.2 Carbon capture and storage

Carbon capture and storage (CCS) has been recognized as a technology that should help reduce CO_2 emissions significantly. The idea behind CCS is simple and can be divided into three steps: capture of CO_2 (for example from a fossil fuel power plant), transportation of the captured CO_2, and permanent storage, with the aim of isolating CO_2 from the atmosphere (see Fig. 1.2). The International Energy Agency (IEA) estimates that CCS

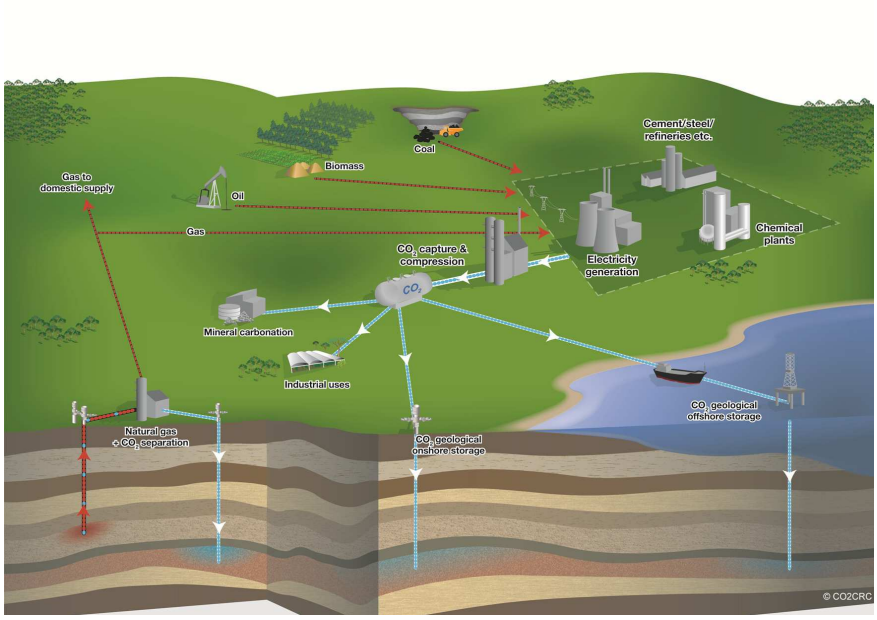

Figure 1.2 – Schematic diagram of possible CCS systems displaying the sources for which CCS might be relevant. (Courtesy CO2CRC).

should contribute to about 15% to 20% of the total greenhouse gas emissions reductions in 2050 [IEA, 2010]. The conversion of the current economies to carbon-free energies requires huge investments on the order of $100 billion per year [Steiner, 2007]. Carbon capture and storage can help streamlining the existing industrial base and spreading over time the investments in new carbon-free power plants and industries. Thus, CCS is a transitory cost-effective solution that can help achieving greenhouse gas concentration stabilization. The International Panel on Climate Change (IPCC) estimates that including CCS in a mitigation portfolio would reduce the cost of stabilizing CO_2 concentration by 30% [Metz et al., 2005]. According to IEA [2010], without CCS the overall costs to halve CO_2 emissions by 2050 would rise by 70%. The global capacity of geological formations to store carbon dioxide is large compared to the cumulated anthropic emissions of carbon dioxide. The estimates of capacity range from 1700 Gt of CO_2 to more than 10000 Gt of CO_2 worldwide [Metz et al., 2005], the former corresponding to about 50 years of CO_2 emissions at the current rate of emission of almost 30 Gt of CO_2 per year [Bernstein et al., 2007].

1.2.1 The three steps of carbon capture and storage

Carbon capture and storage comprises three steps: capture, transport, and storage.

Capture of CO_2 is expected to be most effective at point sources [Metz et al., 2005]. Power plants are the largest point sources of CO_2 emissions in the atmosphere: CO_2 emissions from power production represent around 30% of overall emissions [Metz et al., 2005]. In such plants, large amounts of CO_2 are emitted in diluted streams of flue gases at atmospheric pressure, as the fuel is usually burned in air. Other large single point sources of diluted CO_2 are furnaces, industrial boilers and cement production plants. The emitted CO_2 should be captured at the source. In order to simplify the ensuing steps of transport and storage, a near pure CO_2 product at an absolute pressure of 10 MPa needs to be produced by the capture process [Feron and Hendriks., 2005]. Therefore, a compression step is also needed to achieve the right transport/storage conditions.

Transport of CO_2 is needed as the emissions of CO_2 will not necessarily be at the same location as the storage site. A transport system (via pipelines and/or shipping) is therefore needed to link the CO_2 sources to the CO_2 storage sites. For cost reasons, the distance between the emission sites and the storage sites may determine whether CCS will be developed. The potential sites of injection are distributed in sedimentary basins over all continents, and major sources and prospective sites are separated by distances lower than 300 km [Metz et al., 2005].

Storage of CO_2 is needed in order for CO_2 to remain isolated from the atmosphere for a suitably long period (hundreds of years [Metz et al., 2005]). Storage in underground rock structures is one of the items towards which research is concentrated. In geological storage, CO_2 is injected at depths below 0.3 km.

1.2.2 Options for geological storage

The main geological storage options are [Lokhorst and Wildenborg, 2005]: depleted oil and gas reservoirs, deep saline aquifers, caverns and mines, and deep seated coal beds (see Fig. 1.4).

Oil and gas reservoirs have proven their capability to hold oil and gas over geological periods of time and therefore are expected to act as long term storage sites for CO_2 as well. This option is particularly interesting when one can take advantage of CO_2 injection in order to enhance the recovery of the gas or oil. CO_2 injection has indeed been applied for hundreds of years already to enhance the production of oil from oil reservoirs (EOR), in particular in the United States. In conventional CO_2-EOR, the main aim is to inject a minimum amount of CO_2 to maximise oil production. Conversely, in the case of CO_2 storage, one aims at injecting a maximum amount of CO_2 while possibly increasing oil production. This difference is demonstrated in the Canadian Weyburn project, which is directed to the co-optimization of oil production and CO_2 injection [Cantucci et al., 2009]. For the owners and the operator of the Weyburn oil field, increased oil production is paramount, while an international consortium is focusing on the optimization of the net amount of injected CO_2 [Lokhorst and Wildenborg, 2005]. Improvement of gas recovery (EGR) with the help of CO_2 injection is still in the phase of desk studies [Metz et al., 2005]. EGR includes conventional and unconventional natural gas recovery. Unconventional natural gas is the gas that is more difficult or less economical to extract than

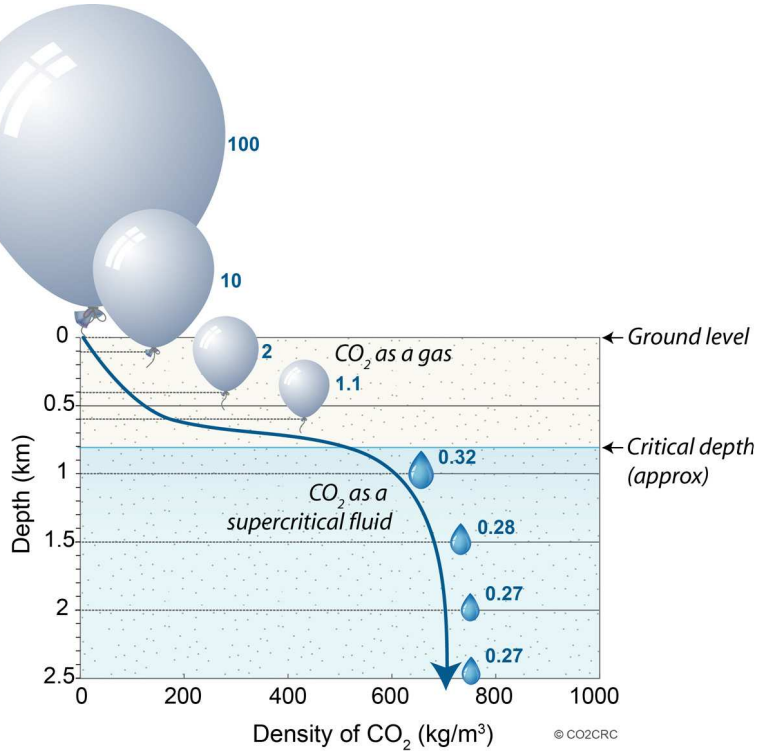

Figure 1.3 – Density of CO_2 at various depths of geological formations. The blue numbers indicate the volume of a given mass of CO_2, in percent of the volume occupied by the same mass at ground level. (Courtesy CO2CRC).

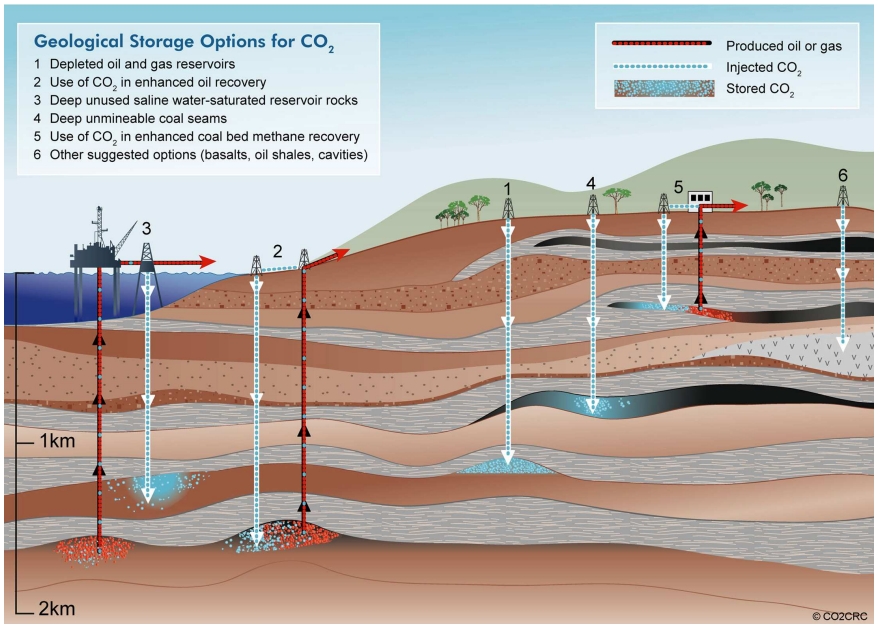

Figure 1.4 – Overview of geological storage options. (Courtesy CO2CRC).

conventional natural gas, usually because of the incomplete development or of the high cost of the technology necessary to reach the gas [Tollefsen et al., 2010]. Essentially, six main categories of unconventional natural gas exist: deep gas, tight gas, shale gas, coal bed methane, geopressurized zones, and methane hydrates.

- Deep gas lies in the very far underground (4.6 km), beyond conventional depths which are traditionally a few hundred meters only. Therefore, deep gas is more expensive to produce than conventional natural gas and is considered as an unconventional gas [Inkpen and Moffett, 2011].
- Tight gas is stuck in a very tight formation underground, trapped in hard rocks such as sandstone or limestone with very low permeability and porosity [Inkpen and Moffett, 2011].
- Shale gas exists in a very fine-grained sedimentary rock called shale, which is easily breakable into thin, parallel layers. It is a very soft rock, but it does not break down when it becomes wet. Because of the low permeability and high toughness of shales, the extraction of natural gas from shale formations is more difficult and nowadays more expensive than that of conventional natural gas [Inkpen and Moffett, 2011].
- Coal bed methane exists naturally in coal seams. This coalbed methane is trapped underground and is generally not released into the atmosphere until coal mining activities unleash it. In the past, the methane that accumulated in a coal mine was intentionally vented into the atmosphere in order to avoid explosions. Today, however, coal bed methane has become a popular unconventional form of natural gas. This methane can be extracted and injected into natural gas pipelines for resale [Inkpen and Moffett, 2011].
- Geopressurized zones are natural underground formations that are under unusually high pressure for their depth. These areas are formed by layers of clay that are deposited and compacted on top of more porous material such as sand or silt. Water and natural gas that are present in this clay are squeezed out by the rapid compression of the clay and migrate toward the more porous sand or silt deposits. Geopressurized zones are typically located at great depths, usually 3 km to 7.5 km below the surface of the earth. The combination of all these factors makes the extraction of natural gas in geopressurized zones quite complicated [Inkpen and Moffett, 2011].
- Methane hydrates are the most recent form of unconventional natural gas to have been discovered and studied. These interesting formations are made up of a lattice of frozen water that traps methane. These hydrates look like melting snow and were first discovered in permafrost regions of the Arctic. However, research into methane hydrates has revealed that resources may be much more plentiful than first expected. In fact, the USGS estimates that methane hydrates may contain more organic carbon than the world's coal, oil, and conventional natural gas combined [Inkpen and Moffett, 2011].

The theoretical storage potential of CO_2 in depleted reservoirs is considerable: an estimate resulted in a theoretical potential of more than 40 Gt CO_2 in European hydrocarbon reservoirs [IEA, 2010], 7 Gt of which could be stored in conventional oil fields. However, a drawback of oil and gas fields is that the majority of them are in the North Sea region, i.e., at considerable distance from the CO_2 emitting power plants.

Deep saline aquifers cannot be used as sources of drinking or irrigation water because of their high salt content. An estimate of the theoretical storage potential revealed

a potential of 150 to 1500 Gt CO_2 in West-European aquifers [IEA, 2010]. But such estimates are uncertain, because of the generally low level of knowledge for deep-seated saline aquifers. A major characterization and testing effort is called for, especially for onshore sites, in order to qualify this type of aquifer for geological storage. The lack of knowledge on deep saline aquifers will increase the lead times for the implementation of CO_2 storage in saline aquifers. The first large scale CO_2 storage plant injecting CO_2 in an aquifer was built in 1996 near the Sleipner gas field in the Norwegian North Sea. At this plant, CO_2 is injected at a depth of 800 to 1000 m below the sea bottom [Metz et al., 2005].

Caverns and mines in rock-salt and abandoned coal mines can serve as potential CO_2 storage structures, although their storage capacity will be limited. For instance, it has been estimated that 3500 Mt of CO_2 can potentially be stored in rock caverns in Alberta Basin and in Saskatchewan, Canada [Manancourt and Gale, 2004]. Salt caverns might be used for temporary storage to buffer exhaust CO_2 streams or to use CO_2 for other commercial purposes. These structures are considered to be less suitable for long-term CO_2 storage, since they could also be used for other applications such as waste disposal. Abandoned coal mines are present in the former German, British, Belgian, and Dutch coal mining districts. These mined coal zones have increased permeability, which improves the CO_2 injectivity. However, the sealing capacity of the overburden is questionable. In Germany and Britain at least, there is abundant evidence of gas leakage to the surface in the major coal mining areas, which makes CO_2 storage in abandoned coal mines less attractive for these regions [Lokhorst and Wildenborg, 2005].

Unmineable coal seams have recently become of interest for the use of CO_2 for Enhanced Coal bed Methane Recovery (ECBM). A primary reason for this growing interest is that the earth's sedimentary basins contain an enormous amount of coal [Kroeger et al., 2011]: the theoretical CO_2 storage potential of European coal seams is estimated at about 6 Gt [IEA, 2010]. In many instances the coal reserves are close to industrial centers with CO_2 emitting power plants. One of the attractive aspects of ECBM is that, for each molecule of CH_4 produced, at least two CO_2 molecules can be stored in the coal matrix [White et al., 2005]. But, the challenge is to unlock the coal bed methane resources in an economically viable manner. Indeed, one of the main problems associated with developing ECBM is the low permeability of most unmineable coals, which is comprised between 1 mD and 10 mD [White et al., 2005]. CO_2 storage in such coal seams is the focus of this thesis and is described in greater detail in Sec. 1.3.

1.2.3 Trapping mechanisms

CO_2 itself has been securely trapped in rock formations in many places around the world [Tajnik et al., 2012]. Geologists searching for sites appropriate for CO_2 storage look for rock formations that already securely hold fluids and therefore have proven their ability to trap fluids [IEA, 2010].

A trap is a configuration of rocks suitable for containing fluids and sealed by a relatively impermeable formation through which fluids will not migrate. CO_2 is held in place in a storage reservoir through one or more of five basic trapping mechanisms: *stratigraphic*, *structural*, *residual*, *solubility*, and *mineral*. Trapping mechanisms (see Fig. 1.5) depend on the local geology and can occur simultaneously depending on the site. Gen-

erally, the initial dominant trapping mechanisms are *stratigraphic trapping* or *structural trapping*, or a combination of the two. Cap rock is a dense layer of impermeable rock that overlays the rocks holding the CO_2 and forms a continuous primary seal. In *stratigraphic trapping*, cap rock, sometimes in association with impermeable rocks at the same level as the CO_2, forms a closed container to trap the CO_2. In *structural trapping*, impermeable rocks shifted by a fault or fold in the geologic strata hold the CO_2 in place. In addition, CO_2 storage rocks are generally separated from the surface by other thick layers of impermeable rock, called *secondary seals*. Over time, other secure trapping mechanisms take

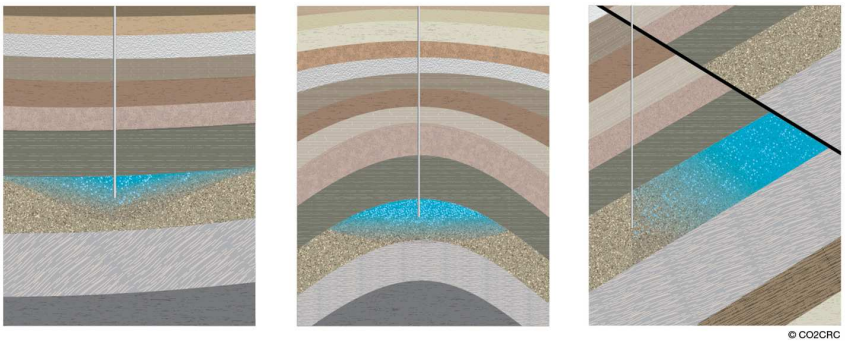

Figure 1.5 – Trapping mechanisms: in stratigraphic trapping (left), CO_2 is trapped by an overlying layer of cap rock coupled with impermeable rock within a narrowing of the storage formation. In structural trapping, CO_2 is trapped by a fold in the rock formations (middle) or by impermeable rock layers shifted along a sealing fault (right) to contain the CO_2. (Courtesy CO2CRC).

over. In *residual trapping*, which usually begins after injection stops, the CO_2 is trapped in the tiny pores of the host rock by capillary pressure effects. After injection stops, water from the surrounding rocks begins to move back into the pore spaces containing the CO_2. As this happens, the CO_2 becomes immobilized by the pressure of the added water. As more CO_2 is injected, the CO_2 moves further from the injection site and, since it is less dense than oil or highly saline water, the CO_2 may also initially rise toward the top of the porous storage rocks, where stratigraphic and structural trapping keep it in place. Injection pressures must be high enough to force the liquid CO_2 into the porous host rock, but must remain low enough not to break the cap rock forming the primary seal right above the storage formation [Metz et al., 2005].

1.3 Geological storage of CO_2 in coal seams

As a possible option for permanent geological storage of carbon dioxide, coal seams have been suggested since the 1970's [Metz et al., 2005]. In particular, unmineable coal seams are potential candidates for such a storage. These unmineable coal seams naturally containe methane, called coal bed methane (CBM). The estimated storage potential of coal seams varies between 3 $GtCO_2$ and 200 $GtCO_2$ worldwide, which is relatively small compared to that of other geological formations [Metz et al., 2005]. The upper estimate is based on the world resources of unmineable bituminous coal seams, whereas the lower

estimate refers only to coal seams for which simultaneous CBM production could be carried out. These values, together with the geographical distribution of potential coal seams (which not always matches the location of large CO_2 sources) suggest that the contribution of coal seams to the underground storage of CO_2 will be limited compared to that of other geological formations. This amount however remains significant with respect to the current anthropogenic emissions of CO_2, which amount to almost 30 $GtCO_2$ per year [Pachauri and Reisinger, 2007]: CO_2 storage in coal seams needs to be taken into account in the effort of finding ways for reducing greenhouse gases emissions.

1.3.1 Criteria for coal seam to be unmineable

The first criterion for a coal seam to be well suited for CO_2 storage is that the coal seam must be unmineable, i.e., the coal can not be recovered for direct energy production. Therefore, for CO_2 storage, it is not only essential to determine the in-place coal resources, but also to identify recoverable reserves from unmineable seams. This distinction is captured by the terms *resources* and *reserves* which, although frequently used interchangeably, hold for different concepts.

In a broad definition, coal *resources* include all coal present in the underground. In contrast, coal *reserves* only include the part of the coal reserves that is realistically available for productions in the foreseeable future [Luppens et al., 2009]. Coal *reserves* are therefore a subset of the coal resources. To be classified as reserves, the coal must be considered as economically producible at the time of classification, but facilities for extraction need not be in place and operative [Wood et al., 1983]. Many factors such as bed thickness, depth of coal, coal rank, coal quality and sulfur content may significantly affect the economics of coal recovery, with no single key parameter being most critical [Luppens et al., 2009].

The first parameter of interest when considering a coal seam is its rank. Coal rank is a function of the degree of coalification (i.e., of metamorphism), which is based on the degree to which the original plant material has been transformed into carbon. Coal rank is a rough indication of how old the coal is: generally, the older the coal, the higher its carbon content. Also, the rank of a coal generally increases with burial depth. The ranks of coal (from the highest to the lowest carbon content) are as follows: anthracite, bituminous coal, subbituminous coal, and lignite (see Fig. 1.6). Lignite (also called brown coal) is a young type of coal, which is brownish black with a high sulfur content and a high moisture content (up to 45 %), where the moisture content is defined as the mass of water in coal per unit mass of dry coal sample. Lignite is more like a soil than like a rock and tends to disaggregate when exposed to weather. Subbituminous coal is also called black lignite. Its moisture content ranges from 20 % to 30 %. Bituminous coal is a soft, dense, black coal. Bituminous coal often has bands of bright and dull material in it. It is the most common coal and its moisture content is below 20 %. Anthracite coal, often referred to as hard coal, is hard, black, and lustrous. In Anthracite, the content of sulfur is low and the content of carbon is high. It is the coal with the highest rank. Its moisture content generally is less than 15 %. The energy content of a coal increases with its rank. Coals with a higher rank can therefore be sold at a higher price than coals with a lower rank.

Bed thickness is one of the most important fundamental factors affecting coal recover-

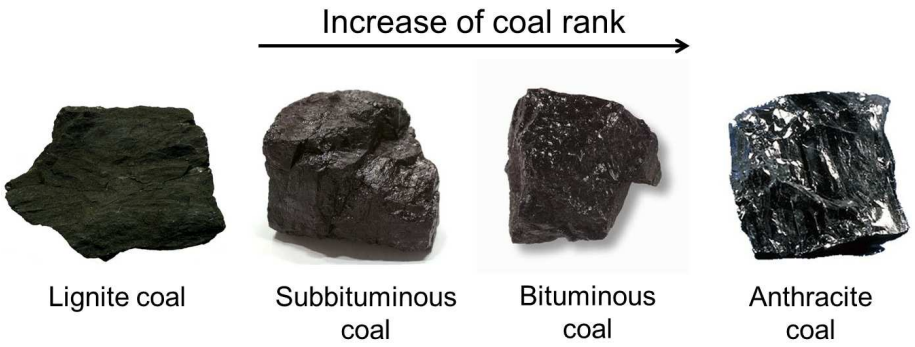

Figure 1.6 – Classifications and rank of coal. (Credit: Wikimedia Commons).

ability. The coal bed thickness varies significantly in the major coal basins. For instance, the bed thickness in most basins in the U.S. is thin to moderate (3 m thick or less). However, the thickness of many coal beds in the western U.S. regions exceed 3 m, sometimes reaching more than 15.2 m. Typically, a direct correlation between bed thickness and recoverability is observed. Very thin coal beds may be nonrecoverable: with current mining technology, minimum bed thicknesses for surface and underground mining are limited to about 0.1 m to 0.2 m, respectively. We also observe that, the lower the thickness of the seam, the greater the surface of the seam must be for the recovery to be economically viable [Luppens et al., 2009]. In a strict definition, coal reserves only include seams with a minimum thickness: this minimum thickness must be of 36.6 cm for anthracite and bituminous coal, and of 76.2 cm for lignite and subbituminous coal.

The depth of the coal beds is also an important factor affecting coal recovery economics. In general, thicker coal beds can be economically recovered to greater depths [Luppens et al., 2009]. Only seams with a depth below 1,828.8 m can be considered as coal reserves [Wood et al., 1983].

Finally, other parameters such as sulfur content, mineral matter, mining costs, location, and transportation infrastructure can make a coal seam mineable or not.

1.3.2 Coal seams for CBM, ECBM, and CCS

Coal seams are fractured porous media, characterized by a relatively large internal surface area of about 30 $m^2.g^{-1}$ to 300 $m^2.g^{-1}$ [Berkowitz, 1985]. Significant amounts of methane (CH_4) are generated and retained during the geological process leading to their formation, the so-called coalification process [Levine, 1993], [Gentzis, 2000]. Such coal bed methane (CBM) can be recovered from the coal seam and used for energy production. Conventional primary recovery of methane (called CBM production), which is performed by pumping out water and depressurizing the reservoir, allows producing 20% to 60% of the methane originally present in the reservoir [White et al., 2005]. As is the case with enhanced oil recovery (EOR), such primary production could be in principle enhanced by injecting CO_2 in the coal seam. This process is schematized in Fig. 1.7 and is called Enhanced Coal Bed Methane (ECBM) recovery [White et al., 2005]. Since the injection of CO_2 may allow to store CO_2 in the underground, ECBM is part of the CCS system.

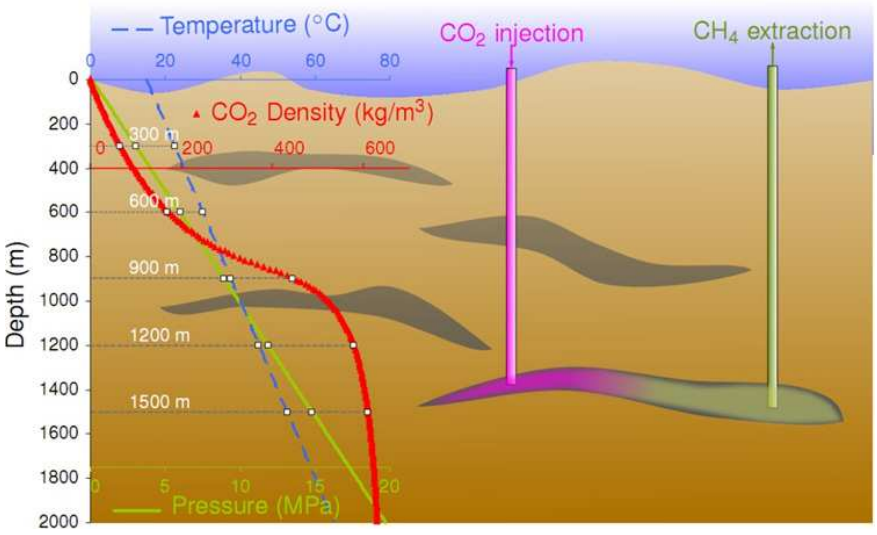

Figure 1.7 – Coal bed methane recovery enhanced by carbon dioxide injection. (Courtesy L. Brochard). The temperature and pressure conditions are obtained by considering a geothermal gradient of 25 °C/km with a surface temperature of 15 °C and a hydrostatic pressure gradient with the water density (1000 kg/m^3), the Earth gravitation field g = 9.81 m.s^2 and a surface pressure of 101325 Pa.

For the selection of a storage site, permeability is a critical parameter. In the earth sciences, permeability k is part of the proportionality constant in Darcy's law [Darcy, 1856] which relates fluid flow velocity v and fluid viscosity μ, to a pressure gradient applied to the porous media ($v = \frac{k}{\mu}\nabla p$) and is presented in m^2. According to Christensen and Holloway [2004], a permeability of 1 mD is necessary for ECBM to be feasible. But the permeability of coal reservoirs varies widely from site to site ranging from $1\mu D = 10^{-18}$ m^2 to about 10 mD, and decreasing generally with an increasing site depth [White et al., 2005]. CBM content increases with increasing rank, so that with greater seam depths gas contents are expected to increase [Beaton, 2003]. With increasing depth also comes increasing overburden pressure, which may decrease the porosity and thus the permeability of the seam. A challenge in ECBM exploration is finding unmineable coals with ranks suitable for gas generation, but relatively shallow in order to guarantee their permeability. A good compromise is medium rank coals with an average gas content of about 8 m^3.t^{-1} and and initial permeability of about 10 mD [Schepers et al., 2010], [Esterle et al., 2006], [Reeves, 2004].

The way fluids are stored in the coal seam differs from the way they are stored in other geological formations in the fact that, besides filling the available fracture and pore volume, the gas is adsorbed in the coal matrix. The density of adsorbed CO_2 is much higher than that of gazeous CO_2 [Sircar, 2001], thus allowing for a better exploitation of the reservoir rock as a storage medium for CO_2. Carbon dioxide and methane can both get adsorbed in the coal matrix, but the affinity of carbon dioxide for coal is greater than that of methane: when immersed in a fluid mixture made of equal amounts of carbon dioxide and methane, at least twice as many molecules of carbon dioxide as of methane are stored in the coal matrix [Ottiger et al., 2008]. Due to the higher adsorptivity of CO_2 in coal with

respect to that of CH_4, the injected carbon dioxide enables to recover larger amounts of methane from the coal, hence the ECBM process.

In coal seams experiments show that the maximum storage capacity of CO_2 in the coal matrix is reached for bulk pressures of CO_2 as low as 3 MPa. For this reason, the storage in coal is considered for sites as shallow as 300 m [White et al., 2005]. Coal seams deeper than 2000 m are not considered for ECBM or for CCS, because their permeability is too low. At a depth below 0.8 km, conditions in temperature and pressure are met for CO_2 to be supercritical the critical temperature and pressure of CO_2 are $T_{cr} = 304$ K and $P_{cr} = 7.4$ MPa, respectively [Washburn, 1933]. Supercritical fluids are denser than gases, as shown in Fig. 1.3, and diffuse better than either gases or ordinary liquids through the pore space in storage rocks [Metz et al., 2005].

From an engineering point of view, ECBM is carried out by injecting CO_2, potentially in supercritical conditions, in natural underground coal formation through one or more injection wells and by collecting CH_4 from one or more production wells. The process of injecting a gas into a reservoir with simultaneous recovery of a value-added product is quite popular in the oil industry, where production of oil is enhanced by injection of CO_2 or N_2 into the reservoir (a process known as enhanced oil recovery or EOR). Thanks to this added value, those techniques that offer a byproduct such as natural gas are expected to be the first commercially practiced storage technologies compared to the other scenarios for long term storage of CO_2. Moreover, since ECBM and EOR make use of similar technologies, ECBM requires no offset of operational costs [White et al., 2005]. Likewise, the expertise gained in the past years for enhanced oil production will play an important role in a faster implementation of the ECBM technology at a commercial scale. In conclusion, ECBM is attractive from two perspectives. On the one hand, if one is interested in the recovered methane as a fuel or a technical gas, ECBM allows also for a net CO_2 sequestration, thanks to the above mentioned high CO_2 adsorptivity. On the other hand, if the goal is to store captured CO_2, the ECBM operation allows also recovering methane, thus making CO_2 storage more interesting economically.

Towards demonstration of its feasibility and as a first step in the direction of its commercial deployment, the ECBM technology has been implemented in a number of field tests, which are reported in Table 1.1. The first ECBM field project, the Coal-Seq project, is the largest such project even. At the San Juan Basin in New Mexico (USA), starting in 1995, pure CO_2 and pure N_2 were injected in the Allison and Tiffany Units, respectively, while CH_4 was successfully produced in a multi-well configuration over a period of more than five years [Reeves, 2004]. The project showed that gas injection indeed enhanced methane recovery. CO_2 injection yielded a reduction in permeability and injectivity, while N_2 injection led to a rapid breakthrough, thus reducing product purity. The former effect was attributed to the porosity reduction associated with coal swelling upon CO_2 injection, particularly evident near the well, where the CO_2 pressure was high.

Field tests at other locations in the world were performed on a much smaller scale, exploiting a single well [Gunter et al., 2004], [Wong et al., 2006] or a two-well configuration [Van Bergen et al., 2006], [Yamaguchi et al., 2006]. The goal of these projects was to test the ECBM technology in reservoirs with different geological characteristics and to observe CO_2 breakthrough within the project life time, usually around 1 year. This information is very useful, in particular when compared to the results obtained from reservoir modeling studies [Van Bergen et al., 2006]. In all cases, the production of CH_4 was

enhanced in response to an injection of fluid and an injection of CO_2 led to a reduction of injectivity. As was the case for the San Juan Basin, this latter effect was attributed to the closing of the fracture associated with coal swelling. The low injection rates could be compensated at least partially and temporarily through shut-in periods in the Alberta CO_2-ECBM project [Gunter et al., 2004], or through fracking in the RECOPOL project [Van Bergen et al., 2006]. In contrast, during the injection of flue gas (mixture of CO_2 and N_2) in the Fenn-Big Valley project, a steady increase of well injectivity was observed [Gunter et al., 2004]. In order to mitigate the effect of the low permeability of a reservoir, one can increase the number of wellbores: in the case of the RECOPOL pilot project in Poland, the recovery wells were only 200 m away from the injection well. One can also increase the pressure of injection [Gaus, 2010]. In this latter case it is necessary to make sure that the overpressure generated would not cause the surrounding rock to fracture and lead to a leakage [White et al., 2005].

Table 1.1 – ECBM pilots. Well configuration: sw (single-well), 2w (two-well) and mw (multi-well)

Location	**Project**	**Year**	**Wells**	**Injection**	**Reference**
San Juan Basin (USA)	Allison Unit	1995	mw	277 kt	Reeves [2004]
Fenn-Big Valley (Canada)	Fenn	1998	sw	0.19 kt	Gunter et al. [2004]
Qinshui Basin (China)	Qinshui	2004	sw	0.19 kt	Wong et al. [2006]
Upper Silesian Basin (Poland)	RECOPOL	2004	2w	0.76 kt	Van Bergen et al. [2006]
Ishikari Coal Basin (Japan)	JCOP	2004	2w	0.15 kt	Yamaguchi et al. [2006]
Illinois Basin (USA)	MGSC	2008	-	0.2 kt	Litynski et al. [2008]
Navajo City (USA)	SWP San Juan	2008	-	68 kt	Litynski et al. [2008]
Tuscaloosa County (USA)	Black Warrior	2009	-	1 kt	Litynski et al. [2008]
Central Appalachian (USA)	SECARB	2009	-	1 kt	Litynski et al. [2008]
Marshall County (USA)	DOE West Virginia	2009	-	18 kt	Litynski et al. [2008]

1.4 Motivation and incentives through research

The feasibility of ECBM depends on several issues such as the permeability of the reservoir, the risks of leakage, and the evolutions of the permeability over the injection process. For field application of ECBM, the variations of permeability cause problems of injectivity: the amount of carbon dioxide injected per unit of time reduces significantly over time while the pressure of injection remains constant, as is shown in Fig. 1.8 for the Allison unit injection pilot [Reeves, 2004]: after one and a half year of injection at constant pressure, the injectivity decreased by 60%. Part of this decrease is due to the fact that the reservoir was being filled, but part is not: well testing indicated that the coal permeability near the well had decreased by about two orders of magnitude. The injection, which was initially planned for three years, lasted six years. Interestingly, the injectivity

increased back slightly after this initial drop: we refer to this phenomenon as to the injectivity rebound. However, such a rebound in injectivity was also due to the cavitation and reopening of new wells [Reeves, 2004]. For commercial applications of CCS, the rate of injection of carbon dioxide must be significantly larger than those experienced in the past and existing pilots [IEA, 2010]. The evaluations of injectivity over the injection process are the focus of the thesis and are discussed in detail in this section.

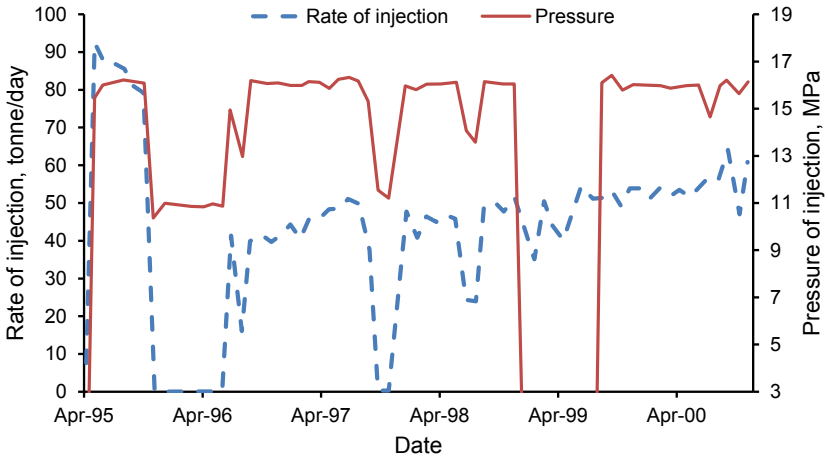

Figure 1.8 – Decrease of injectivity at the Allison Unit injection pilot. (adapted from Reeves [2004]).

Coal reservoirs are made of fractured coal in which the transport of fluid is governed by the network of fractures, also called cleats (Fig. 1.9). Cleats are connected macropores arranged in a network with a typical spacing of 1 cm. The coal matrix in-between, in which most of the fluid is stored, is a porous material with a wide pore size distribution ranging from micropores (diameter lower than 2 nm) to mesopores (diameter comprised between 2 nm and 50 nm) and to macropores (diameter greater than 50 nm) [Sing et al., 1985]. The coal matrix swells when carbon dioxide is injected and replaces methane. In situ, a coal seam is constrained by the surrounding geological layers and is not free to swell. The variations of permeability are the result of a competition between the swelling of the matrix, which tends to close the cleats and the bulk pressure of the fluid which tends to reopen the cleats.

In contrast to confined conditions, some researchers observed coal samples that were merely immersed in pure fluids [Harpalani and Schraufnagel, 1990], [Levine, 1996], [Ottiger et al., 2008]. During an immersion of a coal sample in an adsorbing fluid, its volume varies, and this volume variation depends on the nature of the fluid (see Fig. 1.10): usually a coal sample swells more when immersed in CO_2 at a given pressure than when immersed in CH_4 at the same pressure. As a consequence, during the injection process, the progressive replacement of methane with carbon dioxide leads to a swelling of the coal which is called the *differential swelling*.

At the scale of the coal matrix, the fluids are not in their bulk state but they are stored under an adsorbed form. Adsorption occurs when the molecules of a fluid are interacting

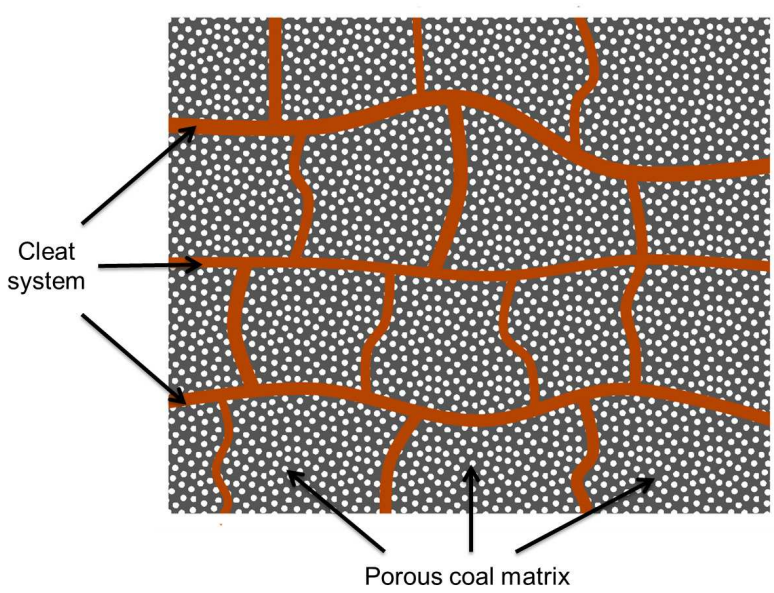

Figure 1.9 – Schematic representation of a coal seam (adapted from Harpalani and Schraufnagel [1990]). Coal matrix is responsible for the differential swelling. The cleats network governs the transport properties of the seam.

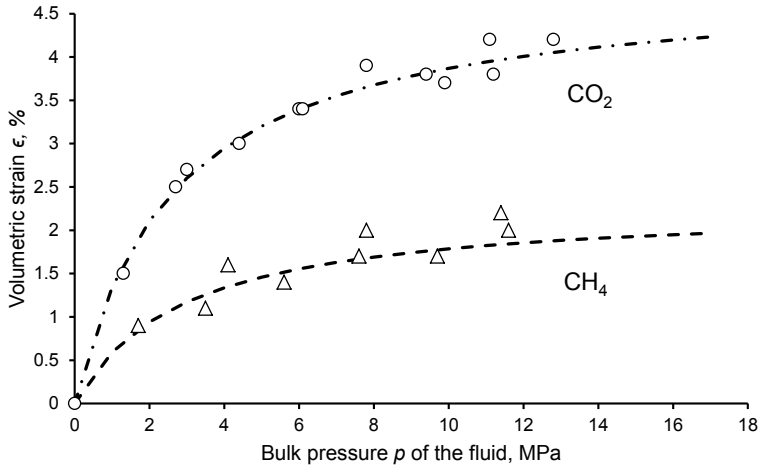

Figure 1.10 – Volumetric strain of coal sample immersed in a pure fluid. The results are adapted from Pini et al. [2009]. The experiments are performed on dry coal samples from the Sulcis coal province (Italy).

with the atoms of a solid. Both carbon dioxide and methane are adsorbed in the coal matrix, but the molecular interactions between carbon dioxide and coal are more significant than between methane and coal, which is the reason why the affinity of carbon dioxide for coal is greater than that of methane (see Fig. 1.11). Helium, which induces no swelling of the coal, is almost not adsorbed in coal, whereas methane and carbon dioxide, which induce significant swellings, are adsorbed [Ottiger et al., 2006]. Adsorption is known to govern the swelling of the coal matrix [Harpalani and Schraufnagel, 1990].

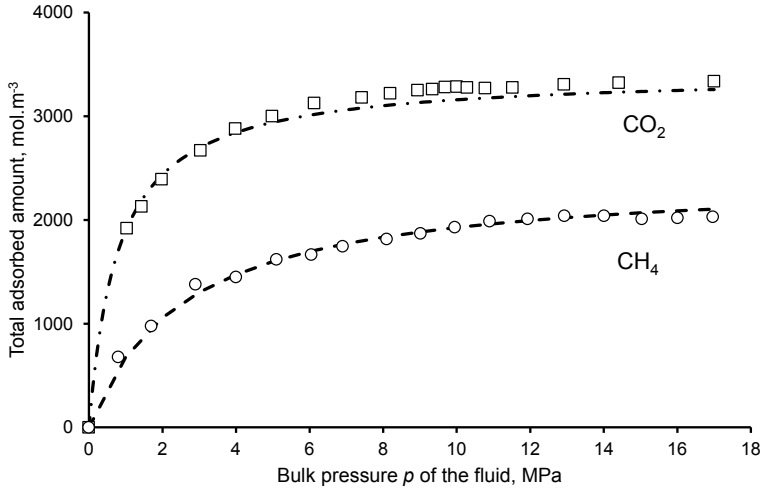

Figure 1.11 – Adsorption amount of coal sample immersed in a pure fluid. (adapted from Pini et al. [2009]). The experiments are performed on dry coal samples from the Sulcis coal province (Italy).

How adsorption modifies the mechanical behavior of the coal matrix and eventually the injectivity of a coal bed reservoir is important for field applications. Indeed, economic analysis of ECBM is based on predictions of rates of injection of CO_2 and of production of CH_4. To obtain relevant predictions, relevant constitutive laws must be available for the coal seam. Such a model must correctly capture the variations of injectivity observed in the field and must therefore explicitly take into account the adsorption-induced differential swelling observed in the laboratory. Empirical models were experimented in the case of the Allison Unit [Pekot and Reeves, 2002], [Reeves et al., 2003], [Shi and Durucan, 2004b]. Such models captured well the general behavior of the coal reservoir, even if significant discrepancies were obtained regarding the bottomhole pressures at the injection, recovery and observation wells. However, if one wants to explore or design innovative solutions for ECBM, one needs to move beyond empirical modeling, the predictive ability of which is limited to the range of conditions on which it has been experimentally verified.

1.5 Outline of the thesis

In this work, we aim at modelling a full ECBM process. As a first step toward this goal, we aim at obtaining constitutive equations that can eventually be used in reservoir

simulations. The model will be derived with the Biot-Coussy poromechanical framework in chapter 2 [Coussy, 2004, 2010]. Two saturated models are proposed in order to estimate the complex evolutions of injectivity over the process of injection. For both models, two porous networks are explicitly taken into account: the cleats of the reservoir and the pores of the coal matrix. The first model uses poromechanical equations that have been extended recently to the effect of surface adsorption [Vandamme et al., 2010], [Coussy, 2010]. For the second model, constitutive equations are derived taking into account the fact that the coal matrix is in fact microporous and coal is considered as a medium containing a generic distribution of pore size. The derived model is then calibrated in chapter 3 with the help of data of adsorption and of adsorption-induced swelling in presence of pure fluids. In chapter 4, making use of the calibrated parameters for adsorption of CO_2 and CH_4 on coal, we perform calculations on Representative Elementary Volumes (REV) of coal reservoir exposed to pure fluids. Numerical simulations are performed, which enable to estimate the variations of injectivity and permeability of coal during primary recovery of coal bed methane (CBM) or during a hypothetical case of an injection of pure carbon dioxide in an empty reservoir. In chapter 5, the model is extended to multi-component fluids, calibrated with experimental data in combination with numerical data obtained by molecular simulations [Brochard et al., 2012a], and then used in order to perform calculations at the scale of a Representative Elementary Volume exposed to a binary mixture such as the one formed by methane and carbon dioxide.

Chapter 2

Poromechanical model of coal bed reservoir saturated by pure fluid

---

This chapter is dedicated to the derivation of two poromechanical dual-porosity models for a coal bed reservoir saturated by a pure fluid. As a prerequisite to any reservoir simulation, we need constitutive equations to better understand and model the link between adsorption, swelling, and variation of permeability for a Representative Elementary Volume of a coal seam. The first poromechanical model is valid for surface adsorption only, while the second is valid for a generic coal matrix and a potentially microporous one. For both models, the pore space of the reservoir is considered to be divided into the macroporous cleats and the pores of the coal matrix. We assume that fluid molecules in the cleats are in a bulk state and that the cleats govern the transport properties of the seam. For the model dedicated to surface adsorption, fluid molecules in the coal matrix are assumed to be either in a bulk state inside the pores of the coal matrix or in an adsorbed state on the surface of those pores; swelling is due to this surface adsorption. For the model valid for a coal matrix with a generic pore size distribution, no assumption is made on the state of the fluid molecules in the coal matrix, which can be in a bulk state, adsorbed on a surface, or adsorbed in a micropore. Since the range of validity of this latter model is greater than the one of the model derived for surface adsorption, in the rest of the thesis, we will therefore only use the dual-porosity model valid for a coal matrix with a generic pore size distribution.

Ce chapitre est dédié à la dérivation de deux modèles poromécaniques à double porosité pour une veine de charbon saturée par un fluide pur. Comme prérequis à toute simulation à l'échelle du réservoir, nous avons besoin d'équations constitutives pour mieux comprendre et modéliser le lien entre adsorption, gonflement et variations de perméabilité pour un Volume Élémentaire Représentatif d'une veine de charbon. Le premier modèle poromécanique est valide pour l'adsorption de surface seulement, alors que le second modèle est valide pour une matrice de charbon générique et potentiellement microporeuse. Pour les deux modèles, l'espace poreux du réservoir est considéré comme pouvant être divisé en les fractures macroporeuses et les pores de la matrice de charbon. Nous supposons que les molécules de fluide dans les fractures sont dans un état bulk et que les fractures gouvernent les propriétés de transport de la veine. Pour le modèle dédié à l'adsorption de surface, les molécules de fluide dans la matrice de charbon sont supposées être soit dans un état bulk à l'intérieur des pores de la matrice de charbon, soit adsorbées à la surface de ces pores ; le gonflement est dû à cette adsorption surfacique. Pour le modèle valide pour une matrice de charbon avec une distribution de taille de pore générique, aucune hypothèse n'est faite sur l'état des molécules de fluide dans la matrice de charbon, qui peuvent être dans un état bulk, adsorbées sur une surface, ou adsorbées dans un micropore. Puisque le domaine de validité de ce second modèle est plus étendu que celui du modèle dérivé pour une adsorption de surface, dans le reste de la thèse, nous n'utiliserons donc plus que le modèle à double porosité valide pour une matrice de charbon avec une distribution générique de tailles de pores.

Contents

2.1 Introduction 44
2.1.1 Models governing adsorption-induced strain 44
2.1.2 Coal permeability models 45
2.2 Dual-porosity model in absence of adsorption 47
2.3 Dual-porosity model considering surface adsorption 49
2.3.1 Physics of swelling induced by surface adsorption 49
2.3.2 Derivation of constitutive equations 51
2.4 Dual-porosity model considering generic adsorption 53
2.4.1 Derivation of constitutive equations 54
2.4.2 Simplification of the adsorption isotherm 58
2.5 Comparison of model for surface adsorption with the model for generic adsorption: meaning of a simplification of the adsorption isotherm 59
2.6 Concluding remarks 61

2.1 Introduction

As explained in Section 1.4, an injection of carbon dioxide into a reservoir initially full of methane results into a differential swelling of the coal matrix. Under the confined conditions that prevail underground, this differential swelling leads to a closure of the cleat system, which translates into a decrease of the permeability of the reservoir. The evolution of the injectivity of the reservoir during the process of injection is therefore the result of a coupling between a preferential adsorption of CO_2, the swelling of the coal matrix, and the pressure dependence of the cleat-driven permeability of the reservoir. As a prerequisite to reservoir simulations, one needs to derive the models which govern adsorption-induced deformation in coal.

2.1.1 Models governing adsorption-induced strain

Pan and Connell [2007] derived a model for coal swelling based on variations of interface energy. They estimated the variation of interface energy due to adsorption by integrating the Gibbs adsorption equation. Using a Langmuir model to relate the bulk pressure of fluid to the adsorbed amount, they related the strain of the solid to the variation of interface energy with the model of Scherer [1986] developed for the swelling of mesoporous glass and assumed valid for coal. Vandamme et al. [2010] also considered the adsorption-induced swelling of coal, by first interpreting it as being due to surface adsorption.

But coupling between adsorption and strain is not observed in coal only. Grosman and Ortega [2008b] developed a thermodynamic approach which relates adsorption to interface stress and to mechanical strain for mesoporous glass. There, they explain why the variation of the surface free energy depends on the deformation and on the elastic constants of the porous solid. Taking into account that the surface free energy of pores is directly related to the deformation of their inner walls and based on the fact that the fluid inside the pores interacts through the deformation of the pore walls, they propose a scenario for the filling and emptying of pores. Furthermore, Grosman and Ortega [2009] show experimentally the influence of the elastic deformation of porous solids on the adsorption process. They show that a stress external to the porous layer can modify the adsorbed amount.

Variations of interface energy can explain adsorption-induced strain in mesoporous solids such as porous silicon [Dolino et al., 1996], [Grosman and Ortega, 2008a], and mesoporous silica [Reichenauer and Scherer, 2000], [Grosman and Ortega, 2005], [Herman et al., 2006], [Gor and Neimark, 2010], [Gor and Neimark, 2011]. However, surface-based models need to be extended for microporous solids [Dolino et al., 1996], [Gunther et al., 2008], since in such solids with sub-nanometric pores, the very notion of surface breaks down. The coupling between adsorption and strain has been studied for microporous solids such as metal-organic frameworks [Coudert et al., 2008], [Neimark et al., 2010],[Neimark et al., 2011], microporous silica materials [Ravikovitch and Neimark, 2006], microporous carbons [Kowalczyk and Neimark, 2008], [Pijaudier-Cabot et al., 2011] or coal [Brochard et al., 2012b].

2.1.2 Coal permeability models

Based on field and laboratory experimental results, various coal permeability models have been proposed based on the fundamental principles of poroelasticity [Seidle and Huitt, 1995] [Palmer and Mansoori, 1996] [Shi and Durucan, 2004a] [Robertson and Christiansen, 2008]. In the literature, the poromechanical models have been introduced for limited cases (various boundary conditions). Permeability models were presented for some unrealistic coal structures as well as specific boundary conditions. For example, Reiss [1980] developed the equations for permeability and porosity based on a collection of matchsticks and a collection of slabs and cubes. Under the assumption of uniaxial strain, the influence of matrix shrinkage on the variations of coal permeability was first translated into a permeability model. Gilman and Beckie [2000] assumed that an individual fracture reacts as an elastic body upon a change in the normal stress component and proposed a simplified mathematical model of methane movement in a coal seam. Their model takes into account the following features: a relatively regular cleat system, adsorptive methane storage, an extremely slow release mechanism of methane from the coal matrix into cleats, and a significant change of permeability due to desorption. Seidle and Huitt [1995] performed modeling of the permeability increase due to matrix shrinkage just by considering a linear relationship between matrix shrinkage and pore pressure. Their model did not consider the impact of coal compressibility and thus was limited to specific conditions in which swelling or shrinkage stunts elastic changes in coal [Robertson and Christiansen, 2008]. Based on the matchstick geometry model and the relationship between permeability and porosity proposed by Seidle and Huitt [1995] and Shi and Durucan [2004a]. Shi and Durucan [2004b] proposed a pore-pressure dependent cleat permeability model for gas-desorbing linear elastic coal beds under uniaxial strain conditions. In this model, the prevailing effective horizontal stresses normal to the cleats govern the changes in the coal permeability of coal beds. Another theoretical model was proposed by Palmer and Mansoori [1996] (called P&M model later). Their permeability in coals is a function of effective stress and matrix shrinkage. The P&M model was improved and summarized by Palmer et al. [2007]. In the same way, Pekot and Reeves [2002] have developed another model with no geomechanical basis, but instead assumed that matrix strain was Langmuir function of the reservoir pressure. It was assumed that strain was proportional to the gas concentration curve and matrix shrinkage was proportional to the adsorbed gas concentration change multiplied by shrinkage compressibility. This model has been compared to the P&M model, and the conclusion was that the two models are essentially equivalent in saturated coals where the strain in function of pressure is proportional to the Langmuir isotherm [Palmer et al., 2007]. Following the above work, Cui and Bustin [2005] derived a stress-dependent permeability model by studying quantitatively the influences of reservoir pressure and adsorption-induced volumetric strain on coal seam permeability with constraints from the adsorption isotherm and related swelling. Gu and Chalaturnyk [2005a], Gu and Chalaturnyk [2005b], and Gu and Chalaturnyk [2006] developed a permeability model by considering the full separation of strain between coal matrix and cleat system. Recently, Gu and Chalaturnyk [2010] have established new porosity and permeability models used for reservoir and geomechanical coupled simulation in order to simulate the influence of permeability alterations in predicting or evaluating CBM production. Gu and Chalaturnyk [2010] modeled the fractured coal as an equivalent continuum elastic medium and took into account the anisotropy of

the permeability of the seam, by considering a matrix shrinkage/swelling due to gas desorption/adsorption and a thermal expansion due to temperature change and mechanical parameters. Pan and Connell [2007] developed a theoretical model for sorption-induced strain and applied it to single-component adsorption strain experimental data. Clarkson [2008] recently extended this theoretical model to calculate the sorption-strain component of the P&M model.

Robertson and Christiansen [2008] derived a coal permeability model for a fractured coal, under variable stress conditions. This model was derived for a cubic geometry rather than a matchstick geometry under biaxial or hydrostatic confining pressures. It was also designed to handle changes in permeability caused by adsorption and desorption of gasses from the coal matrix. In contrast with previous models developed for field conditions, their model mainly deals with variable stress conditions which are commonly used during measurement of permeability in the laboratory. Two similar models were presented analytically by Connell et al. [2010] for standard triaxial strain and stress conditions. They established a novel approach to distinguish the sorption strains of the coal matrix and the cleats. Zhang et al. [2008] proposed a general porosity and permeability model based on the theory of poroelasticity. While interpreting laboratory experimental results, a matchstick or cubic coal model is typically considered with the matrix blocks completely separated from each other. In such a model, the permeability should not change under conditions of constant confining pressure [Liu et al., 2011a] [Liu and Rutqvist, 2009]. This phenomenon is not consistent with laboratory observations [Harpalani and Chen, 1997], Pan et al. [2010], which display reduction in permeability with the injection of carbon dioxide. Liu and Rutqvist [2009] assumed that coal matrix blocks were connected to each other by coal matrix bridges and they developed a new permeability model based on the concept of internal swelling stress in order to explicitly consider cleat-matrix interaction during coal deformation processes. Another alternative option has been proposed by Liu et al. [2010], Liu et al. [2011a] on this issue. They considered that the above phenomena may be due to the ignorance of the internal actions between coal fractures and matrix. Izadi et al. [2011] considered coal as a collection of unconnected cleat system in an elastic swelling medium. The cleats are isolated from each other and swelling results in a reduction in cleat aperture. Ma et al. [2011] proposed a model based on the volumetric balance between the bulk coal and the pores, by applying the constant volume theory of Massarotto et al. [2009]. It demonstrates primarily the changes in cleat volumes and is therefore different from other models that put heavy emphasis on the pore volume/-cleat compressibility. Liu et al. [2011b] have recently applied a coupling approach for free swelling of an unconstrained homogeneous medium, with which free swelling scales with gas pressure, porosity must increase as pressure increases, and hence permeability must increase with swelling.

As reviewed above, a large variety of coal models have been developed and applied for a variety of boundary conditions. All these models were derived from the theory of poroelasticity or from more empirical continuum approaches. But for all those models the adsorption-induced swelling of the coal matrix is considered as an empirical input. In contrast, we aim at deriving models with a thermodynamical basis for this swelling. In this chapter, two dual-porosity models are proposed for the behavior of a representative elementary volume of coal bed reservoir. Both approaches are based on the Biot-Coussy poromechanical framework [Coussy, 2004] and two porous networks are explicitly taken

into account: the cleats of the reservoir and the pores of the coal matrix. The resulting constitutive equations require directly as an input the adsorption isotherm of the fluid considered on coal. The first model uses poromechanical equations that have been extended recently to the effect of surface adsorption [Coussy, 2010] [Vandamme et al., 2010]. In the second approach, constitutive equations are derived for a generic porous medium, and in particular for a microporous one such as coal, in which adsorption occurs by pore filling more than by surface covering. Before aiming at capturing the effect of adsorption, we derive in the next section the classical constitutive equations of a dual-porosity medium.

2.2 Dual-porosity model in absence of adsorption

In this section, a dual-porosity poromechanical model for the coal bed reservoir is derived, in which no effect of adsorption is considered. The reservoir is made of two types of pores: the pores of the coal matrix and the cleat system. Fig. 2.1 displays the three scales considered. Fig. 2.1b shows a representative elementary volume (REV) of the coal bed reservoir, which is made of coal fractured by cleats. Neglecting the effect of adsorption in the coal matrix is equivalent to considering that all fluid molecules in the coal matrix are in their bulk state (see Fig. 2.1c).

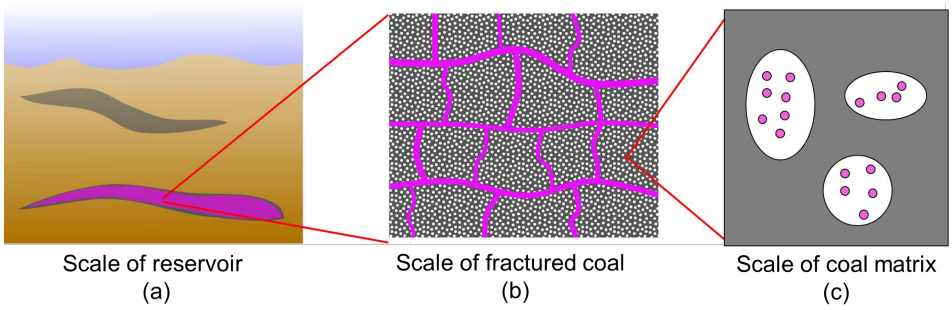

Figure 2.1 – Different scales considered for a coal bed reservoir in absence of any adsorption.

The general assumptions for our modeling are: (i) The coal bed reservoir is homogeneous and isotropic; (ii) Only isothermal conditions are considered; (iii) Only the pure component case (i.e., carbon dioxide only, or methane only) is considered. The pressure p_c of the fluid in the cleats can differ from the pressure p_m of the fluid in the pores of the coal matrix.

We consider a Representative Elementary Volume (REV) of reservoir (see Fig. 2.1) and note f_{skel} the Helmholtz free energy stored in its solid skeleton per unit volume of undeformed medium. If no adsorption occurs in the reservoir, the reservoir is a classical dual-porosity medium. For such a system, the energy balance for the solid skeleton is Coussy [2004]:

$$df_{skel} = \sigma d\epsilon + s_{ij} de_{ij} + p_c d\phi_c + p_m d\phi_m \tag{2.1}$$

where σ is the volumetric confining stress, ϵ is the volumetric strain, s_{ij} are the deviatoric confining stresses, e_{ij} are the deviatoric strains, ϕ_c is the Lagrangian porosity associated to the cleats (i.e., the volume of the cleats divided by the volume of the undeformed REV), and ϕ_m is the Lagrangian coal matrix porosity (i.e., the volume of the pores of coal matrix divided by the volume of the undeformed REV).

For a non-linear dual-porosity medium, making use of Maxwell's symmetry relations Eq. (2.1) yields [Coussy, 2004]:

$$d\sigma = Kd\epsilon - b_c dp_c - b_m dp_m \tag{2.2}$$

$$d\phi_c = b_c d\epsilon + \frac{dp_c}{N_c} + \frac{(dp_c - dp_m)}{N_{cm}} \tag{2.3}$$

$$d\phi_m = b_m d\epsilon + \frac{dp_m}{N_m} + \frac{(dp_m - dp_c)}{N_{cm}} \tag{2.4}$$

$$ds_{ij} = 2Gde_{ij} \tag{2.5}$$

where the bulk modulus K, the shear modulus G, the Biot coefficients b_c, b_m, and Biot moduli N_c, N_m, and N_{cm} of the reservoir may all depend on the confining stress σ and on the pressures p_c and p_m of the fluid in the cleats and in the coal matrix, respectively.

If we apply $p_c = p_m$, we must retrieve the classical constitutive equations of a porous medium with a single porosity. Assuming that the solid phase is a homogenous isotropic linear material, its bulk modulus K_s is constant. Classical poromechanical relations exist, which link the different poroelastic parameters [Coussy, 2004]:

$$b_c + b_m = 1 - \frac{K}{K_s} \tag{2.6}$$

$$\frac{1}{N_c} = \frac{(b_c - \phi_c)}{K_s} \tag{2.7}$$

$$\frac{1}{N_m} = \frac{(b_m - \phi_m)}{K_s} \tag{2.8}$$

In contrast, if we apply a pressure p_c in the cleats while keeping a zero pressure $p_m = 0$ in the coal matrix pores, the reservoir must behave like a single-porosity medium for which the porosity reduces to the cleat porosity only. In that case, we must again retrieve the classical constitutive equations of a porous medium with a single porosity. But, for such a medium, the solid phase is now the coal matrix itself, whose bulk modulus is noted K_m. The classical poromechanical relations which link the different poroelastic parameters [Coussy, 2004] now are:

$$b_c = 1 - \frac{K}{K_m} \tag{2.9}$$

$$\frac{1}{N_c} + \frac{1}{N_{cm}} = \frac{(b_c - \phi_c)}{K_m} \tag{2.10}$$

In the above equations, the different bulk moduli introduced (K_s for the solid skeleton, K_m for the coal matrix, and K for the reservoir) characterize the reservoir at different

scales and must verify the condition $K_s \geqslant K_m \geqslant K$.

2.3 Dual-porosity model considering surface adsorption

In this section, a dual-porosity poromechanical model for the coal bed reservoir is derived by now taking into account the effect of surface adsorption in the coal matrix. The different scales here considered for the reservoir are identical to the ones considered in Sec. 2.2, but fluid molecules can now be adsorbed on the surface of the pores of the coal matrix (Fig. 2.2c).

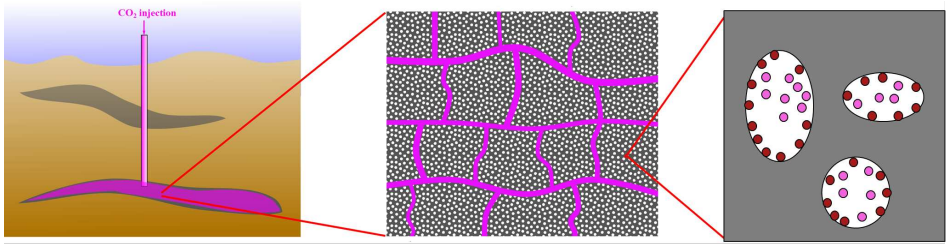

Figure 2.2 – Different scales considered for a coal bed reservoir considering surface adsorption.

Given the very low specific surface of cleats with regard to that of the microporous coal matrix, adsorption at the surface of the cleats is considered to be negligible. Therefore, fluid molecules can be found either in a bulk state in the cleats, or in a bulk state in the pores of the coal matrix, or in an adsorbed state at the surface of the pores of the coal matrix (see Fig. 2.2). As a prerequisite to the derivation of relevant constitutive equations, we explain in the next section how surface adsorption can lead to a swelling.

2.3.1 Physics of swelling induced by surface adsorption

As was shown early on by De Laplace [1806] and Young [1805], creating surfaces requires providing energy to the system. For this reason, the energy of a film of soap is an increasing function of its area. Therefore, if one wants to increase the area of this film, he will need to provide energy by working against the so-called surface stress σ^s, which, for an interface between two liquids, is equal to its surface tension. By mechanical analogy, a soap bubble behaves like a stretched membrane.

In coal, the surface of the coal matrix pores is an interface between a solid (the solid skeleton) and a fluid (e.g., carbon dioxide or methane). For the same reasons, the surface of the pores behaves like a stretched membrane. Adsorption of fluid at the surface of the pore modifies how this membrane is stretched, thus leading to a deformation of the coal sample.

Energy can be provided to the surface of the pores either by straining this surface (and working against the surface stress) or by adding fluid molecules on the surface. The

energy balance for the surface of the pores is therefore:

$$df_{surf} = \sigma^s ds_m + \mu_m dn_m^a \tag{2.11}$$

where f_{surf} is the Helmholtz free energy of the pore surface per unit volume of undeformed porous medium, σ^s is the surface stress, s_m is the surface of the coal matrix pores per unit volume of undeformed porous medium, μ_m is the molar chemical potential of the fluid in the coal matrix, and n_m^a is the molar density of fluid molecules adsorbed at the surface of the pores (in excess of the bulk density) per unit volume of undeformed porous medium. Gibbs showed that adsorption, an accumulation of molecules of fluid on an interface, can modify the surface tension γ, which, for a fluid-fluid interface, is equal to the surface stress σ^s. More precisely, the celebrated Gibbs adsorption law [Gibbs, 1928] shows that adsorption leads to a decrease of surface tension:

$$d\gamma = -\Gamma d\mu \tag{2.12}$$

where μ is the molar chemical potential of the adsorbed molecules of fluid, and where Γ is the molar amount of adsorbed molecules of fluid in excess of the bulk density per unit area of interface.

The pore surface is an interface between a solid and a liquid. For such an interface, the dependence of the surface stress on adsorption is more complex and is given by Shuttleworth equation [Shuttleworth, 1950]:

$$\sigma^s = \gamma + \left.\frac{\partial \gamma}{\partial \epsilon_T}\right|_{\mu} \tag{2.13}$$

where ϵ_T is the surface strain of the interface. Combined with Gibbs adsorption law (2.12), Shuttleworth equation yields how the surface stress evolves with adsorption:

$$\left.\frac{\partial \sigma^s}{\partial \mu}\right|_{\epsilon_T} = -\Gamma - \left.\frac{\partial \Gamma}{\partial \epsilon_T}\right|_{\mu} \tag{2.14}$$

If the adsorption does not depend on the strain of the surface, Gibbs law (2.12), which was initially derived for an interface between two fluids, remains valid and reads in an integrated form:

$$\Delta\sigma^s = -\int_{\mu=-\infty}^{\mu} \Gamma(\mu) d\mu = -\int_{p=0}^{p} \Gamma(p) \overline{V}_b(p) dp \tag{2.15}$$

where p and $\overline{V}_b(p)$ are the bulk pressure and the bulk molar volume of the fluid, respectively.

2.3.2 Derivation of constitutive equations

We consider a representative elementary volume (REV) of the reservoir and denote f its Helmholtz free energy per unit volume of undeformed porous medium. The pressure p_c of the fluid in the cleats can differ from the pressure p_m of the fluid in the pores of the coal matrix. Energy can be provided to the REV of the reservoir by straining it, by adding molecules of fluid in the cleats, or by adding molecules of fluid in the coal matrix:

$$df = \sigma d\epsilon + s_{ij} de_{ij} + \mu_c dn_c + \mu_m dn_m \tag{2.16}$$

where μ_c is the molar chemical potential of the molecules of fluid in the cleats, n_c is the molar density of the molecules of fluid in the cleats per unit volume of undeformed porous medium, μ_m is the molar chemical potential of the molecules of fluid in the coal matrix, and n_m is the molar density of fluid molecules in the coal matrix per unit volume of undeformed porous medium.

In the pores of the coal matrix, the molecules of fluid can either be in their bulk state inside the pore (with a molar density n_m^b per unit volume of undeformed medium) or adsorbed at the surface of the coal matrix pore (with a molar density n_m^a per unit volume of undeformed medium), so that: $n_m = n_m^b + n_m^a$. In contrast, in the cleats, all molecules of fluid are in a bulk state. We now introduce the Helmholtz free energy f_l of the fluid that is in a bulk state in the medium per unit volume of undeformed porous medium. This energy is equal to the sum of the Helmholtz free energy of the fluid in the cleats with the Helmholtz free energy of the fluid in a bulk state in the coal matrix. By definition of the Helmholtz free energy with respect to the Gibbs free energy, we obtain:

$$f_l = n_c \mu_c - p_c \phi_c + n_m^b \mu_m - p_m \phi_m \tag{2.17}$$

Combining Eq. (2.16) with Eq. (2.17) and using the Gibbs-Duhem relations $n_c d\mu_c - \phi_c dp_c = 0$ and $n_m^b d\mu_m - \phi_m dp_m = 0$, we obtain the energy balance for the system made of the reservoir without its bulk fluids [Coussy, 2010] [Vandamme et al., 2010]:

$$d(f - f_l) = \sigma d\epsilon + s_{ij} de_{ij} + p_c d\phi_c + p_m d\phi_m + \mu_m dn_m^a \tag{2.18}$$

Identifying that the reservoir without its bulk fluids is in fact made of the solid skeleton and of the surface of the pores, we find that: $f - f_l = f_{skel} + f_{surf}$, where f_{skel} is the Helmholtz free energy stored in the solid skeleton per unit volume of undeformed porous medium. Combining Eq. (2.18) with Eq. (2.11) eventually yields the energy balance for the solid skeleton [Coussy, 2010] [Vandamme et al., 2010]:

$$df_{skel} = \sigma d\epsilon + s_{ij} de_{ij} + p_c d\phi_c + p_m d\phi_m - \sigma^s ds_m \tag{2.19}$$

For an isotropic medium under small deformations, for reasons of symmetry, the surface s_m of the pores of the coal matrix can not depend on the deviatoric strains. Moreover, this surface s_m must only depend on the variables that define the state of the coal matrix, i.e., the porosity ϕ_m and the volumetric strain ϵ_m of the coal matrix: $s_m = s_m(\epsilon_m, \phi_m)$.

A macroscopic strain being the space average of its microscopic counterparts [Coussy, 2010], we have:

$$\epsilon = (1 - \phi_{c0})\epsilon_m + \phi_c - \phi_{c0} \tag{2.20}$$

where ϕ_{c0} is the porosity associated to the cleat system in the state of reference, from what follows: $s_m = s_m(\epsilon - \phi_c, \phi_m)$. Therefore the variation ds_m of surface of the pores of the coal matrix is given by:

$$ds_m = c_{\phi_c} d\epsilon - c_{\phi_c} d\phi_c + c_{\phi_m} d\phi_m \tag{2.21}$$

where c_{ϕ_c} and c_{ϕ_m} are, in first order, constant material parameters equal to:

$$c_{\phi_c} = \left.\frac{\partial s_m}{\partial(\epsilon - \phi_c)}\right|_{\phi_m} \tag{2.22}$$

$$c_{\phi_m} = \left.\frac{\partial s_m}{\partial \phi_m}\right|_{\epsilon - \phi_c} \tag{2.23}$$

The energy balance (2.19) can therefore be rewritten as:

$$df_{skel} = (\sigma + p_c^a)\, d\epsilon + s_{ij} de_{ij} + (p_c - p_c^a) d\phi_c + (p_m - p_c^a) d\phi_m \tag{2.24}$$

where $p_c^a = c_{\phi_c}\sigma^s = \left.\frac{\partial s_m}{\partial(\epsilon-\phi_c)}\right|_{\phi_m} \sigma^s$ and $p_m^a = c_{\phi_m}\sigma^s = \left.\frac{\partial s_m}{\partial \phi_m}\right|_{\epsilon-\phi_c} \sigma^s$. Comparing the two energy balances (2.24) and (2.1), one infers that the constitutive equations for a reservoir in which surface adsorption occurs can readily be derived from the constitutive equations (2.2-2.5) for a reservoir in which no adsorption occurs, by replacing in the latter σ with $\sigma + p_c^a$, p_c with $p_c - p_c^a$, and p_m with $p_m - p_m^a$:

$$d\sigma = K d\epsilon - b_c dp_c - b_m dp_m - (1 - b_c) dp_c^a + b_m dp_m^a \tag{2.25}$$

$$d\phi_c = b_c d\epsilon + \frac{(dp_c - dp_c^a)}{N_c} + \frac{(dp_c - dp_c^a) - (dp_m - dp_m^a)}{N_{cm}} \tag{2.26}$$

$$d\phi_m = b_m d\epsilon + \frac{(dp_m - dp_m^a)}{N_m} + \frac{(dp_m - dp_m^a) - (dp_c - dp_c^a)}{N_{cm}} \tag{2.27}$$

$$ds_{ij} = 2G de_{ij} \tag{2.28}$$

If we now assume that the characteristic time of transfer of fluid between the cleat system and the coal matrix porosity is much smaller than any other characteristic time of fluid transport in the reservoir, at any location in the reservoir the chemical potential of the fluid in the cleats is equal to the chemical potential of the fluid in the coal matrix pores. Under such an assumption, imposing an identical pressure of the fluid in the cleats and in the coal matrix pores (i.e., $p_c = p_m = p$), and noting $b_c + b_m = b$, we obtain another

version of the constitutive equations for our dual porosity reservoir:

$$d\sigma = Kd\epsilon - bdp + b_c dp_c^a + b_m dp_m^a - dp_c^a \tag{2.29}$$

$$d\phi_c = b_c d\epsilon + \frac{(dp - dp_c^a)}{N_c} - \frac{(dp_c^a - dp_m^a)}{N_{cm}} \tag{2.30}$$

$$d\phi_m = b_m d\epsilon + \frac{(dp - dp_m^a)}{N_m} - \frac{(dp_m^a - dp_c^a)}{N_{cm}} \tag{2.31}$$

$$ds_{ij} = 2Gde_{ij} \tag{2.32}$$

where the poroelastic parameters of the reservoir may depend on the confining stress σ and on the pressure p of the fluid, and where the micromechanical relations (2.6-2.8) and (2.9-2.10) still hold. Therefore, surface adsorption modifies the poromechanical behavior of the reservoir through the introduction of a pre-pore pressure p_c^a which acts in the cleat system and of a pre-pore pressure p_m^a which acts in the pores of the coal matrix. How adsorption modifies the surface stress σ^s is governed by Eq. (2.12). In a final simplification, if we consider that the poromechanical behavior of the medium is linear, the poroelastic coefficients depend no more on stresses or pressure, and the above equations can be integrated as:

$$\sigma = K\epsilon - bp + b_c p_c^a + b_m p_m^a - p_c^a \tag{2.33}$$

$$\varphi_c = b_c \epsilon + \frac{p - p_c^a}{N_c} - \frac{p_c^a - p_m^a}{N_{cm}} \tag{2.34}$$

$$\varphi_m = b_m \epsilon + \frac{p - p_m^a}{N_m} - \frac{p_m^a - p_c^a}{N_{cm}} \tag{2.35}$$

$$s_{ij} = 2Ge_{ij} \tag{2.36}$$

where $p_c^a = c_{\phi_c}\sigma^s = \frac{\partial s_m}{\partial(\epsilon-\phi_c)}\Big|_{\phi_m} \sigma^s$ and $p_m^a = c_{\phi_m}\sigma^s = \frac{\partial s_m}{\partial \phi_m}\Big|_{\epsilon-\phi_c} \sigma^s$, the coefficients c_{ϕ_c} and c_{ϕ_m} being constant material parameters.

2.4 Dual-porosity model considering generic adsorption

The coal matrix being microporous, the applicability of the equations derived in the previous section is questionable: indeed, in micropores adsorption occurs by pore filling more than by surface covering, and defining pore surface or pore volume in an unambiguous manner is not possible (see Fig. 2.3c). In contrast to what was done in the previous section, we here aim at deriving constitutive equations that are valid for a generic coal matrix, and in particular for such a microporous coal matrix. We still consider the different scales introduced in Fig. 2.1.

Fluid molecules in the reservoir are located either in the cleats or in the coal matrix. Molecules in the cleats are assumed to be in a bulk state. In contrast, molecules in the microporous coal matrix can be in a bulk state as well as in an adsorbed state, since in such micropores, fluid molecules are in intermolecular interaction with the atoms of the solid skeleton. For such microporous media, conventional poromechanics breaks down

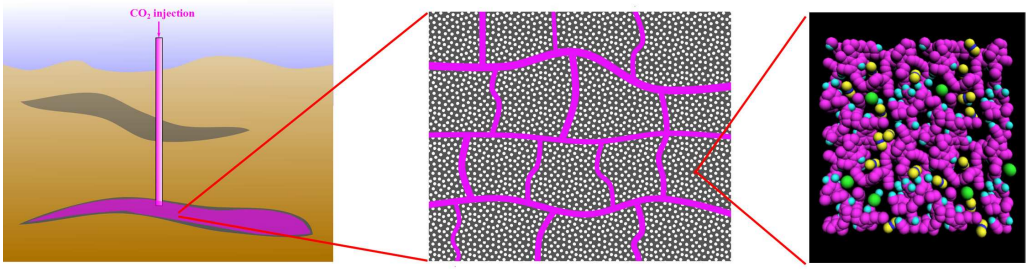

Figure 2.3 – Schematic multi-scale model for a coal bed reservoir with a microporous matrix.

[Brochard et al., 2012b]. The next section is devoted to the derivation of constitutive equations for a dual-porosity model for a reservoir made of a coal matrix with a generic (and potentially microporous) pore system.

2.4.1 Derivation of constitutive equations

We consider the system made of the coal matrix only, i.e., the reservoir without the fluid in the cleats. The Helmholtz free energy of such a system per unit undeformed volume of reservoir is noted f. The pressure p_c (or the molar chemical potential μ_c) of the fluid in the cleats and the thermodynamic pressure p_m (or the molar chemical potential μ_m) of the fluid in the coal matrix can differ from each other. Energy can be added to such a system either by straining it with a volumetric confining stress σ (the corresponding work being '$\sigma d\epsilon$', where ϵ is the volumetric strain), by straining it with a deviatoric confining stress s_{ij} (the corresponding work being '$s_{ij}de_{ij}$', where e_{ij} is a deviatoric stain), by deforming the cleat porosity ϕ_c with the pressure of the fluid in the cleats (the corresponding work being '$p_c d\varphi_c$', where φ_c is the variation of the Lagrangian porosity associated to the cleats), or by adding fluid molecules in the coal matrix (the added energy being '$\mu_m dn_m$', where n_m is the number of moles of fluid in the coal matrix per unit undeformed volume of reservoir):

$$df = \sigma d\epsilon + s_{ij}de_{ij} + p_c d\varphi_c + \mu_m dn_m \tag{2.37}$$

The above equation can be rewritten as follows:

$$d(f - \mu_m n_m) = \sigma d\epsilon + s_{ij}de_{ij} + p_c d\varphi_c - n_m d\mu_m \tag{2.38}$$

From the above equation one concludes that the constitutive equations can be four equations which link σ, s_{ij}, p_c, n_m to ϵ, e_{ij}, φ_c, μ_m.

We first consider the constitutive equation that governs the deviatoric stresses s_{ij}. For symmetry reasons, under the hypotheses of isotropy and of small deformations, this

constitutive equation remains the same as in regular poroelasticity:

$$s_{ij}(\epsilon, e_{ij}, \varphi_c, \mu_m) = 2Ge_{ij} \tag{2.39}$$

where G is the shear modulus of the reservoir.

We now consider the constitutive equation that governs the amount n_m of fluid in the coal matrix per unit undeformed volume of reservoir. Previous studies have shown that the amount n^{ads} of fluids in the coal matrix per unit volume of undeformed coal matrix depends on the pressure p_m of the fluids in the coal matrix and on the strain ϵ_m of the coal matrix [Brochard et al., 2012b]. Experimental data or molecular simulations of adsorption on a microporous coal can provide this amount $n^{ads}(\epsilon_m, p_m)$ or $n^{ads}(\epsilon_m, \mu_m)$ of fluid in the coal matrix [Brochard et al., 2012b]. The amount n_m of fluid per unit volume of undeformed porous media (i.e., of fractured coal) can be obtained geometrically from the adsorption isotherm n^{ads} that is defined at the scale of the coal matrix (see Figs. 2.3b and 2.3c):

$$n_m(\epsilon, e_{ij}, \varphi_c, \mu_m) = (1 - \phi_{c0})n^{ads}(\epsilon_m, p_m) \tag{2.40}$$

where ϕ_{c0} is the cleat porosity in the state of reference, $p_m(\mu_m)$ is obtained from the state equation of the fluid considered, and the volumetric strain ϵ_m of the coal matrix is obtained from the classical micro-macro relation [Coussy, 2010]:

$$\epsilon = (1 - \phi_{c0})\epsilon_m + \varphi_c \tag{2.41}$$

$$\epsilon_m = \frac{\epsilon - \varphi_c}{1 - \phi_{c0}} \tag{2.42}$$

The next constitutive equation is derived by using a Maxwell relation based on Eq. (2.38):

$$\left.\frac{\partial \sigma}{\partial \mu_m}\right|_{\epsilon, e_{ij}, \varphi_c} = -\left.\frac{\partial n_m}{\partial \epsilon}\right|_{\mu_m, e_{ij}, \varphi_c} \tag{2.43}$$

for which the right-hand term can be rewritten with the help of Eqs. (2.40) and (2.42):

$$\left.\frac{\partial n_m}{\partial \epsilon}\right|_{\mu_m, e_{ij}, \varphi_c} = \frac{1}{1 - \phi_{c0}} \left.\frac{\partial n_m}{\partial \epsilon_m}\right|_{\mu_m, e_{ij}, \varphi_c} = \left.\frac{\partial n^{ads}}{\partial \epsilon_m}\right|_{\mu_m} \tag{2.44}$$

Equation (2.43) can be rewritten as follows:

$$\left.\frac{\partial \sigma}{\partial \mu_m}\right|_{\epsilon, e_{ij}, \varphi_c} = -\left.\frac{\partial n^{ads}}{\partial \epsilon_m}\right|_{\mu_m} \tag{2.45}$$

An integration of the above equation yields:

$$\sigma = f_1(\epsilon, e_{ij}, \varphi_c) - \int_{\mu=-\infty}^{\mu_m} \left.\frac{\partial n^{ads}}{\partial \epsilon_m}\right|_{\mu_m} d\mu \tag{2.46}$$

which, with the help of the Gibbs-Duhem relation $d\mu = \overline{V}_b dp$ (where $\overline{V}_b$ is the bulk molar volume of the fluid), can be rewritten as:

$$\sigma = f_1(\epsilon, e_{ij}, \varphi_c) - \int_{0}^{p_m} \left.\frac{\partial n^{ads}}{\partial \epsilon_m}\right|_{p_m} \overline{V}_b dp \tag{2.47}$$

The function f_1 is determined by soliciting the material at $p_m = 0$ in the coal matrix (i.e., with no fluid in the coal matrix). In such a case, for which $\sigma = f_1(\epsilon, e_{ij}, \varphi_c)$, regular poroelasticity must be recovered, from what follows that:

$$f_1(\epsilon, e_{ij}, \varphi_c) = (K + b^2 N)\epsilon - bN\varphi_c \tag{2.48}$$

where K is the bulk modulus of the reservoir, b is the Biot coefficient associated to the cleat system, N is the Biot modulus associated to the cleat system, and where the poroelastic coefficients verify the classical relations [Coussy, 2004]:

$$b = 1 - \frac{K}{K_m} \tag{2.49}$$

$$\frac{1}{N} = \frac{b - \phi_{c0}}{K_m} \tag{2.50}$$

where K_m is the bulk modulus of the coal matrix. The third constitutive equation can therefore be written as:

$$\sigma(\epsilon, e_{ij}, \varphi_c, \mu_m) = (K + b^2 N)\epsilon - bN\varphi_c - \int_{0}^{p_m} \left.\frac{\partial n^{ads}}{\partial \epsilon_m}\right|_{p_m} \overline{V_b} dp \tag{2.51}$$

The last constitutive equation is derived by using a Maxwell relation based on Eq. (2.38):

$$\left.\frac{\partial p_c}{\partial \mu_m}\right|_{\epsilon, e_{ij}, \varphi_c} = -\left.\frac{\partial n_m}{\partial \varphi_c}\right|_{\epsilon, e_{ij}, \mu_m} \tag{2.52}$$

for which the right-hand term can be rewritten with the help of Eqs. (2.40), (2.41) and (2.42):

$$\left.\frac{\partial n_m}{\partial \varphi_c}\right|_{\epsilon, e_{ij}, \mu_m} = -\frac{1}{1 - \phi_{c0}} \left.\frac{\partial n_m}{\partial \epsilon_m}\right|_{\epsilon, e_{ij}, \mu_m} = -\left.\frac{\partial n^{ads}}{\partial \epsilon_m}\right|_{\mu_m} \tag{2.53}$$

Equation (2.52) can be rewritten as follows:

$$\left.\frac{\partial p_c}{\partial \mu_m}\right|_{\epsilon, e_{ij}, \varphi_c} = \left.\frac{\partial n^{ads}}{\partial \epsilon_m}\right|_{\mu_m} \tag{2.54}$$

An integration of the above equation yields:

$$p_c = f_2(\epsilon, e_{ij}, \varphi_c) + \int_{\mu=-\infty}^{\mu_m} \left.\frac{\partial n^{ads}}{\partial \epsilon_m}\right|_{\mu_m} d\mu \tag{2.55}$$

which, with the help of the Gibbs-Duhem relation $d\mu = \overline{V}_b dp$, can be rewritten as:

$$p_c = f_2(\epsilon, e_{ij}, \varphi_c) + \int_{0}^{p_m} \left.\frac{\partial n^{ads}}{\partial \epsilon_m}\right|_{p_m} \overline{V}_b dp \tag{2.56}$$

The function f_2 is determined by soliciting the material at $p_m = 0$ in the coal matrix (i.e., with no fluid in the coal matrix). In such a case, for which $p_c = f_2(\epsilon, e_{ij}, \varphi_c)$, regular poroelasticity must be recovered, from what follows that:

$$f_2(\epsilon, e_{ij}, \varphi_c) = -Nb\epsilon + N\varphi_c \tag{2.57}$$

The last constitutive equation can therefore be written as:

$$p_c(\epsilon, e_{ij}, \varphi_c, \mu_m) = -Nb\epsilon + N\varphi_c + \int_{0}^{p_m} \left.\frac{\partial n^{ads}}{\partial \epsilon_m}\right|_{p_m} \overline{V}_b dp \tag{2.58}$$

In summary, the constitutive equations for a dual-porosity medium whose pore space is made of cleats (in which the pressure of the fluid is p_c) and of micropores (in which the thermodynamic pressure of the fluid is p_m) is:

$$\begin{aligned}
\sigma &= (K + b^2 N)\epsilon - bN\varphi_c - p^a(\epsilon_m, p_m) && (2.59)\\
p_c &= -Nb\epsilon + N\varphi_c + p^a(\epsilon_m, p_m) && (2.60)\\
n_m &= (1 - \phi_{c0}) n^{ads}(\epsilon_m, p_m) && (2.61)\\
s_{ij} &= 2Ge_{ij} && (2.62)
\end{aligned}$$

where the pressure $p^a(\epsilon_m, p_m)$ induced by adsorption in the coal matrix is written as:

$$p^a(\epsilon_m, p_m) = \int_{0}^{p_m} \left.\frac{\partial n^{ads}}{\partial \epsilon_m}\right|_{p_m} \overline{V}_b dp \tag{2.63}$$

Note that in the above equation, the integrand can be interpreted as a tangent Biot

coefficient b_m^{tan} associated to the coal matrix:

$$b_m^{tan} = \left.\frac{\partial n^{ads}}{\partial \epsilon_m}\right|_{p_m} \overline{V}_b \tag{2.64}$$

If we now set $p_m = p_c = p$, which corresponds to the assumption that the fluid in the cleats is in thermodynamic equilibrium with the fluid in the coal matrix, we obtain the following constitutive equations:

$$\begin{aligned}
\sigma &= (K + b^2 N)\epsilon - bN\varphi_c - p^a(\epsilon_m, p) && (2.65)\\
p &= -Nb\epsilon + N\varphi_c + p^a(\epsilon_m, p) && (2.66)\\
n_m &= (1 - \phi_{c0}) n^{ads}(\epsilon_m, p) && (2.67)\\
s_{ij} &= 2Ge_{ij} && (2.68)
\end{aligned}$$

In order to derive those equations, no assumption was made on the state of the fluid molecules (bulk or adsorbed) in the coal matrix. Those equations are expected to apply for a coal matrix with a generic pore system.

2.4.2 Simplification of the adsorption isotherm

Brochard et al. [2012b] demonstrated recently with the help of molecular simulations that the adsorption isotherm of methane in coal can be well approximated by its first-order expansion with respect to the strain ϵ_m of the coal matrix:

$$n^{ads}(\epsilon_m, p) \approx n_0^{ads}(p)(1 + C(p)\epsilon_m) \tag{2.69}$$

where $n_0^{ads}(p)$ is the amount of fluid adsorbed in the coal matrix when the matrix is kept at zero deformation, and where $C(p)$ is a dimensionless coupling coefficient which captures the dependence of adsorption on the strain of the adsorbing medium. Assuming that this approximation holds for the adsorption isotherm of any pure fluid on coal, from such a first-order expansion follows:

$$\begin{aligned}
\left.\frac{\partial n^{ads}}{\partial \epsilon_m}\right|_p &= n_0^{ads}(p)C(p) && (2.70)\\
b_m^{tan} &= n_0^{ads}(p)C(p)\overline{V}_b(p) && (2.71)
\end{aligned}$$

The above equation is a function of the fluid thermodynamic pressure p only. Therefore, in coal, the adsorption-induced pressure p^a and the tangent Biot coefficient b_m^{tan} associated to the coal matrix also are functions of the fluid thermodynamic pressure only: $p^a(\epsilon_m, p) = p^a(p)$ and $b_m^{tan}(\epsilon_m, p) = b_m^{tan}(p)$. With such a simplification, Eq. (2.67) can be rewritten

as:

$$n_m = n_0^{ads}(p)\left[1-\phi_{c0}+C(p)(\epsilon-\varphi_c)\right] = \frac{1}{\overline{V}_b}(1-\phi_{c0})\left(\phi_m^{eq}(p)+b_m^{tan}(p)\epsilon_m\right) \quad (2.72)$$

where $\phi_m^{eq} = n_0^{ads}\overline{V}_b$ is the volume (per unit of undeformed coal matrix) that the adsorbed molecules would occupy if they were in a bulk state. Eq. (2.72) makes it possible to modify the set of constitutive equations (2.65)-(2.68) in order to express σ, φ_c, n_m and s_{ij} as functions of ϵ, e_{ij} and p, thus yielding the constitutive equations of the coal bed reservoir here considered:

$$\begin{aligned}
\sigma &= K\epsilon - bp - (1-b)p^a && (2.73)\\
\varphi_c &= b\epsilon + \frac{p-p^a}{N} && (2.74)\\
n_m &= n_0^{ads}(p)\left[1-\phi_{c0}+C(p)\left[(1-b)\epsilon - \frac{p-p^a}{N}\right]\right] && (2.75)\\
s_{ij} &= 2Ge_{ij} && (2.76)
\end{aligned}$$

where p^a is given by:

$$p^a(p) = \int_0^p b_m^{tan}(p)dp = \int_0^p n_0^{ads}(p)C(p)\overline{V}_b(p)dp \quad (2.77)$$

2.5 Comparison of model for surface adsorption with the model for generic adsorption: meaning of a simplification of the adsorption isotherm

In Secs. 2.3.2 and 2.4.1, we derived two poromechanical models for coal bed reservoirs. In the first model (Sec. 2.3), the coal matrix was considered as a porous medium in which only surface adsorption takes place, while in the second model (Sec. 2.4) a generic (and potentially microporous) coal matrix was considered. Since the model in Sec. 2.4.1 was derived for a generic medium, its range of validity is obviously wider than that of the model derived in Sec. 2.3.2. In Sec. 2.4.2, for the case of a generic porous medium, we simplified the constitutive equations by considering that the amount n^{ads} of fluid in the coal matrix was well captured by a first-order expansion with respect to the volumetric strain ϵ_m of the coal matrix (see Eq. 2.69). In this section, we aim at determining what the meaning of this simplification is, if we consider that all adsorption occurring in the coal matrix occurs by surface covering only.

Let us consider such a porous medium in which adsorption would occur only by surface covering. For the sake of simplicity, we consider that there is no cleat in the medium. We introduce a Lagrangian adsorbed amount Γ^L of fluid, defined as the molar amount of adsorbed molecules in the bulk density per unit area of the surface of the pores in the reference state. This Lagrangian adsorbed amount Γ^L differs from the (Eulerian) adsorbed

amount Γ defined earlier in Sec. 2.3.1, in the sense that this latter is defined per unit area of the surface of the pores in the actual deformed state. By definition of the surface strain ϵ_T of the surface of the pores, both adsorbed amounts are linked for small strains by:

$$\Gamma^L = \Gamma(1+\epsilon_T) \tag{2.78}$$

The amount n^{ads} of fluid in the medium is given by:

$$n^{ads} = \frac{\phi_m}{\overline{V}_b} + \Gamma^L s_0 \tag{2.79}$$

In this equation, the variations φ_m of porosity ϕ_m are given by Eq. (2.35):

$$\phi_m - \phi_{m0} = \varphi_m = b_m \epsilon + \frac{p}{N_m} + c\sigma^s \tag{2.80}$$

where ϕ_{m0} is the porosity in the state of reference and where c is a constant material parameter. How the surface stress σ^s is linked to the Lagrangian adsorbed amount Γ^L can readily be inferred from Eq. (2.14) combined with Eq. (2.78):

$$\begin{aligned} \left.\frac{\partial \sigma^s}{\partial \mu}\right|_{\epsilon_T} &= -\left(\Gamma + \left.\frac{\partial \Gamma}{\partial \epsilon_T}\right|_\mu\right) = -\left(\Gamma^L(1-\epsilon_T) + \frac{\partial}{\partial \epsilon_T}\left(\Gamma^L(1-\epsilon_T)\right)\right)\Big|_\mu \\ &= -\left(\Gamma^L + \left.\frac{\partial \Gamma^L}{\partial \epsilon_T}\right|_\mu - \Gamma^L\right) = -\left.\frac{\partial \Gamma^L}{\partial \epsilon_T}\right|_\mu \end{aligned} \tag{2.81}$$

so that Eq. (2.79) can eventually be rewritten as:

$$n^{ads} = -\left[\phi_{m0} + b_m\epsilon + \frac{p}{N_m} - c\int_{\mu=-\infty}^{\mu} \left.\frac{\partial \Gamma^L}{\partial \epsilon_T}\right|_\mu d\mu\right] / \overline{V}_b + \Gamma^L s_0 \tag{2.82}$$

In linear poroelasticity, the surface strain ϵ_T of the surface of the pores is related to the volumetric strain ϵ in a linear manner. Therefore, if we assume that, at a given pressure p of the fluid, the Lagrangian adsorbed amount Γ^L depends in an affine manner on the strain ϵ^T of the surface of the pores, one readily finds out that all terms in Eq. (2.82) depend in an affine manner on the volumetric strain ϵ, thus implying that the adsorbed amount n^{ads} also depends in an affine manner on the volumetric strain ϵ, and that the first-order expansion (2.69) used to simplify the constitutive equations for a generic adsorption (see Sec. 2.4.2) is valid.

Reversely, we now assume that the first-order expansion (2.69) is valid. Given the form of Eq. (2.82), we can reasonably assume that the validity of this first-order expansion implies that each term of the summation on the right-hand side of Eq. (2.82) must depend in an affine manner on the volumetric strain epsilon. Since in linear poroelasticity the surface strain ϵ_T of the surface of the pores is related to the volumetric strain ϵ in a linear manner, one concludes that the Lagrangian adsorbed amount Γ^L must depend in an affine

manner on the surface strain ϵ_T of the surface of the pores.

In conclusion, assuming that the adsorbed amount n^{ads} of fluid in the coal matrix per unit undeformed volume depends in an affine manner on the volumetric strain of the medium is equivalent to assuming, if adsorption occurs by surface covering, that the Lagrangian adsorbed Γ^L of fluid per unit area of the undeformed surface of the pores depends in an affine manner on the surface strain ϵ^T of the surface of the pores.

2.6 Concluding remarks

In this chapter we aimed at deriving two dual-porosity models for saturated coal bed reservoirs. Both models considered two types of pores, i.e., the pores of the coal matrix and the cleat system. The first model (see Sec. 2.3) took into account the effect of surface adsorption only, thus assuming that adsorption in coal occurs mainly by surface covering. We know however that the coal matrix is not only made of mesopores but also of micropores, in which adsorption occurs by pore filling more than by surface covering. Such an observation motivated the derivation of a more general model (see Sec. 2.4), in which no assumption was made on the state of the fluid in the coal matrix: this fluid could be in a bulk state (as it is in macropores for instance), adsorbed on a surface (as it is at the surface of a mesopore for instance), or adsorbed in a micropore. Moreover for the coal matrix, this latter model does not make use of the notions of porosity, of surface of the pores, or of density of the liquid, since all those notions are ambiguous in a microporous medium.

The generic model was compared with the model derived for surface adsorption (see Sec. 2.5). In particular, we discussed for both models an assumption on how adsorption depends on the strain of the medium. Because of the underlying assumptions on which they were derived, the range of validity of the generic model is greater than the one of the model derived for surface adsorption. For this reason, in the next chapters, the poromechanical behavior of the coal bed reservoir will only be modeled with these equations derived for a coal matrix with a generic pore size distribution (i.e., with the equations derived in Sec. 2.4).

Chapter 3

Calibration of constitutive equations

This chapter presents a calibration of the parameters of the constitutive equations derived for a dual-porosity coal seam with a generic porous (and potentially microporous) coal matrix. This calibration requires the knowledge of adsorption isotherms and of adsorption-induced swellings. Two sets of parameters are calibrated on two coals with different sorption and swelling properties, on which adsorption experiments of pure CO_2 and of pure CH_4 are available. For coal, coupling between adsorption and swelling is condensed into one coupling coefficient. The calibration of the model for the coal samples and the fluids of interest lets us identify some parameters associated to the microporous coal matrix: a pressure-dependent tangent Biot coefficient and an apparent microporosity. For the smallest pressures considered for the fluid, the tangent Biot coefficient can be greater than unity, i.e., is out of the usual range observed for regular macroporous media. Finally, we investigate the effect of the compressibility of the coal matrix on the calibration of the parameters.

Ce chapitre présente une calibration des paramètres des équations constitutives dérivées pour une veine de charbon à double porosité avec une matrice de charbon poreuse générique (et potentiellement microporeuse). Cette calibration requiert la connaissance d'isothermes d'adsorption et de gonflements induits par adsorption. Deux jeux de paramètres sont calibrés sur deux charbons avec des propriétés de sorption et de gonflement différentes, sur lesquels des expériences d'adsorption de CO_2 pur et de CH_4 pur sont disponibles. Pour le charbon, le couplage entre adsorption et gonflement est condensé en un coefficient de couplage. La calibration du modèle pour les échantillons de charbon et les fluides d'intérêt nous permet d'identifier certains paramètres associés à la matrice de charbon microporeuse : un coefficient de Biot tangent dépendant de la pression et une microporosité apparente. Pour les plus faibles pressions de fluide considérées, le coefficient de Biot tangent peut être plus grand que l'unité et est donc en dehors de l'intervalle usuellement observé pour des milieux macroporeux classiques. Finalement, nous investiguons l'effet de la compressibilité de la matrice de charbon sur la calibration des paramètres.

Contents

3.1 Introduction 66

3.2 Calibration of adsorption isotherm 66

3.3 Calibration of adsorption-induced swelling 71

3.4 Effect of matrix compressibility on calibration 76

3.5 Conclusions 78

3.1 Introduction

In the previous chapter, we derived poromechanical models for coal bed reservoirs saturated with a pure fluid in which adsorption could occur by surface covering and/or by pore filling. The model derived in Sec. 2.4.1 for a generic porous medium possesses a wider range of validity than the model derived in Sec. 2.3.2 for a medium in which only surface adsorption would take place. In addition, we consider that, in coal, the adsorbed amount of fluid depends linearly on the strain, which makes it possible to use the set of linearized constitutive equations $(2.73 - 2.76)$. It is this set of equations that we will use to model the poromechanical behavior of a coal bed saturated with a pure fluid. However, as a prerequisite to any reservoir simulation, the constitutive equations $(2.73 - 2.76)$ must be calibrated.

The calibration of the parameters of the model will be performed in this chapter by using experimental data of adsorption of fluid in a coal sample and of adsorption-induced swellings of the same coal sample. The bulk modulus of the coal matrix K_m will not be calibrated but will be set to a typical value for coal. While aiming at modeling a complete ECBM process, we restrict ourselves for now to coal bed reservoirs saturated with a pure fluid. With carbon dioxide as the pore fluid, the constitutive equations could be used to simulate an injection of CO_2 in an empty reservoir. With CH_4 as the pore fluid, the constitutive equations could be used to simulate CBM production.

As a basis for the calibration of the parameters, we use experimental data gathered by Pini on two coal samples [Pini et al., 2010b]: the Ribolla and Sulcis coals from Italy. The Ribolla sample was excavated from the Ribolla Coal Mine (Grosseto, Italy), whereas the Sulcis sample comes from the Monte Sinni coal mine (Carbosulcis, Cagliari, Italy) in the Sulcis Coal Province [Pini et al., 2010b]. Table 3.1 provides the main properties of these samples [Pini, 2009]. These values allow classifying Sulcis coal as high volatile C bituminous [Ottiger et al., 2006] and Ribolla coal as medium volatile bituminous [Vassilev et al., 1996].

On both Ribolla and Sulcis coal samples, Pini measured total adsorbed amounts $n^{ads}(p)$ of pure CO_2 and pure CH_4 at a temperature $T = 318$ K. On those two samples and at the same temperature, he also measured the swelling $\epsilon^u(p)$ when the sample was immersed in the fluid. For this same temperature, the molar volume $\overline{V}_b$ of carbon dioxide and of methane are displayed in Fig. 3.1. Such measurements of total adsorbed amount $n^{ads}(p)$ and swelling $\epsilon^u(p)$ will enable us to calibrate the derived model, as will be shown in sections 3.2 and 3.3. The effect of the choice of the bulk modulus K_m of the coal matrix will be discussed in section 3.4.

3.2 Calibration of adsorption isotherm

This section is dedicated to the calibration of the adsorption isotherms on both the Ribolla and the Sulcis coal samples. On those samples, Pini performed measurements of adsorption of pure carbon dioxide and of pure methane at a temperature $T = 318$ K. All high pressure adsorption measurements were performed in a Rubotherm magnetic suspension balance (Rubotherm, Bochum, Germany), whose characteristics and details are extensively described elsewhere [Keller and Staudt, 2005], [Ottiger et al., 2006]. A

Table 3.1 – Properties of the Ribolla and Sulcis coal samples tested by Pini and used for the calibration of the constitutive equations Pini et al. [2010b]. All percentages are mass fractions. *Volatile matter* refers to the components of coal, except for moisture, which are liberated at high temperature in the absence of air. *Fixed carbon content* of the coal is the carbon found in the material which is left after volatile materials are driven off. *Ash* represents the bulk mineral matter after carbon, oxygen, sulfur and water has been driven off during combustion. R_0 is the term reactivity which is used to describe a critical property or behavior during reaction or conversion in a chemical or a metallurgical process of coal [Raaness, 1990].

Sample	Ribolla	Sulcis
Moisture (%)	7.80	5.32
Volatile Matter (%)	30.99	40.25
Fixed Carbon (%)	50.09	45.72
Ash (%)	11.12	8.71
R_0 (%)	0.74	0.70
Density (kg/m^3)	1435	1370

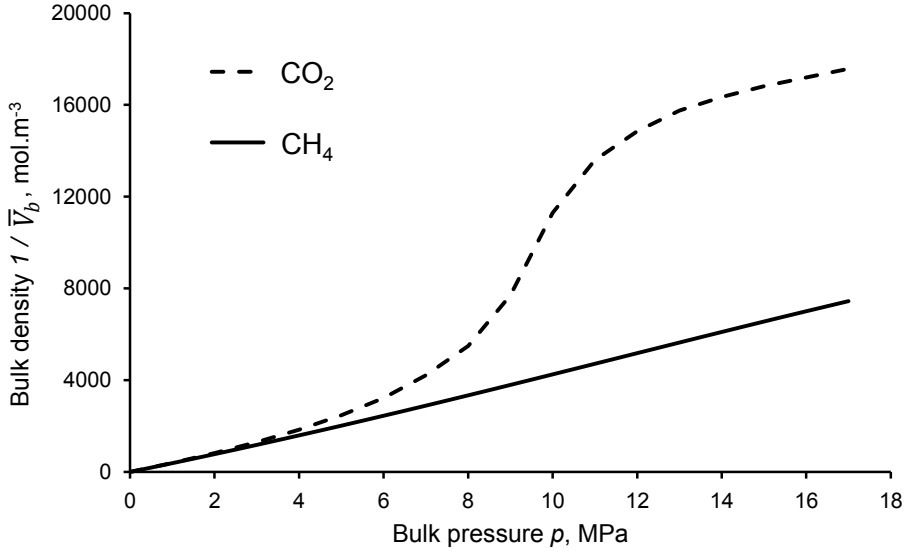

Figure 3.1 – Equation of state for CO_2 and for CH_4 at a temperature $T = 318$ K. The data is from NIST Chemistry WebBook (http://webbook.nist.gov/chemistry/).

schematic of the device is shown in Fig. 3.2. A typical adsorption experiment consists of the following steps: the high pressure cell containing about 3 g of the powdered coal sample is evacuated and the mass of the vacuumed sample is measured. Then, the system is filled with helium to determine the volume of the metal parts and of the coal sample. In this determination, helium is assumed not to be adsorbed by coal. After evacuating it again, the cell is filled with the gas to be adsorbed, i.e., CO_2 or CH_4, and the mass of the sample is measured at the pressures of interest. The experimental setup and methods

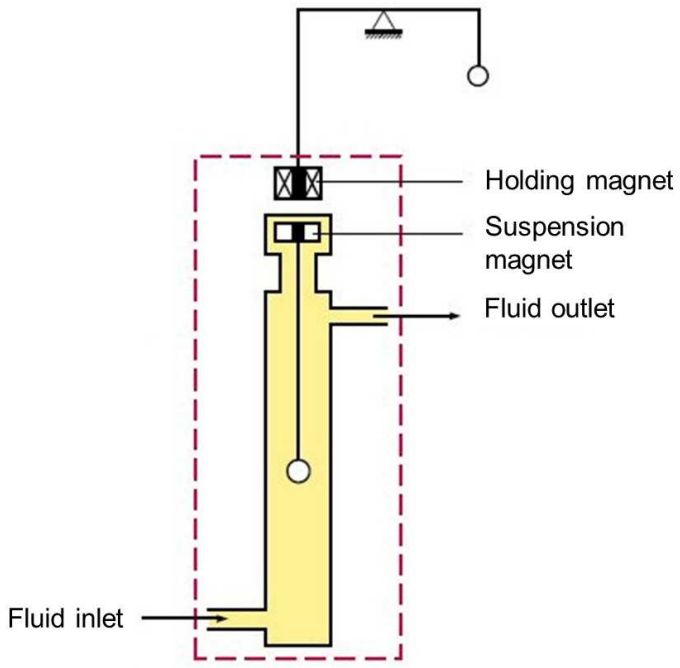

Figure 3.2 – Rubotherm magnetic suspension balance (Source: www.rubotherm.de/magnet/).

have been described extensively in Pini [2009] and Ottiger et al. [2006]. However, the most important equations used for data reconciliation are summarized here. After the coal sample is placed in the basket, and after the magnetic suspension balance is evacuated, a mass M_1^0 under vacuum is measured:

$$M_1^0 = m^{met} + m_0^{coal} \tag{3.1}$$

where m^{met} and m_0^{coal} are the masses of the lifted metal parts and the initial mass of the coal sample, respectively. Then, the system is filled with helium and the sum $V^{met} + V_0^{coal}$ of the volume V^{met} of the metal parts and of the volume V_0^{coal} of the coal sample is calculated from the measured mass $M_1(\rho_{He}^b, T)$ and from the elsewhere measured bulk density ρ_{He}^b of helium:

$$V^{met} + V_0^{coal} = \frac{M_1^0 - M_1(\rho_{He}^b, T)}{\rho_{He}^b} \tag{3.2}$$

In this equation, adsorption of helium can be neglected, because in general the affinity of helium for adsorbents is much lower than that of CO_2 or of CH_4 and because the injection of helium is performed at the highest possible temperature and density [Ottiger et al., 2006]. After evacuating it again, the cell is filled with the gas to be adsorbed and the mass $M_1(\rho^b, T)$ is measured at the desired conditions, i.e., at given temperature T and pressure p of the fluid:

$$M_1(\rho^b, T) = M_1^0 + m^{ads} - \rho^b \left[V^{met} + V_0^{coal} + V^{ads}\right] \tag{3.3}$$

where m^{ads} and V^{ads} are the total absolute amount adsorbed and the volume of the adsorbed phase, respectively, and where $\rho^b(p, T)$ is the density of the fluids at pressure p and temperature T. Since the volume V^{ads} of the adsorbed phase cannot be directly measured, adsorption is characterized by the molar excess amount n^{excess}, which requires no more information about the volume of the adsorbed phase:

$$\frac{n^{excess}}{\rho_{coal}} = \frac{m^{ads} - \rho^b V^{ads}}{M_m m_0^{coal}} = \frac{M_1(\rho^b, T) - M_1^0 + \rho^b \left[V^{met} + V_0^{coal}\right]}{M_m m_0^{coal}} \tag{3.4}$$

where M_m is the gas molar mass. The molar excess amount n^{excess} is expressed as a quantity of fluid (in moles) divided by the mass of coal. For a practical application like ECBM, the molar absolute adsorption n^{ads} per unit volume of coal is needed, which is given by:

$$\frac{n^{ads}}{\rho_{coal}} = \frac{m^{ads}}{M_m m_0^{coal}} = n^{excess} + \frac{\rho^b V^{ads}}{M_m m_0^{coal}} \tag{3.5}$$

Therefore, the volume V^{ads} of the adsorbed phase needs to be determined to evaluate this quantity. In order to do so, CO_2 adsorption is considered at high pressures, at which we can assume that the coal is saturated and that the mass m^{ads} and the volume V^{ads} of the adsorbed phase depend no more on the pressure. Under such assumptions, Eq. (3.4) yields a linear relationship between n^{excess} and ρ^b, the slope of which is the volume V^{ads} of the adsorbed phase [Murata et al., 2001]. In the case of CH_4, Pini could not determine the volume of the adsorbed phase with the same method because he only performed measurements below the critical density of methane. Due to the good agreement between the volume of the adsorbed phase estimated from CO_2 injection and the microporous volume estimated by Pini [2009] and Ottiger et al. [2006], Pini considered that this estimated volume also held for injection of CH_4. Therefore, the adsorption isotherm n^{ads} which was given by Pini is in fact the adsorption isotherm at zero strain, i.e., $n^{ads}(\epsilon = 0)$ or n_0^{ads}. Figure 3.3 displays the adsorption isotherms n_0^{ads} on both the Sulcis and the Ribolla coal samples at a temperature $T = 318$ K: one can observe that the affinity of carbon dioxide for Sulcis coal is significantly lower than its affinity for Ribolla coal, while the affinity of methane for Sulcis coal is nearly the same as its affinity for Ribolla coal. To fit the adsorption isotherms observed experimentally, Pini used the Langmuir equation, which is

given by:

$$n_0^{ads} = \frac{n^{max} b_p p}{1 + b_p p} \tag{3.6}$$

where n^{max} and b_p are the Langmuir adsorption parameters. n^{max} is the maximal amount of fluid that can be adsorbed. $1/b_p$ is the pressure at which half of this maximal amount is adsorbed. Table 3.2 provides those parameters for CO_2 and CH_4 on the Sulcis and Ribolla coals at $T = 318$ K. In our modeling, we will readily use the adsorption isotherms (3.6) together with the parameters given in Table 3.2.

Table 3.2 – Parameters of Langmuir isotherms fitted on adsorption data of CO_2 and CH_4 on Ribolla and Sulcis samples at $T = 318$ K, adapted from Pini [2009]. The meaning of n^{max} and b_p is provided in the text.

Sample	**Ribolla**		**Sulcis**	
Fluid	CO_2	CH_4	CO_2	CH_4
n^{max} (mol.m^{-3})	4922	2425	3411	2137
b_p (Pa^{-1})	5.18×10^{-7}	3.87×10^{-7}	1.25×10^{-6}	6.27×10^{-7}

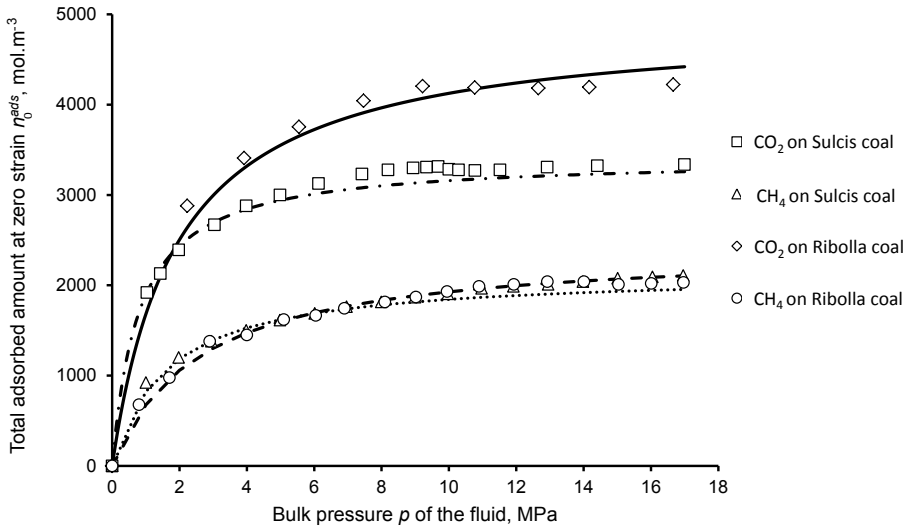

Figure 3.3 – Total adsorbed amount of CO_2 and CH_4 at zero strain in Sulcis and Ribolla coals at $T = 318$ K. Symbols are experimental data adapted from Pini [2009], whereas lines are fitted Langmuir isotherms.

3.3 Calibration of adsorption-induced swelling

This section is dedicated to calibrating the coefficient $C(p)$ that couples adsorption and deformation (see Eq. 2.69). In order to do so, we use both the adsorption isotherms displayed in Fig. 3.3 and experimental data of swelling of coal immersed in pure CO_2 and in pure CH_4. The experimental procedure leading to this latter measurement has been described in detail elsewhere [Rajendran et al., 2005], [Pini, 2009]). However, the most important steps of the data reconciliation and the main equations are briefly summarized in the following. In the swelling experiments, a disc of coal is placed on a brass holder in a high pressure cell, as depicted in Fig. 3.4. The cell is equipped with sapphire windows, which allows continuous imaging. Beside keeping the coal sample in horizontal position, the brass holder is the reference for evaluating the diameter of the swollen coal sample from digital imaging. Such quantity is estimated by comparing its size to that of the brass holder, while assuming that the strain of the holder induced by fluid pressure is negligible with respect to the strain of the sample. The cell is brought to the desired temperature, evacuated, flushed with the fluid of interest, and then filled to the required pressure. The disc of coal is allowed to expand for two days to reach equilibrium conditions before a picture is taken and the diameter of the disc is determined using a commercial image analysis software [Pini, 2009]. With this procedure, Pini carried out measurements of

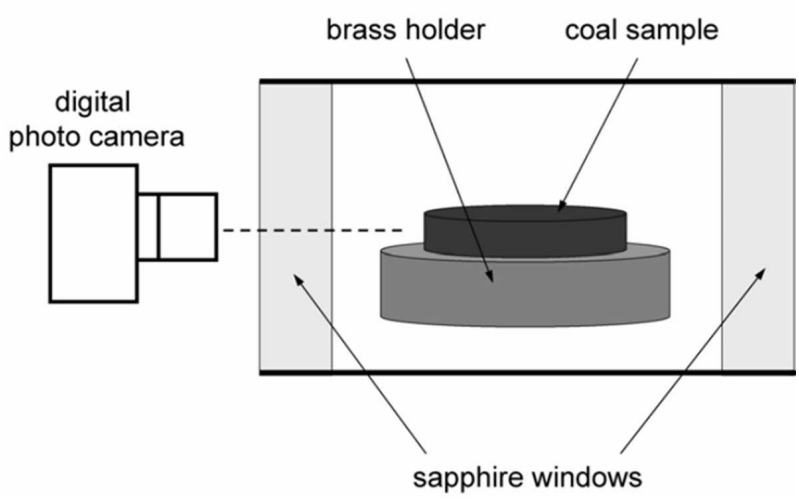

Figure 3.4 – Schematic of the high pressure view cell used for the swelling experiments, adapted from Pini [2009].

swelling of Ribolla and Sulcis coals using the two adsorbing fluids CO_2 and CH_4 at a temperature $T = 318.15$ K. The obtained experimental data is displayed in Fig. 3.5. In order to fit the volumetric strains ϵ^u measured experimentally, Pini used a Langmuir-like equation given by:

$$\epsilon^u = \frac{\epsilon^u_{max} b_s p}{1 + b_s p} \tag{3.7}$$

where ϵ^u_{max} and b_s are the calibrated parameters. ϵ^u_{max} is the maximal strain that one could observe by immersing the sample in a fluid. In the experiment of immersion, since all the particles of coal swell homothetically, $\epsilon^u = \epsilon = \epsilon_m$. Table 3.3 provides those parameters for CO_2 and CH_4 and for the Sulcis and Ribolla coals at $T = 318.15$ K[1]. Table 3.4

Table 3.3 – Parameters obtained for the fit of Eq. (3.7) to the swelling of Ribolla and Sulcis samples for CO_2 and CH_4 at a temperature $T = 318.15$ K, adapted from Pini [2009]. The meaning of ϵ^u_{max} and b_s is provided in the text.

Sample	**Ribolla**		**Sulcis**	
Fluid	CO_2	CH_4	CO_2	CH_4
ϵ^u_{max} (-)	0.044	0.024	0.049	0.023
b_s (Pa^{-1})	5.91×10^{-8}	4.88×10^{-8}	3.8×10^{-7}	3.47×10^{-7}

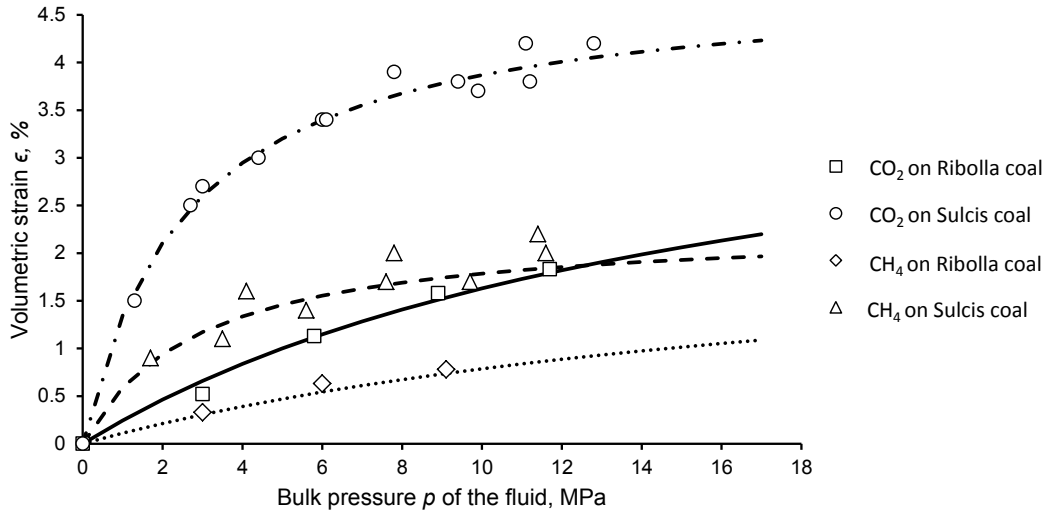

Figure 3.5 – Swelling of Ribolla and Sulcis coal samples immersed in carbon dioxide and methane (experimental data adapted from Pini [2009]). Symbols are experimental data, whereas lines are the calibrated poromechanical model.

provides mechanical properties for Ribolla and Sulcis coals. The bulk modulus $K = 0.78$ GPa and Poisson's ratio $\nu = 0.26$ of a small element of fractured coal are given by Pini for Sulcis coal [Pini, 2009]. We choose the same elastic properties for the Ribolla coal: by doing so, both coals only differ by their adsorptive properties. In the absence of any mechanical information relative to the scale of the coal matrix, we set for now, the bulk modulus K_m of the coal matrix to 1.04 GPa given by [Pini, 2009], which, with the help of Eq. (2.49), leads to a Biot coefficient $b = 0.25$. Other values for the Biot coefficient b and the bulk modulus K_m for the coal matrix could be considered as well: the impact of such a choice on the results of the calibration will be discussed later on. For a sample

1. It is worth mentioning that b_p and b_s have different values.

Table 3.4 – Mechanical properties of the Ribolla and Sulcis coals

Parameter	Definition	Value
E	Young's modulus, GPa	1.12
G	Shear modulus, GPa	0.45
ν	Poisson's ratio	0.26
K	Bulk modulus of reservoir, GPa	0.78
b	Biot coefficient of reservoir	0.25
K_m	Bulk modulus of coal matrix, GPa	1.04

immersed in a fluid, for which the boundary conditions verify $\sigma = -p$, a combination of Eqs. (2.73), (2.77) and (2.49) enables to express the coupling coefficient $C(p)$ as:

$$C(p) = \frac{1 + K_m d\epsilon^u/dp}{n_0^{ads}\overline{V_b}} \tag{3.8}$$

where ϵ^u is the volumetric strain of the immersed sample.

For a given bulk modulus K_m of the coal matrix, the above expression enables to calculate the coupling coefficient $C(p)$ from the measured adsorption isotherms displayed in Fig. 3.3 together with the measured swellings displayed in Fig. 3.5. The resulting coupling coefficient $C(p)$ calculated with Eq. (3.8) combined with the experimental data on Sulcis and Ribolla coals is displayed in Fig. 3.6. We observe that this coefficient and therefore how adsorption and strain are coupled depends significantly on the pressure of the fluid for carbon dioxide, especially near $p = 10$ MPa, a pressure at which the density of carbon dioxide significantly varies, while for methane such a coupling coefficient depends less significantly on the pressure of the fluid. The dependency of the coupling coefficient on the pressure of the fluid was studied recently by Brochard et al. [2012b], who performed molecular simulations of methane on a fully flexible coal structure at different levels of strain.

The poromechanical model is now calibrated. On top of the swellings of the coal samples measured upon immersion in a fluid, Fig. 3.5 displays the swelling predicted by the set of constitutive equations (2.73)-(2.77). The calibrated model is in very good agreement with the experimental data, thus providing the ability of the generic poromechanical model to capture the swelling of coal observed experimentally in presence of fluid.

Figure 3.5 also shows that, in the experiment of sample immersed in pure CO_2, Sulcis coal swells about twice as much as Ribolla coal, while the affinity of carbon dioxide for Sulcis coal is lower than for Ribolla coal (see Fig. 3.3). We also observe from Fig. 3.5 that, upon immersion in pure CH_4, Sulcis coal swells about twice as much as Ribolla coal, while the affinity of methane for Sulcis coal is almost the same as for Ribolla coal (see Fig. 3.3): as was already noted by Day et al. [2008] and by Pini [2009], coals with high sorption capacity are not necessarily coals with a high swelling potential, which shows that swelling and adsorption are linked in a nontrivial manner. Figure 3.7 shows how the adsorption-induced pressure p^a depends on the bulk pressure of the fluid. Like

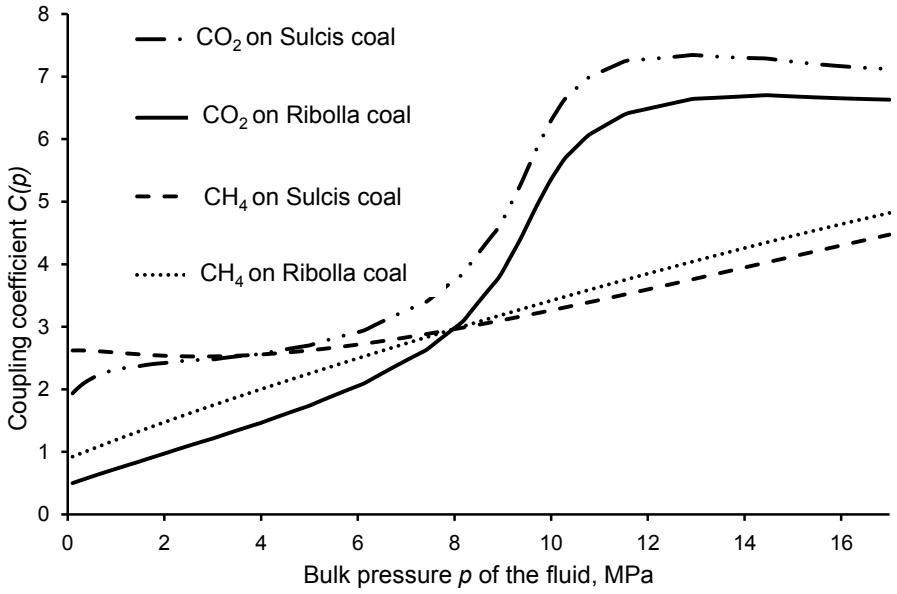

Figure 3.6 – Coupling coefficient $C(p)$ for Ribolla and Sulcis coals in presence of pure carbon dioxide or pure methane.

the swelling curves displayed in Fig. 3.5, for the coals and fluids here considered, the adsorption-induced pressure evolves in a concave manner with the pressure of the fluid.

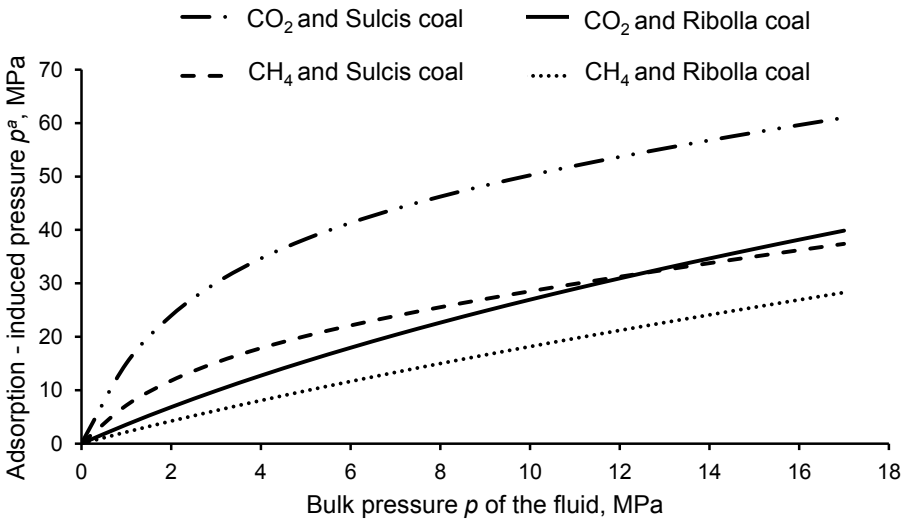

Figure 3.7 – Adsorption-induced pressure p^a for Ribolla and Sulcis coals immersed in pure carbon dioxide and pure methane.

We also identified from the model an apparent tangent Biot coefficent $b_m^{tan} = n_0^{ads} C(p) \overline{V_b}(p)$ associated to the coal matrix (see Eq. 2.64). Figure 3.8 displays this tangent Biot coefficient b_m^{tan} as a function of the bulk pressure p of the fluid. For Sulcis coal, this Biot co-

efficient can be as high as 17.7 at the smallest fluid pressures, while for Ribolla coal this coefficient can reach a value of 3.6. Figure 3.8 also shows that such a tangent Biot coefficient b_m^{tan} is lower for CH_4 than for CO_2. In any case, for both coals this Biot coefficient is out of the usual range $[0, 1]$ observed for regular macroporous media. Those unconventional values are a direct consequence of the interaction forces taking place between the atoms of the solid and the molecules of the fluid, which overcome the effects of the bulk pressure effect [Brochard et al., 2012b].

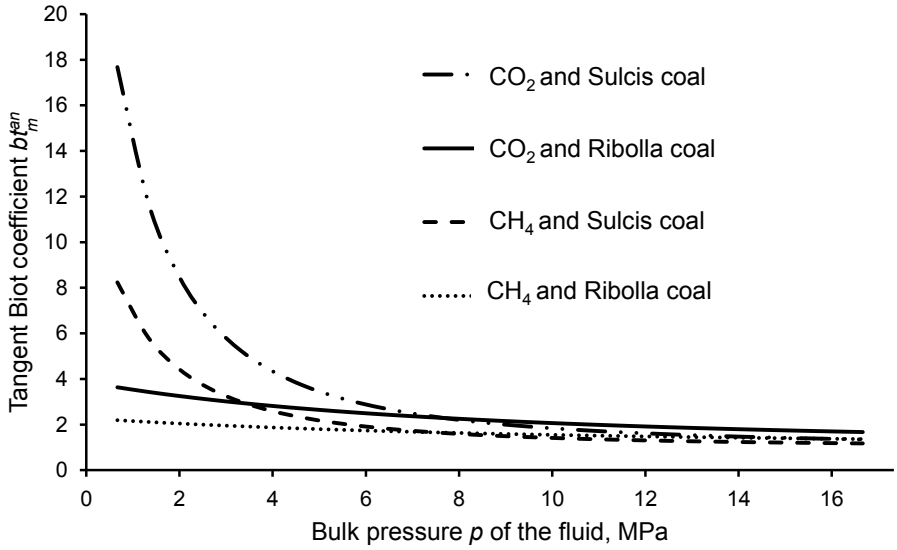

Figure 3.8 – Tangent Biot coefficient b_m^{tan} associated to coal matrix for Sulcis and Ribolla coals in presence of pure carbon dioxide and pure methane.

In the microporous coal matrix, fluid molecules can be in a bulk as well as in an adsorbed state. We can introduce a parameter $n^{ads}\overline{V}_b$ which is analogous to a porosity: in a chunk of coal matrix of volume Ω_0, $n^{ads}\overline{V}_b\Omega_0$ is the volume that the adsorbed molecules would occupy if they were in their bulk state. The parameter $n^{ads}\overline{V}_b$ is therefore an apparent porosity of the microporous coal matrix. Rewriting the constitutive equation (2.69) enables to rewrite this parameter as:

$$n^{ads}(p)\overline{V}_b(p) = n_0^{ads}(p)\overline{V}_b(p) + b_m^{tan}(p)\epsilon \tag{3.9}$$

where $n_0^{ads}(p)\overline{V}_b(p)$ is the apparent porosity of the coal matrix kept at zero deformation. Figure 3.9 displays such an apparent porosity $n_0^{ads}(p)\overline{V}_b(p)$ at zero deformation as a function of the fluid bulk pressure p: this apparent porosity of the coal was higher in presence of CO_2 than in presence of CH_4 and always decreased with the pressure of the fluid, independent of the type of coal or of the type of fluid. For Sulcis coal in presence of CO_2, this apparent porosity of the coal matrix could be as high as 8 at the smallest fluid pressures, while for Ribolla coal under the same fluid this porosity reached a value of 6.9. Above a pressure of the fluid of about 10 MPa, we observed that such a porosity converged toward a value below unity, for both samples and both fluids. However, whithin the range of small pressures (below 7 MPa in general) for both coals and fluids this porosity was out of the

range $[0, 1]$ usually observed for regular macroporous media. Such surprising values are a direct consequence of the microporous feature of the medium.

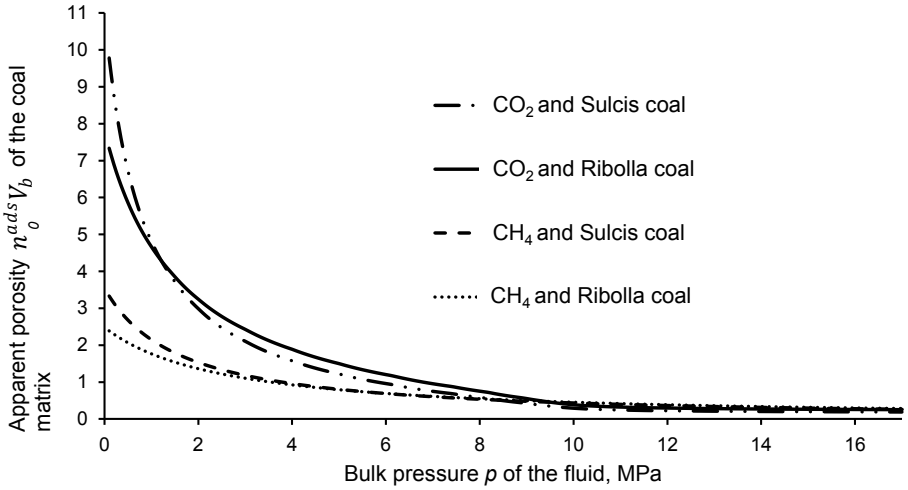

Figure 3.9 – Apparent porosity $n_0^{ads}(p)\overline{V}_b(p)$ for Sulcis and Ribolla coals in presence of pure carbon dioxide and pure methane.

3.4 Effect of matrix compressibility on calibration

The coupling coefficient $C(p)$ between adsorption and strain depends on the bulk modulus K_m of the coal matrix (see Eq. 3.8). A variation of the coupling coefficient will modify the dependence of the adsorption-induced pressure on the bulk pressure of the fluid (see Eq. 2.77) and thus, as will be discussed in Chapter 4, how injectivity and permeability will evolve with time at the scale of the reservoir. Therefore, in this section we aim at analyzing the sensitivity of the adsorption-induced pressure p^a and of the apparent tangent Biot coefficient b_m^{tan} of the coal matrix to the bulk modulus K_m of the coal matrix. The bulk modulus K_m of the coal matrix should verify the inequality $K_m \geq K/(1-\phi_{c0})$ where K is the bulk modulus of the reservoir and where ϕ_{c0} is the porosity of the cleats in the state reference. For three different values of the bulk modulus K_m of the coal matrix that fall in the range $K_m \geq K/(1-\phi_{c0})$, Fig. 3.10 displays the adsorption-induced pressure p_a calibrated by following the procedure explained in Sections 3.2 and 3.3. The displayed values were calibrated on a Sulcis coal sample immersed in pure CO_2. One can observe in this figure that a less compressible coal matrix resulted in higher adsorption-induced pressures p_a. Such a higher value translates into a higher apparent tangent Biot coefficient b_m^{tan} of the coal matrix, as is observed in Fig. 3.11. In contrast, Fig. 3.12 shows that the bulk modulus K_m chosen for the calibration had very little impact on the back - calculated apparent porosity of the microporous coal matrix.

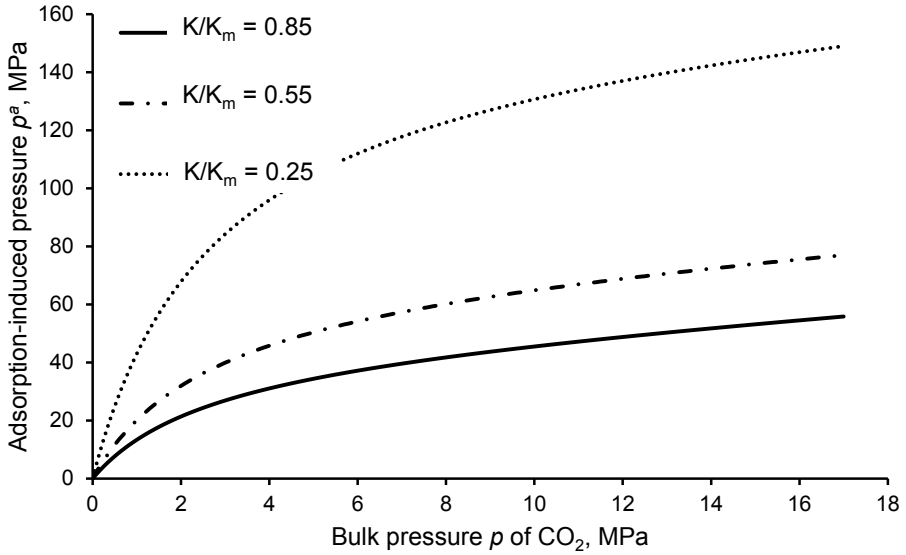

Figure 3.10 – Effect of matrix compressibility on the calibrated adsorption - induced pressure p^a for Sulcis coal in presence of pure carbon dioxide. K and K_m are the bulk moduli of the fractured coal and of the coal matrix, respectively.

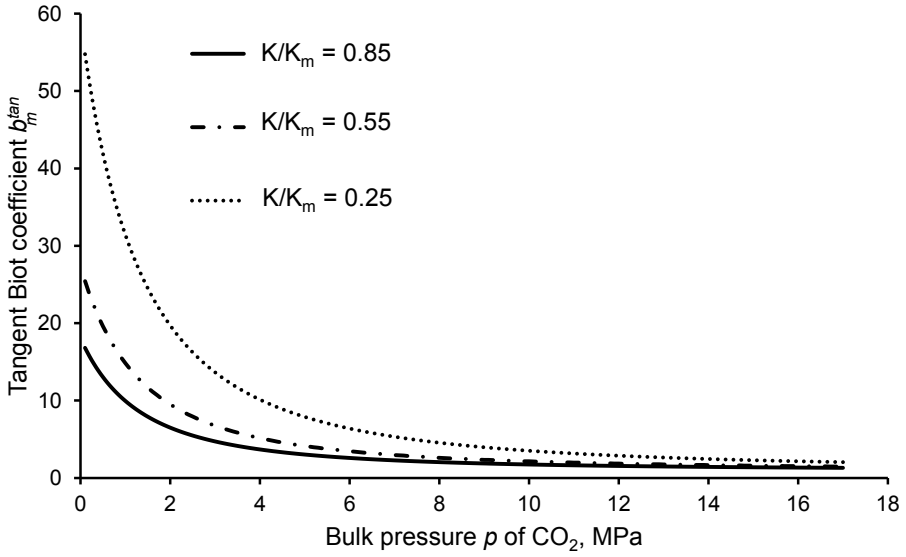

Figure 3.11 – Effect of matrix compressibility on the calibrated tangent Biot coefficient b_m^{tan} of the coal matrix for Sulcis coal in presence of pure carbon dioxide. K and K_m are the bulk moduli of the fractured coal and of the coal matrix, respectively.

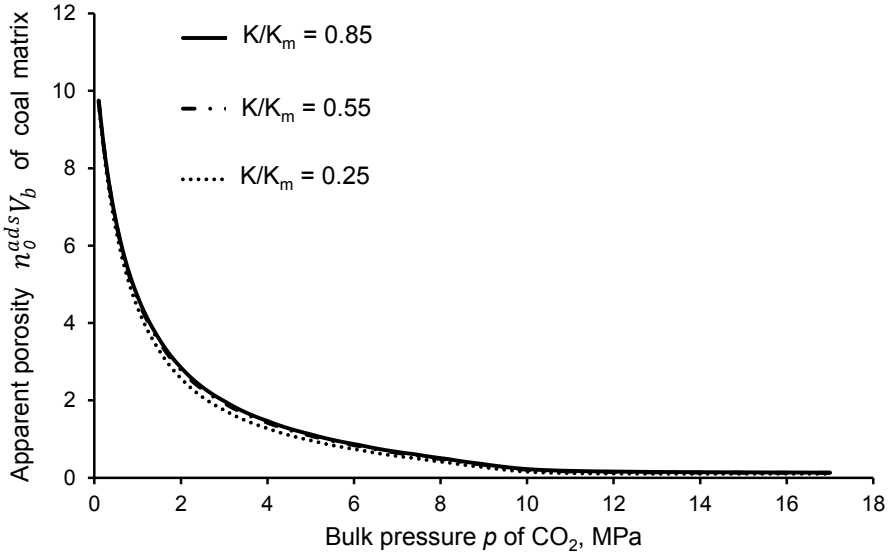

Figure 3.12 – Effect of matrix compressibility on the apparent porosity of the Sulcis coal matrix in presence of pure carbon dioxide. K and K_m are the bulk moduli of the fractured coal and of the coal matrix, respectively.

3.5 Conclusions

After deriving constitutive equations of a coal bed reservoir with a microporous coal matrix saturated with a pure fluid in Chapter 2, we needed to calibrate those constitutive equations. Such a calibration is a prerequisite to simulate a coal bed reservoir under various conditions (see Chapter 4). In the present chapter, we showed that this calibration could be performed if adsorption isotherms and swellings upon adsorption have been measured. We considered two coals with different sorption and swelling properties, subjected to adsorption of pure CO_2 and of pure CH_4. The coefficient $C(p)$ that couples adsorption and swelling was calibrated. We observed that this coefficient depended significantly on the pressure of the fluid for carbon dioxide, especially near $p = 10$ MPa, a pressure at which the density of carbon dioxide significantly varies. In contrast, for methane such a coupling coefficient was less pressure-dependent (see Fig. 3.1). From the calibration of the model on coal samples and fluids of interest, we could identify additional parameters of the microporous coal matrix. The tangent Biot coefficent b_m^{tan} of the coal matrix was identified as a function of the fluid bulk pressure: interestingly, especially at the smallest pressures considered, this Biot coefficient was out of the usual range $[0, 1]$ observed for regular macroporous media. An apparent porosity was also defined, which also fell out of the usual range $[0, 1]$ at low pressures. Those unconventional values are a direct consequence of the intermolecular forces between the molecules of fluid in the microporous coal matrix and the atoms of the solid skeleton of the coal matrix. Finally, we investigated how the choice of the compressibility of the coal matrix impacts the calibration of the parameters. The adsorption-induced pressure p_a and the tangent Biot coefficient b_m^{tan} of the coal matrix increase with an increasing bulk modulus K_m. This choice is expected to have a significant impact on simulations at the scale of a representative elementary volume or

at the scale of the reservoir. Such simulations are the focus of the next Chapter.

Chapter 4

Simulations

This chapter is dedicated to simulations at the scale of a coal sample, of a Representative Elementary Volume, and of a coal seam, based on the constitutive equations derived and calibrated in previous chapters. Simulations are limited to cases for which the medium is saturated with a pure fluid (CH_4 or CO_2). The numerical model is first validated at the scale of a coal sample by comparison with available permeability measurements of coal injected with carbon dioxide. At the scale of a Representative Elementary Volume, we show that adsorption-induced variations of permeability depend significantly on the boundary conditions and on the compressibility of the coal matrix. The effect of the kinetics of transfer of fluid between cleats and coal matrix is also discussed. At the scale of a reservoir, simulations of production of methane from the reservoir (a process known as primary recovery of coal bed methane) or of injection of carbone dioxide in a methane-free reservoir are performed. We discuss the effects of the compressibility of the coal matrix, of the boundary conditions, and of the kinetics of transfer of fluid between cleats and coal matrix on the rates of production or of injection.

Ce chapitre est dédié à des simulations à l'échelle d'un échantillon de charbon, d'un Volume Élémentaire Représentatif, et d'une veine de charbon, basées sur les équations constitutives dérivées et calibrées dans les chapitres précédents. Les simulations sont limitées aux cas où le milieu est saturé par un fluide pur (CH_4 ou CO_2). Le modèle numérique est tout d'abord validé à l'échelle d'un échantillon de charbon par comparaison avec des mesures de perméabilité disponibles de charbon injecté par du dioxyde de carbone. A l'échelle d'un Volume Élémentaire Représentatif, nous montrons que les variations de perméabilité induites par l'adsorption dépendent significativement des conditions aux limites et de la compressibilité de la matrice de charbon. L'effet de la cinétique de transfert de fluide entre fractures et matrice de charbon est aussi discuté. A l'échelle du réservoir, des simulations de production de méthane d'une veine (un processus connu sous le nom de récupération primaire de coal bed methane) et des simulations d'injection de dioxyde de carbone dans une veine préalablement vidée de son méthane sont effectuées. Nous discutons les effets de la compressibilités de la matrice de charbon, de la température, des conditions aux limites, et de la cinétique de transfert de fluide entre fractures et matrice de charbon sur les débits de production ou d'injection.

Contents

4.1 Introduction 84

4.2 Coal sample: comparison with experiment 84

4.3 Representative Elementary Volume 88

4.3.1 Effect of boundary conditions 89

4.3.2 Effect of compressibility of coal matrix 91

4.3.3 Effect of kinetics of transfer of fluid between cleats and coal matrix 92

4.4 Primary recovery of coal bed methane (CBM) 97

4.4.1 Effect of compressibility of coal matrix 99

4.4.2 Effect of temperature 100

4.5 Injection of carbon dioxide in methane-free coal bed 102

4.5.1 Effect of boundary conditions 106

4.5.2 Effect of compressibility of coal matrix 108

4.5.3 Effect of kinetics of transfer of fluid between cleats and coal matrix 111

4.6 Conclusion 114

4.1 Introduction

In Chapter 2 we derived a poromechanical model for a saturated coal bed reservoir that explicitly takes into account the fact that the coal matrix is microporous. The derived model is a dual-porosity one: in addition to the porosity of the coal matrix, we also considered the macroporous cleat system. In Chapter 3, we calibrated the derived model on experimental data of adsorption and of swelling. Two sets of data were used for that purpose: data gathered on the so-called Sulcis coal and on the so-called Ribolla coal.

In the present Chapter, we aim at using the calibrated model for numerical simulations. Such simulations will be performed at the scale of a coal sample (Section 4.2), at the scale of a Representative Elementary Volume (Section 4.3), and at the scale of a reservoir (Sections 4.5 and 4.4). At the scale of the coal sample (Section 4.2), simulations will be compared with experimental data in order to validate the calibrated model. At the scales of a Representative Elementary Volume and a reservoir, we will consider how the following parameters affect the outputs of the simulation: the boundary conditions, the compressibility of the coal matrix, and the kinetics of transfer of fluid from the cleat system to the microporous coal matrix. Our ultimate goal is to study Enhanced Coal Bed Methane (ECBM), which requires considering mixtures of carbon dioxide and of methane. Such mixtures will be considered in the next Chapter. In the present Chapter, we restrain ourselves to cases in which one pure fluid only is present. We will therefore consider two cases only: production of methane in the absence of any injection of carbon dioxide (a process known as Coal Bed Methane Recovery, or CBM), and the hypothetic (and unrealistic) case of an injection of carbon dioxide into a coal bed reservoir that would initially have been emptied of all its methane.

All simulations are performed with the modeling platform Bil, a finite-element and finite-volume code developed in-house by Patrick Dangla [1]. Bil is written in C language and can run on Linux-based OS. Bil is developped for 1D, 2D, and 3D problems. It includes no mesh generator or postprocessing treatment of outputs. However, it can read mesh files created by the free open-source software Gmsh [2]. The output files created by Bil can easily be used by some plotting programs such as Gnuplot [3].

4.2 Coal sample: comparison with experiment

This section is dedicated to a comparison of our calibrated model with experimental data. Mazzotti et al. [2009] measured the permeability of a coal sample at different levels of confining stresses and of pore fluid pressure. They performed this experiment with a coal sample from the Monte Sinni coal mine in the Sulcis Coal Province (Sardinia, Italy), i.e., with a coal which we already considered in Chapter 3, and on which we calibrated our model.

Properties of the coal sample used in this experiment are given in Table 4.1. On the same type of coal, sorption and swelling isotherms were also measured, as was explained in Sections 3.2 and 3.3. In order to measure the permeability, Mazzotti et al. [2009] used

1. http://perso.lcpc.fr/dangla.patrick/bil/
2. http://www.geuz.org/gmsh/
3. http://www.gnuplot.info/

Table 4.1 – Input parameters of the model for the permeability experiments performed on Sulcis coal (adapted from Mazzotti et al. [2009]

Property	Definition	Value
T	Temperature, K	318.15
E	Young's modulus, GPa	1.12
ν	Poisson's ratio	0.26
K	Bulk modulus of coal sample, GPa	0.78
b	Biot coefficient of coal sample	0.25
ϕ_{c0}	Porosity of cleats	0.032
K_m	Bulk modulus of coal matrix, GPa	1.04
L	Length of coal sample, m	0.036
A	Section area of coal sample, m^2	4.73×10^{-4}
V_{US}	Volume of upstream reservoir, m^3	5.04×10^{-5}
V_{DS}	Volume of downstream reservoir, m^3	1.52×10^{-5}

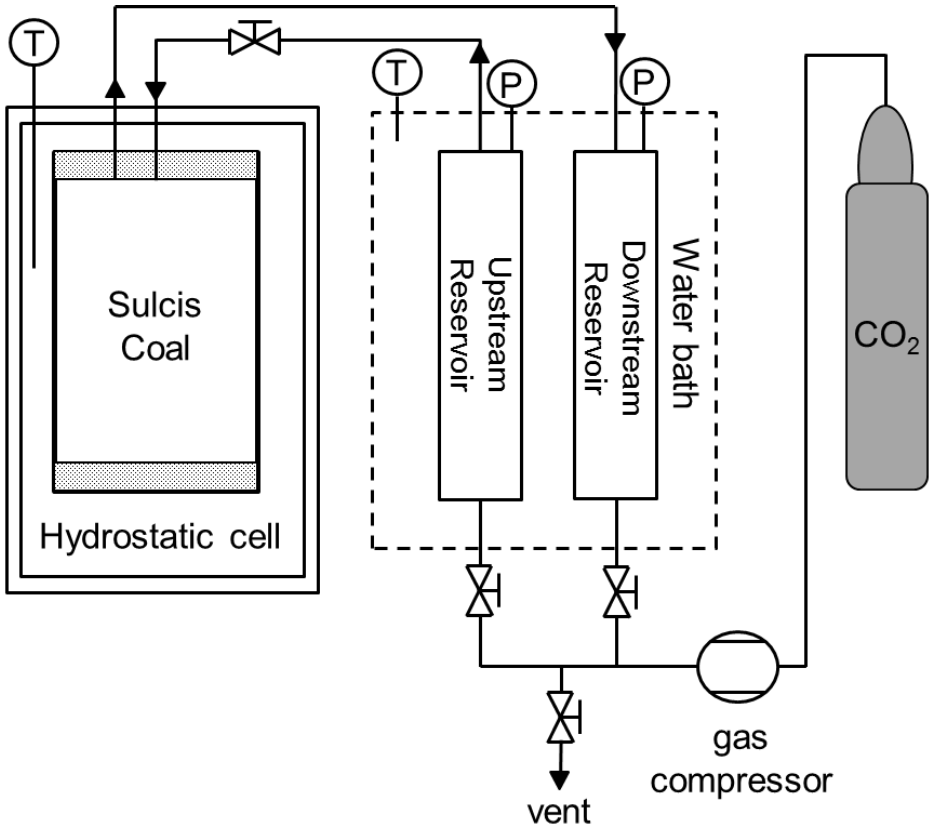

Figure 4.1 – Experimental setup used by Mazzotti et al. [2009] to measure the permeability of a Sulcis coal sample at different levels of confining stress and of pore fluid pressure (adapted from Mazzotti et al. [2009]).

the transient step method. The experimental setup is sketched in Fig. 4.1: a hydrostatic cell is at the heart of the setup and can accomodate the coal sample, which here was 2.54 cm (1 inch) in diameter and 3.6 cm in length. The cell was designed to work with confining stresses up to 100 MPa. The hydrostatic cell was kept at the desired temperature with a heating jacket: the temperature in the experiences of interest was 318.15 K, a temperature which is representative of the conditions of the coal seam in the Sulcis coal Province. The confining stress was controlled to $\pm$ 0.1 MPa. The cylindrical sample was isolated from the confining fluid with a rubber jacket and placed between two stainless steel disks with interconnected circular grooves to distribute the fluid over the cross-sectional area of the sample. The two stainless steel disks were connected to the tubing system and finally to two reservoirs: the upstream reservoir (the volume of which was 50.4 cm^3), which could be pressurized with the gas to be injected, and the downstream reservoir (the volume of which was 15.2 cm^3), which was used to collect the gas exiting the sample. In the experiments of interest, the injected fluid was carbon dioxide. The reservoirs were placed in a water bath maintained at the same temperature as the hydrostatic cell.

In a typical experiment, the assembled sample was placed into a hydrostatic cell and a confining stress was applied and held constant. The sample was then injected with carbon dioxide: as an initial condition, reservoirs and sample were equilibrated with CO_2 at an identical pressure. The upstream reservoir was then disconnected from the sample and fluid was added into the reservoir in order to increase the pressure in it. This upstream reservoir was then connected back to the upstream end of the sample and fluid pressures in the upstream and in the downstream reservoirs were recorded over time until equilibration. Equilibration would take at least two days, which was the time necessary for the fluid to get adsorbed in the coal matrix. The pressure in the upstream reservoir was then risen again to a new level, and a new measurement was carried out. In this study, the confining stresses ranged from 5.5 to 10 MPa and fluid pressures in the reservoirs varied from 0.5 to 6 MPa. These values were chosen to cover the range of conditions representative for a Sulcis coal seam at a 500 m depth. Two types of experiments were carried out: those in which the confining stress was kept constant and the fluid pressure in the reservoir was raised and those in which the same increment of fluid pressure was repeated at different levels of confining stress.

For the different experiments performed, we aim at comparing the variations of pressures measured experimentally in the upstream and downstream reservoirs with those predicted by our model. In order to do so, we perform 2D axisymmetric simulations of the experiments. The input parameters used for the model calculations are summarized in Table 4.1. Remaining required material properties, such as the coupling coefficient $C(p)$ or the tangent Biot coefficient $b_m^{tan}(p)$ are given in Section 3.3. The mesh used to simulate the above experiment is shown in Fig. 4.2. To perform the simulation, we choose values of permeability $k_{us} = 0.1$ mD for the upstream reservoir and $k_{ds} = 0.1$ mD for the downstream reservoir which are large compared to the value of permeability for the sample, which was on the order of 0.0001 mD. We consider no adsorptive properties for the reservoirs. All simulations of the transient step experiments are carried out at a temperature $T = 318.15$ K. The permeability of the sample is assumed to depend only on the porosity ϕ_c associated to the cleat system and to be governed by the Kozeny-Carman equation [Carman, 1937]. Practically, the permeability k is given by the following equation, in

which k_0 is the permeability in the state of reference:

$$\frac{k}{k_0} = \frac{\phi_c^3}{(1-\phi_c)^2} \times \frac{(1-\phi_{c0})^2}{\phi_{c0}^3} \tag{4.1}$$

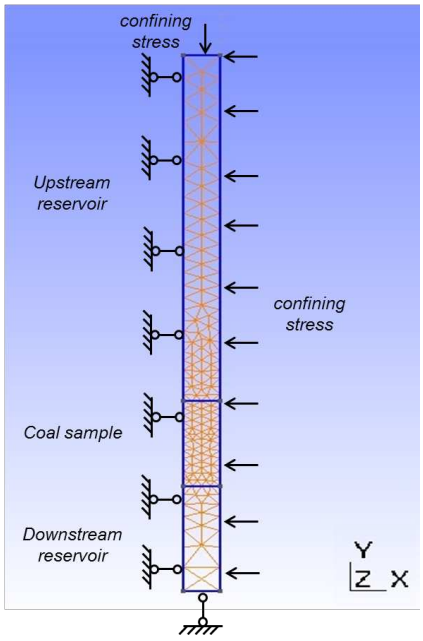

Figure 4.2 – Numerical model for the experiment performed by Mazzotti et al. [2009] to measure permeabilities of coal samples to carbon dioxide.

We perform both simulations of experiments in which the confining stress is kept constant and the fluid pressures are varied and of experiments in which the confining stress is varied. Figure 4.3 shows simulations for which the confining stress is varied between 5 and 10 MPa, whereas Fig. 4.4 reports a simulation of transient steps obtained when the confining stress is kept constant at 10 MPa. The symbols are the experimental data, whereas the solid lines correspond to numerical predictions of the model, obtained by fitting the permeability k_0 of the coal sample in the state of reference: $k_0 = 4.34 \times 10^{-4}$ mD. It is worth noting that the obtained permeability k_0 is much smaller than the one for typical coal beds measured in the field, which usually ranges between 1 and 10 mD [White et al., 2005]: it is possible that, given its centimetric size, the tested sample contained very few cleats.

Simulations of permeability experiments performed at various levels of confining stresses and comparison with experiments are displayed in Fig. 4.3. The agreement between experimental data and model predictions is very satisfactory at the two largest levels of confining stress (7.5 MPa and 10 MPa) but is not good at the lowest level of confining stress (5.5 MPa). This discrepancy is probably due to the fact that the confining stress can lead to a closure of microcracks: in other words, the presence of microcracks likely makes the coal sample behave nonlinearly in the elastic domain, while our model for a drained sample is linear elastic.

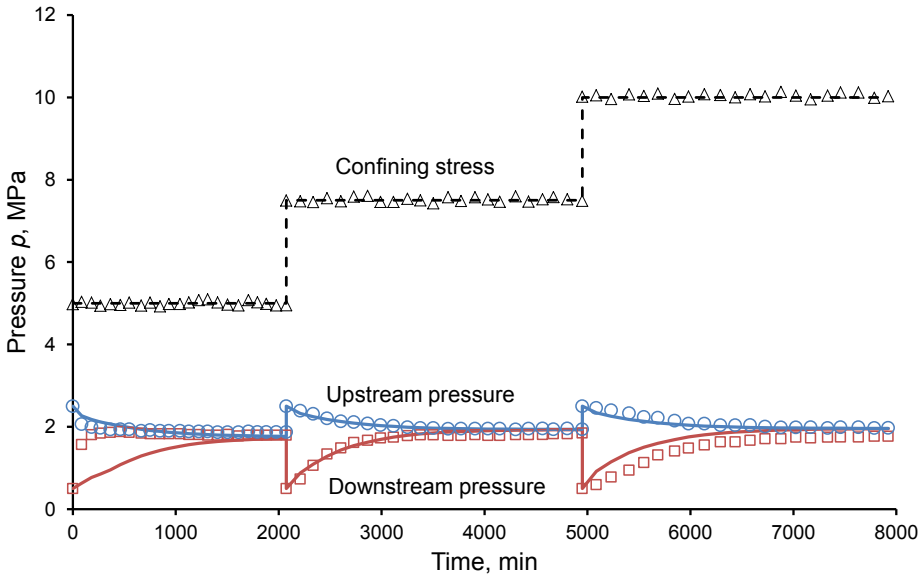

Figure 4.3 – Simulation of transient steps experiment performed at 318.15 K with CO_2 at various levels of confining stresses. Symbols correspond to experimental data by Mazzotti et al. [2009] and lines correspond to model results. Both the pressures in the upstream reservoir (○) and in the downstream reservoir (□) are represented.

For experiments performed at a constant level of confining stress (see Fig. 4.4), an excellent agreement is achieved between experiments and model predictions, which validates our model and its calibration. In particular, the model captures very well the fact that, at a given level of confining stress, the greater the pressure of the fluid, the smaller the time needed to reach equilibrium (see Fig. 4.4). Such a feature is due to the fact that a greater fluid pressure leads to a swelling of the sample, which translates into an increase of the cleat porosity and therefore of the permeability (see Fig. 4.5).

Now that we gained confidence in the quality of the predictions made possible by our calibrated model, the next sections are dedicated to study the effect of various parameters on the variations of permeability of a Representative Elementary Volume of fractured coal.

4.3 Representative Elementary Volume

This section is dedicated to simulations at the scale of a Representative Elementary Volume. We use our models calibrated on both Sulcis and Ribolla coal in order to study how the evolutions of permeability of a Representative Elementary Volume are affected by the boundary conditions (Section 4.3.1) and by the compressibility of the coal matrix (Section 4.3.2). In a last part (Section 4.3.3), we make our model more complex by explicitly considering the kinetics of transfer of fluid between the cleat system and the micropores of the coal matrix. The effect of this kinetics on the evolutions of permeability of the Representative Elementary Volume over time is discussed.

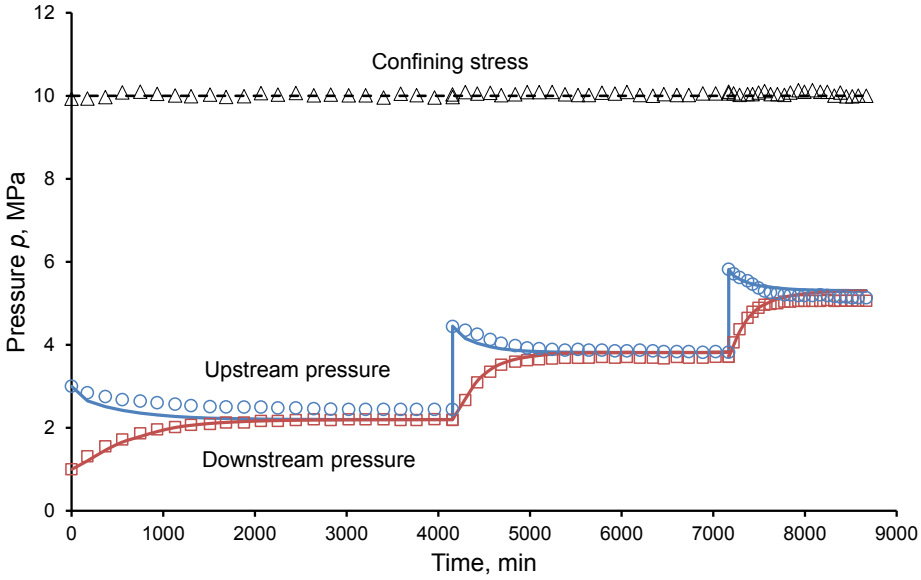

Figure 4.4 – Simulation of transient steps experiment performed at 318.15 K with CO_2 at a constant level of confining stress. Symbols correspond to experimental data by Mazzotti et al. [2009] and lines correspond to model results. Both the pressures in the upstream reservoir (○) and in the downstream reservoir (□) are represented.

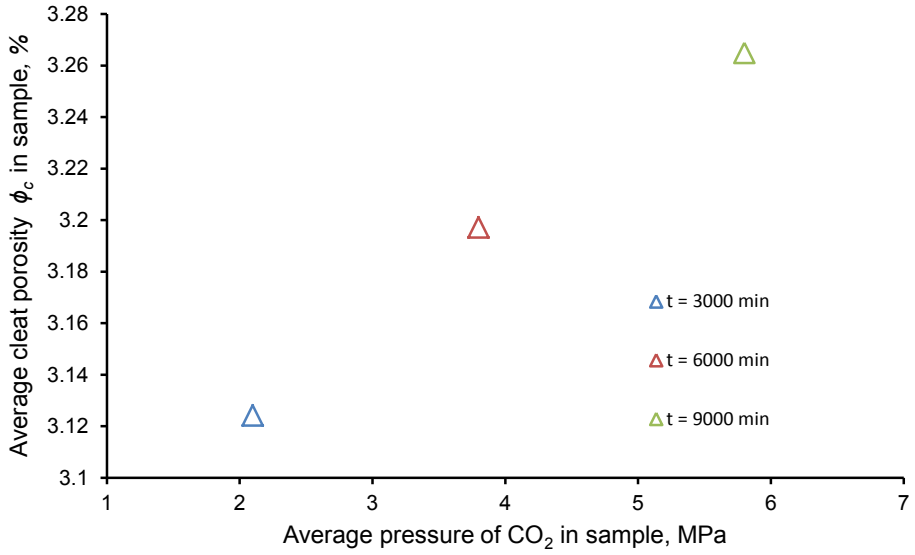

Figure 4.5 – Variations of the cleat porosity of the coal sample at 318.15 K with the CO_2 pressure at constant level of confining stress.

4.3.1 Effect of boundary conditions

We now consider two Representative Elementary Volumes, made of Sulcis and Ribolla coals, respectively. The model was calibrated for those two coals in Chapter 3. The general coal parameters are given in Table 3.4. We consider that the permeability of a Representa-

tive Elementary Volume is still governed by the Kozeny-Carman equation (4.1). For both coals, two types of boundary conditions are considered: either the volumetric confining stress is imposed (at levels of 4 MPa, 8 MPa, and 12 MPa), or the volume of the sample is kept constant (see Fig. 4.6). All simulations are performed on a Representative Elementary Volume, meaning that all state parameters are homogeneous within the sample.

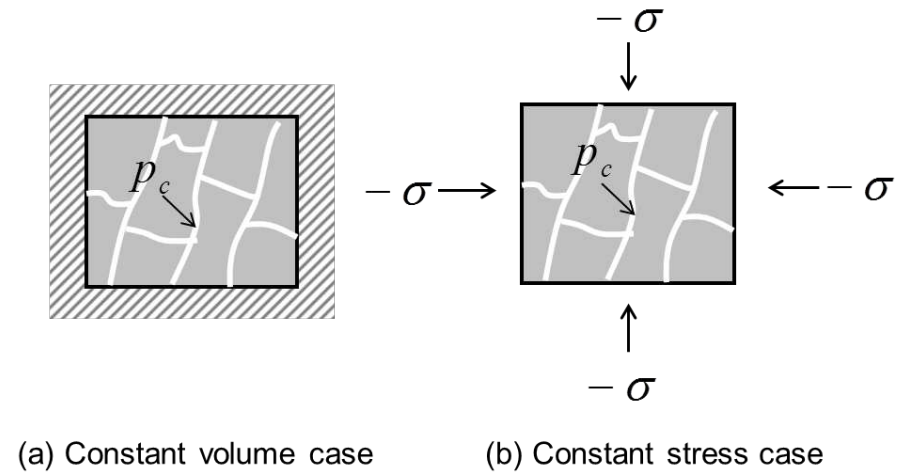

Figure 4.6 – Schematic diagram of applied boundary conditions: (a) constant volume case, for which the volume of the REV is kept constant throughout the process, and (b) constant stress case, for which the confining stress is kept constant throughout the process.

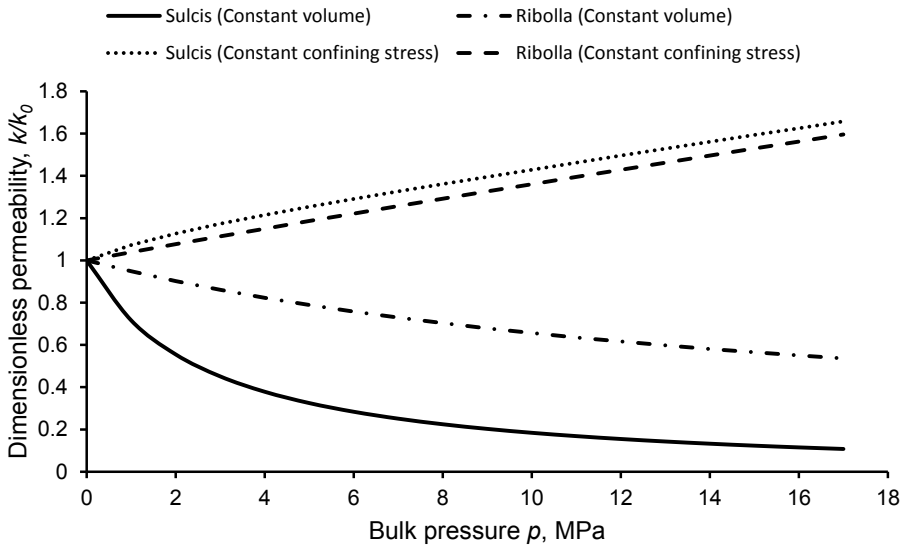

Figure 4.7 – Effect of boundary conditions on dimensionless permeability for Ribolla and Sulcis coal samples. For both Sulcis and Ribolla coals, imposing a confining stress of 4 MPa, 8 MPa, or 12 MPa yields identical results.

Figure 4.7 displays the dimensionless permeability for Ribolla and Sulcis coal samples for both types of boundary conditions. Because of adsorption, with an increasing fluid pressure the coal matrix swells. If the volume of the sample is kept constant, the swelling of the coal matrix leads to a closure of the cleat system: the cleats porosity, and therefore the permeability, decrease. For the coal which swells more (i.e., Sulcis), the porosity and the permeability decrease more with an increasing fluid pressure than for the coal which swells less (i.e., Ribolla). Fig. 4.7 also shows that, when the volumetric confining stress is imposed, increasing the pressure of the fluid increases the permeability of the sample. Such an enhancement of permeability is more pronounced for the coal which swells more. With our model, at a given level of confining stress, the adsorption-induced pressure leads to a homothetic swelling of the sample and thus to an increase of the cleats porosity. From a dry reference state, the swelling predicted by our model is independent of the level of confining stress. Therefore, as can be observed in Fig. 4.7, the variations of dimensionless permeability with fluid pressure are identical for confining stresses of 4 MPa, 8 MPa, and 12 MPa.

Comparing the case of an imposed confining stress with the case of an imposed volume shows that, depending on the boundary conditions, opposite trends can be observed: when the confining stress is fixed, the permeability readily starts increasing with the fluid pressure, while the permeability starts decreasing with the fluid pressure when the volume of the sample is fixed. Boundary conditions therefore play a tremendous role on adsorption-induced variations of permeability.

4.3.2 Effect of compressibility of coal matrix

We now aim at understanding the effect of matrix compressibility in the interpretation of experimental data on the variations of permeability of a Representative Elementary Volume injected with carbon dioxide. Like in the previous section, both a Representative Elementary Volume with a constant volume and a Representative Elementary Volume on which a constant confining stress is applied will be considered. As was explained in Sec. 3.4, the bulk modulus K_m of the coal matrix must verify $K_m \geq K/(1-\phi_{c0})$, where K is the bulk modulus of the reservoir and ϕ_{c0} is the cleat porosity in the state of reference. For the Sulcis coal sample, for which the cleat porosity is equal to 3.2%, this requirement translates into a Biot coefficient b_m that must be greater than 0.032. During the calibration of the model, we needed to assume the Biot coefficient b of the reservoir (see Sec. 3.3). By doing so, Eq. (2.49) shows that we imposed the ratio of the bulk modulus K of the reservoir to the bulk modulus K_m of the coal matrix. For a given bulk modulus K of the reservoir, another value for the Biot coefficient b thus implies another value for the bulk modulus K_m of the coal matrix: Eq. (3.8) shows that, as a consequence, the calibration of the model on the swelling data displayed in Fig. 3.6 will lead to a different coupling coefficient $C(p)$ and thus, through Eq. (2.77), to a different calibration for the adsorption-induced pressure $p^a(p)$.

Figure 4.8 displays the variation of permeability of a Sulcis coal sample kept at fixed volume for three values of matrix compressibility (i.e., for three Biot coefficients). One observes that, in a sample with a less compressible coal matrix (i.e., with a lower ratio K/K_m), the decrease of permeability with an increasing fluid pressure is more pronounced than in the sample with a more compressible coal matrix. Such a phenomenon

is due to the fact that, if the Biot coefficient is high (i.e., if $K_m \gg K$), the coal matrix is almost incompressible: in such a case, if the volume of the sample is kept constant, all swelling observed upon an increase of the pressure of the fluid will translate into a loss of pore volume. In contrast, if the Biot coefficient is low (i.e., if $K_m \sim K$), if the volume of the sample is kept constant, only part of the swelling observed upon an increase of the pressure of the fluid will translate into a loss of pore volume: therefore, in this latter case, the decrease of porosity and thus of permeability with an increasing pressure of carbon dioxide is less pronounced than if the Biot coefficient is high.

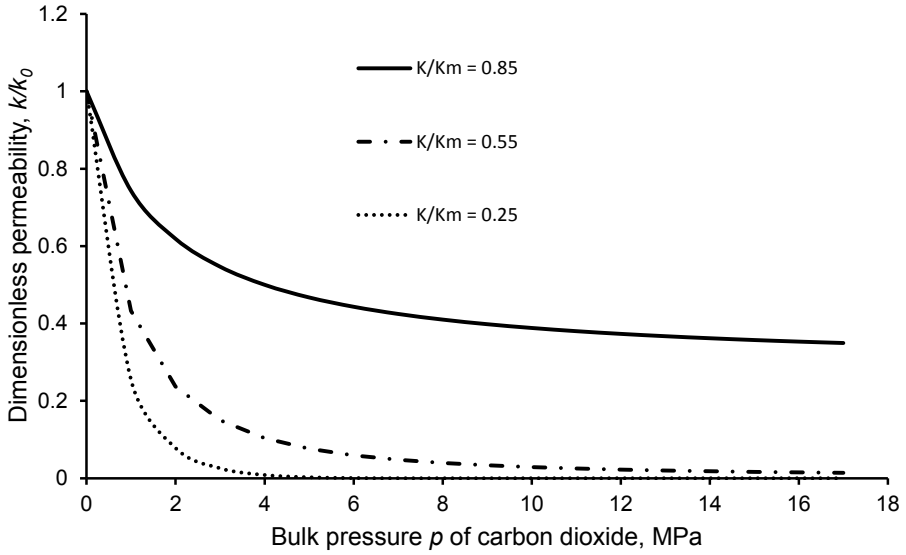

Figure 4.8 – Dimensionless permeability of a Representative Elementary Volume of Sulcis coal kept at constant volume and injected with carbon dioxide, for various ratios K/K_m of the bulk modulus K of the reservoir to the bulk modulus K_m of the coal matrix.

Figure 4.9 displays the variations of permeability of a Sulcis coal sample submitted to a given confining stress and injected with carbon dioxide, for three different values of matrix compressibility. We observe that, for a less compressible coal matrix (i.e., with a lower ratio K/K_m), the increase of permeability with an increasing pressure of carbon dioxide is more pronounced than in the coal with a more compressible coal matrix. Again, this is due to the fact that, if the coal matrix is compressible, only part of the swelling of the coal matrix translates into a swelling of the coal sample and thus into an increase of cleat porosity.

Therefore, the compressibility of the coal matrix plays a significant role on adsorption-induced variations of permeability.

4.3.3 Effect of kinetics of transfer of fluid between cleats and coal matrix

In the simulations performed up to now, we considered that the fluid in the cleats was in thermodynamic equilibrium with the fluid in the coal matrix. Assuming such a thermo-

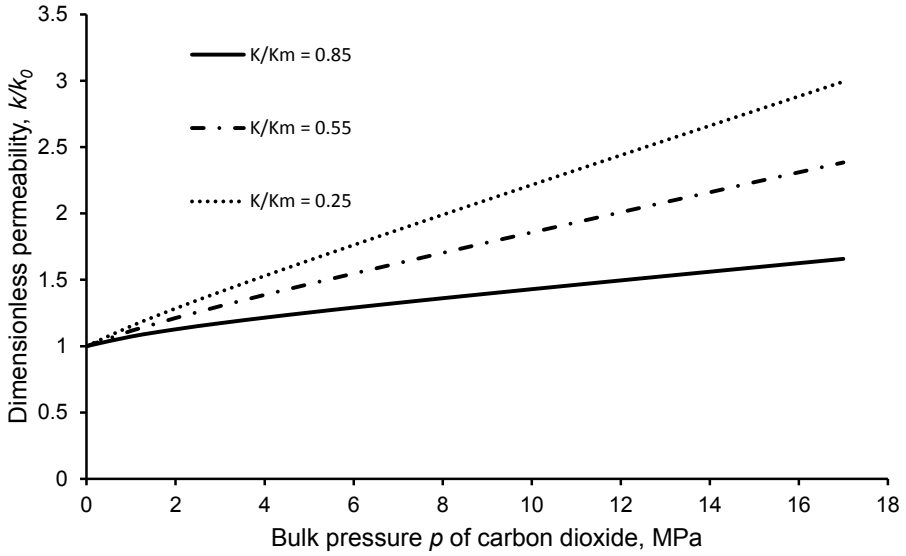

Figure 4.9 – Dimensionless permeability of a Representative Elementary Volume of Sulcis coal injected with carbon dioxide and submitted to a given confining stress, for various ratios K/K_m of bulk modulus K of the reservoir to the bulk modulus K_m of the coal matrix.

dynamic equilibrium is equivalent to assuming that the characteristic time of transfer of fluid between cleats and coal matrix is much smaller than any other characteristic time of interest. In this section, we aim at relaxing this assumption and studying the effect of this kinetic of transfer on the response of the Representative Elementary Volume.

In order to do so, we come back to the derivation of the constitutive equations performed in Sec. 2.4.1. For the sake of convenience, the pressure p_c in the cleats and the thermodynamic pressure p_m in the coal matrix were first considered to be independent, before being equated at the end of the derivation. We here recall the constitutive equations (2.59)-(2.62), for which the pressures p_c in the cleats and p_m in the coal matrix were still considered to be independent from each other:

$$\sigma = K\epsilon - bp_c - (1-b)p^a(p_m) \tag{4.2}$$

$$\varphi_c = b\epsilon + \frac{p_c - p^a(p_m)}{N} \tag{4.3}$$

$$n_m = n_0^{ads}(p_m)\left[1 - \phi_{c0} + C(p_m)\left[(1-b)\epsilon - \frac{p_c - p^a(p_m)}{N}\right]\right] \tag{4.4}$$

$$s_{ij} = 2Ge_{ij} \tag{4.5}$$

where p^a is the adsorption-induced pressure, now governed by the thermodynamic pressure p_m in the coal matrix. This set of equations is the one which we will use to study the effect of the kinetics of transfer of fluid between cleats and coal matrix for various boundary conditions. But, in order to do so, the equation that governs this transfer must be derived.

Using the mass balance equations [Coussy, 2004], two separate continuity equations for the fluid flowing through the cleat system and for the fluid flowing through the coal matrix are obtained:

$$\frac{\partial n_c}{\partial t} + \nabla.\underline{W}_c = -\mathring{n}_{c\to m} \tag{4.6}$$

$$\frac{\partial n_m}{\partial t} + \nabla.\underline{W}_m = \mathring{n}_{c\to m} \tag{4.7}$$

where n_c and n_m are the moles of fluid per unit volume in the cleats and in the coal matrix, respectively and where $\underline{W}_c$ and $\underline{W}_m$ are the relative vectors of the molar flow of fluid with respect to cleats and coal matrix, respectively. Those relative vectors of the molar flow of fluid are set to zero (i.e., $\nabla.\underline{W}_m = 0$ and $\nabla.\underline{W}_c = 0$). $\mathring{n}_{c\to m}$ stands for the rate of the moles of fluid per unit volume which flow from the cleats into the coal matrix and is considered to be given by Darcy's law [Darcy, 1856]:

$$\mathring{n}_{c\to m} = \beta(p_c - p_m) \tag{4.8}$$

so that the transfer is finally governed by:

$$-\frac{\partial n_c}{\partial t} = \frac{\partial n_m}{\partial t} = \beta(p_c - p_m) \tag{4.9}$$

where β is:

$$\beta = \frac{\rho k_m}{\mu l^2} \tag{4.10}$$

In Eq. (4.10), ρ is the molar density of the fluid, k_m is the intrinsic permeability of the coal matrix, μ is the viscosity of the fluid (The viscosity of the fluid is chosen equal to $\mu = 1.79 \times 10^{-5}$ Pa.s, which is the viscosity of carbon dioxide at a temperature $T = 318.15$ K and a pressure $p = 6$ MPa.) and l is the characteristic distance between cleats (in all simulations chosen equal to $l = 1$ cm). Dimensional analysis provides the characteristic time τ_d of diffusion in the coal matrix:

$$\tau_d = \frac{\mu l^2}{p_f k_m} \tag{4.11}$$

where p_f is a characteristic pressure of the fluid (in all simulations chosen equal to $p_f = 1$ MPa).

We perform simulations of a Representative Elementary Volume in which the pressure of the fluid in the cleats is increased from 0 MPa up to 17 MPa. The time needed to reach the maximal pressure is τ_l, so that the response of the Representative Elementary Volume is governed by the dimensionless ratio $\alpha = \tau_d/\tau_l$. Various ratios α ranging from 10^{-8} to 10^8 are considered. The simulations are performed for three types of boundary conditions (see Fig. 4.10): immersion, for which the confining stress is governed by the pressure

of the fluid (i.e., $\sigma = -p$), constant volume case, for which the volume of the REV is kept constant throughout the process (i.e., $\epsilon = 0$), and constant stress case, for which the confining stress is kept constant throughout the process (i.e., $\sigma =$ constant).

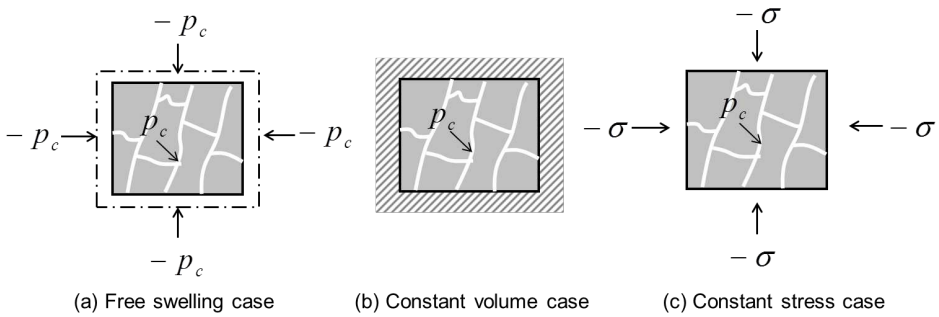

Figure 4.10 – Schematic diagram of applied boundary conditions: (a) immersion, for which the loading stress is governed by the pressure of the fluid, (b) constant volume case, for which the volume of the Representative Elementary Volume is kept constant throughout the process, and (c) constant stress case, for which the confining stress is kept constant throughout the process.

Figure 4.11 shows the variations of cleat porosity with CO_2 pressure in case of immersion. As is observed, the Representative Elementary Volume swells freely when the characteristic time τ_d of diffusion is much lower than the characteristic time τ_l of loading (i.e., for $\alpha = 10^{-8}$), which results from the fact that the permeabilty k_m of the coal matrix is so high that we can consider that there is a thermodynamic equilibrium between coal matrix and cleats ($p_m = p_c$). The greater the characteristic time τ_d of diffusion, the greater the difference between the pressure p_c in the cleats and the pressure p_m in the coal matrix, and thus the smaller the adsorption-induced pressure $p^a(p_m)$ and the cleat porosity ϕ_c. For large values of α, the cleat porosity decreases linearly with the pressure p_c of the fluid, as is the case for a regular linear elastic porous medium with one type of porosity: fluid has no time to invade the coal matrix. For intermediate values of α, the cleat porosity ϕ_c first decreases, following the trend observed for larger values of α, since fluid needs some time to diffuse into the coal matrix.

The case for which the deformation ϵ is set to zero is displayed in Fig. 4.12. If the permeabilty k_m of the coal matrix is high, i.e., when the diffusion takes places rapidly (i.e., $\alpha = 10^{-8}$), the cleat porosity ϕ_c decreases with the CO_2 pressure p_c in the cleats, as was observed in Fig. 4.7 in the case of thermodynamic equilibrium between cleats and coal matrix. In contrast, when the permeability k_m of the coal matrix is small (i.e., $\alpha = 10^8$), the cleat porosity ϕ_c increases linearly with the pressure in the cleats, as is expected for a regular porous medium with one type of porosity. For intermediate values of α, the cleat porosity ϕ_c first increases because fluid needs some time to diffuse into the coal matrix; for large times, the behavior observed at thermodynamic equilibrium (i.e., where $p_m = p_c$) is recovered.

The third case, corresponding to a Representative Elementary Volume subjected to a constant confining stress σ, is displayed in Fig. 4.13. When diffusion is very slow with respect to the time of loading (i.e., $\alpha = 10^8$), the cleat porosity ϕ_c increases linearly with the CO_2 pressure p_c in the cleats, as is expected for a regular porous medium with one

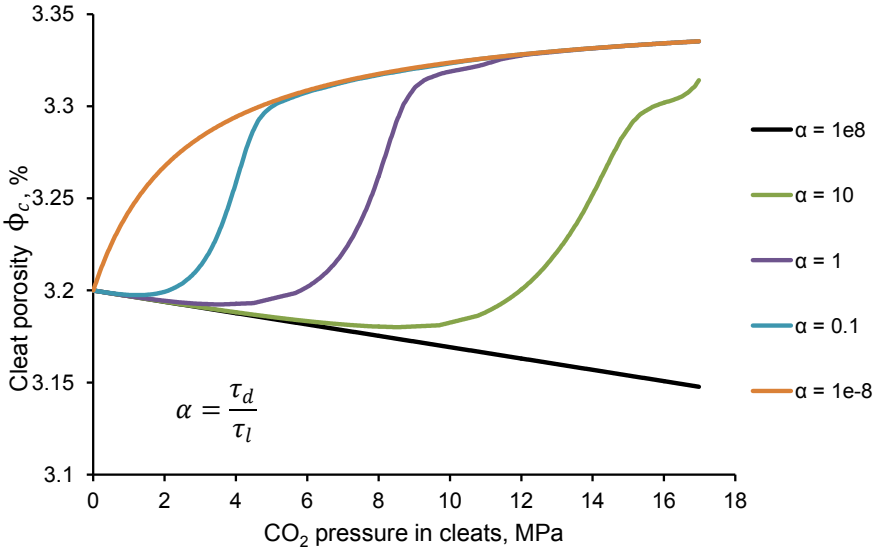

Figure 4.11 – Variation of cleat porosity of a Representative Elementary Volume of Sulcis coal immersed in a fluid with a pressure that increases linearly with time, for various ratios $\alpha = \tau_d/\tau_l$ of the characteristic time τ_d of diffusion to the characteristic time τ_l of loading.

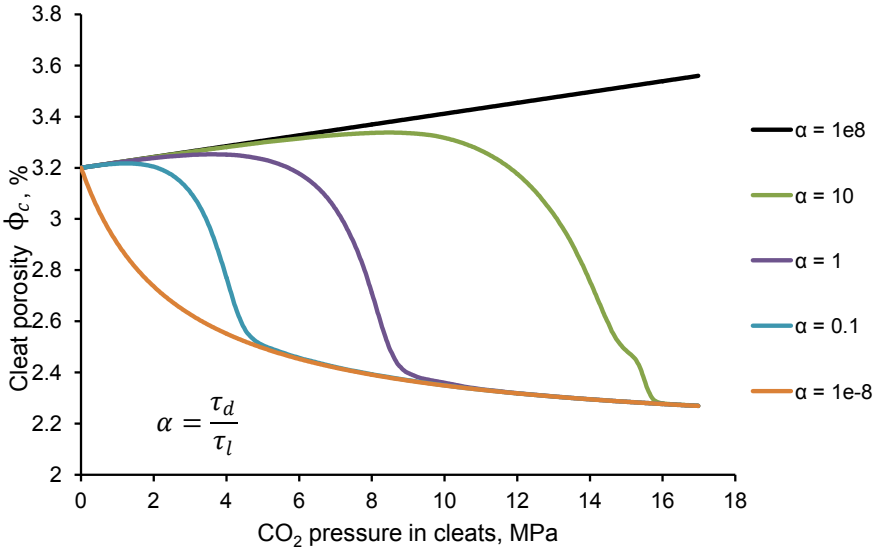

Figure 4.12 – Variation of cleat porosity of a Representative Elementary Volume of Sulcis coal the deformation ϵ of which is set to zero and subjected to a pore pressure in the cleats that increases linearly with time, for various ratios $\alpha = \tau_d/\tau_l$ of the characteristic time τ_d of diffusion to the characteristic time τ_l of loading.

type of porosity: fluid has no time to penetrate into the coal matrix. In contrast, for high values of the permeability k_m of the coal matrix (i.e., $\alpha = 10^{-8}$), the cleat porosity ϕ_c increases with the CO_2 pressure p_c in the cleats, as was observed in Fig. 4.7 in the case of thermodynamic equilibrium between the cleats and the coal matrix (i.e., $p_m = p_c$). Again, for intermediate values of α, the cleat porosity ϕ_c first follows the variations observed for small values of α (since fluid needs time to penetrate into the coal matrix) and then converges towards the values observed in the case of thermodynamic equilibrium.

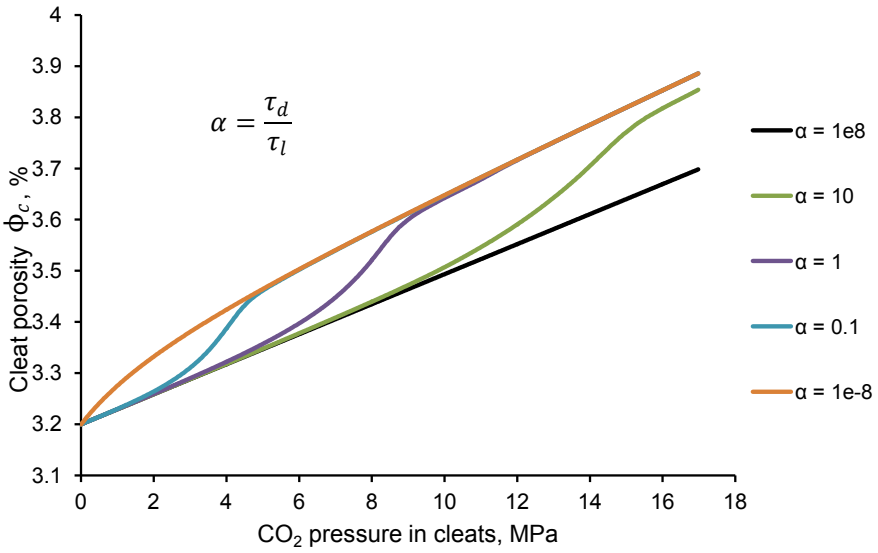

Figure 4.13 – Variation of cleat porosity of a Representative Elementary Volume of Sulcis coal subjected to a constant confining stress σ and to a pressure of fluid in the cleats that increases linearly with time, for various ratios $\alpha = \tau_d/\tau_l$ of the characteristic time τ_d of diffusion to the characteristic time τ_l of loading.

4.4 Primary recovery of coal bed methane (CBM)

Coal reservoirs are naturally fractured systems which contain methane. CO_2-enhanced coal bed methane recovery (CO_2-ECBM) involves the injection of CO_2 into a coal seam to promote the desorption of methane, while simultaneously storing CO_2 in the coal seam. In this section, we aim at performing the simulations of the primary recovery of coal bed methane (CBM). The total recovery process (CO_2-ECBM) will be discussed in the next chapter. We perform simulations of pure CH_4 recovery from a coal bed reservoir to investigate how adsorption and swelling take effect on the variations of permeability and production rate of CH_4.

Using the coal parameters for Ribolla and Sulcis coals, 1D simulations are performed. The input parameters are recalled in Table 4.2 and the calibration parameters $C(p)$ and $b_m^{tan}(p)$ for adsorption of pure CH_4 on Sulcis and Ribolla coal are given in Sec. 3.3. The performed simulations are axisymmetric plane-strain one-dimensional. The radius of the reservoir is set to 500 m, the radius of the bore hole is 10 cm. Before CH_4 production, the

Table 4.2 – Model input parameters of the coal seam for simulation of CBM production

Property	Definition	Value
T	Temperature, K	318.15
E	Young's modulus of coal seam, GPa	1.12
ν	Poisson's ratio of coal seam	0.26
ϕ_{c0}	Initial porosity of coal seam	0.032
k_0	Initial permeability of coal seam, mD	10
p_0	Initial pressure of CO_2, MPa	4
p_{pro}	Production pressure of pure CH_4, MPa	0.1
K	Bulk modulus of coal seam, GPa	0.78
b	Biot coefficient of coal seam	0.25
K_m	Bulk modulus of coal matrix, GPa	1.04
L	Radius of coal seam, m	500

initial methane pressure in the reservoir is considered to be equal to 4 MPa. Production pressure of 0.1 MPa is applied and kept constant over time. We impose zero displacement and no flow on the edge of reservoir. Permeability is given by Eq. (4.1). The pressure distribution at different times during the production from a reservoir made of Sulcis coal is displayed in Fig. 4.14: for CBM production without CO_2 injection, the pressure decreases continuously everywhere in the reservoir, until it reaches the pressure in the production well (see Fig. 4.14).

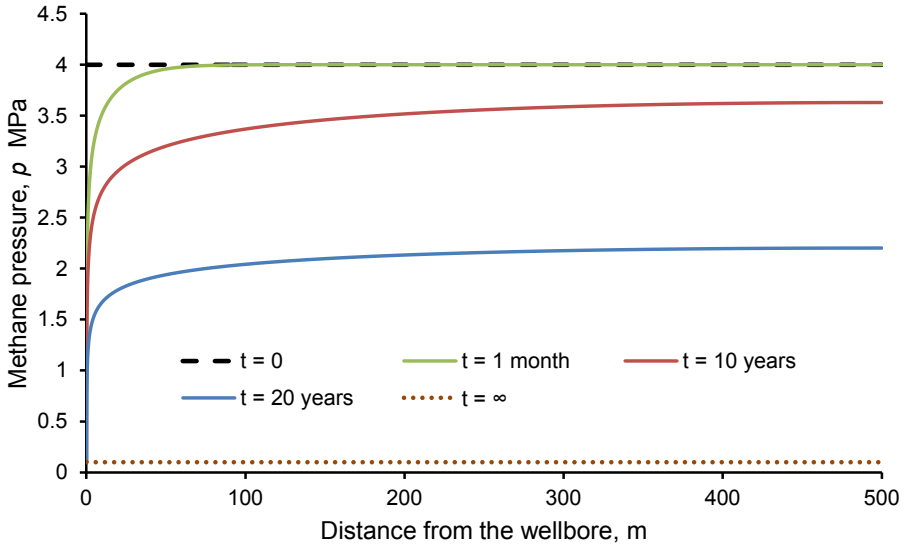

Figure 4.14 – CH_4 pressure in reservoir made of Sulcis coal at different times of the production process.

The rates of methane production calculated on reservoirs made of each coal are displayed in Fig. 4.15. The rate of production is very slightly lower for the reservoir made of Ribolla coal than for the reservoir made of Sulcis coal. Such a difference is due to the fact that Sulcis coal swells more than Ribolla coal in presence of pure methane (see Fig. 3.5): the shrinkage of the coal matrix upon CH_4 desorption leads to an opening of the cleat system, which itself leads to an increase of the production from the reservoir.

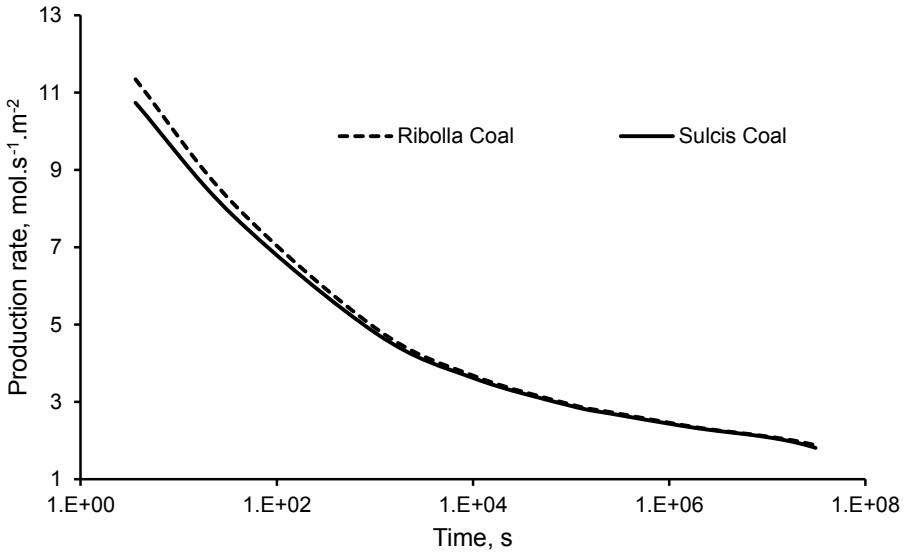

Figure 4.15 – CH_4 production rate of reservoirs made of Ribolla coal and of Sulcis coal.

Starting from this base case, in the next sections we will study the effect of various parameters on the behavior of the seam while producing methane. Those parameters are the compressibility of the coal matrix (Sec. 4.4.1) and the temperature of the seam (Sec. 4.4.2).

4.4.1 Effect of compressibility of coal matrix

This section is dedicated to study the effect of the compressibility of the coal matrix on the behavior of the seam. We restrict our discussion to a reservoir made of Sulcis coal since this coal exhibits larger swellings than Ribolla coal. During the calibration of the model, we needed to assume the Biot coefficient b of the reservoir (see Sec. 3.3). As already explained in Sec. 4.3.2, for a given bulk modulus K of the reservoir, another value for the Biot coefficient b implies another value for the bulk modulus K_m of the coal matrix, which as a consequence, leads to a different coupling coefficient $C(p)$ and to a different calibration for the adsorption-induced pressure $p^a(p)$.

Figure 4.16 displays the production rate and Fig. 4.17 displays the dimensionless permeability k/k_0 along the reservoir at different times of the coal bed methane production process, when the Biot coefficient b is set to 0.15 (and thus when $K/K_m = 0.85$), and when the Biot coefficient b is set to 0.75 (and thus when $K/K_m = 0.25$). With different Biot coefficients, significant differences are observed: the production rates are larger for

lower K/K_m, as a consequence of larger permeabilities. Such a behavior comes from a phenomenon already presented at the scale of a Representative Elementary Volume in Sec. 4.3.2. For the coal matrix which is almost incompressible (for which the Biot coefficient is high), most of its swelling translates into a loss of pore volume. Therefore, variations of permeability are more pronounced when the coal matrix is almost incompressible.

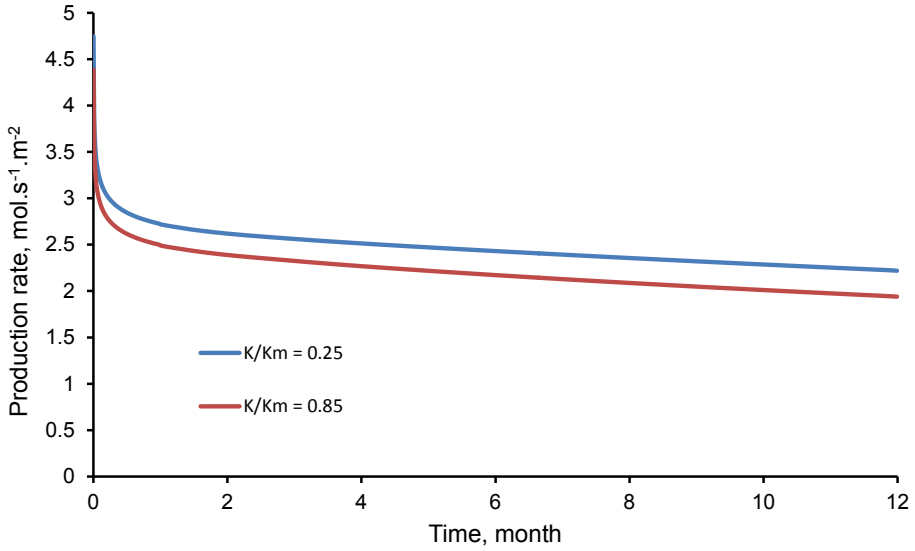

Figure 4.16 – Variations of production rate of CH_4 over a year for the reservoir made of Sulcis coal at various ratios K/K_m of the bulk modulus K of the reservoir to the bulk modulus K_m of the coal matrix.

4.4.2 Effect of temperature

In practice, coal seams can be located at various depths. As explained in Sec. 1.3.2, the depths of interest for ECBM applications are between 300 m and 2000 m. Among various parameters which will change with depth, one of the most important ones is the temperature. This part is dedicated to study the effect of temperature on the production process.

We consider that, during the process of the production of methane from the coal bed reservoir, the temperature remains constant and equal to the geothermal temperature. We select three temperatures: 33 °C, 45 °C, 60 °C. Assuming an average geothermal gradient of 25 °C.km^{-1} with a surface temperature of 15 °C, these temperatures cover the range of depths for which CO_2 storage in coal seams is considered to be feasible (i.e., between 750 and 2000 m). For the three geothermal temperatures considered, the equation of state of methane is displayed in Fig. 4.18. At those three temperatures, Pini et al. [2010a] measured experimentally the adsorption isotherms of CH_4 on Ribolla coal (see Table 4.4).

Now, we can simulate a coal seam to understand how the depth (i.e., the temperature) of the seam can affect the productivity of the reservoir. Using the coal parameters for

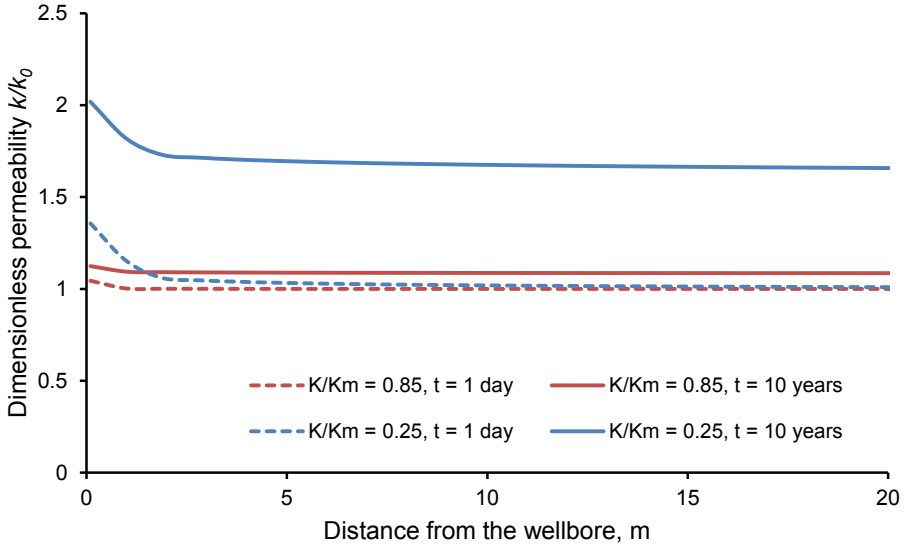

Figure 4.17 – Dimensionless permeability in the reservoir made of Sulcis coal during production of methane at different ratios K/K_m of the bulk modulus K of the reservoir to the bulk modulus K_m of the coal matrix.

Table 4.3 – Geothermal temperature at various depths of the coal bed reservoir.

Temperature, °C	**Depth, m**
33	750
45	1200
60	2000

Table 4.4 – Langmuir model parameters for CH_4 adsorption on Ribolla coal at three temperatures (33 °C, 45 °C, 60 °C). Data is from [Pini et al., 2010a]. The langmuir isotherm is given in Eq. (3.6).

Temperature	**33 °C**	**45 °C**	**60 °C**
n^{max} (mol.m^{-3})	2597.4	2539.9	2396.5
b_p (Pa^{-1})	1.21×10^{-3}	0.99×10^{-3}	0.87×10^{-3}

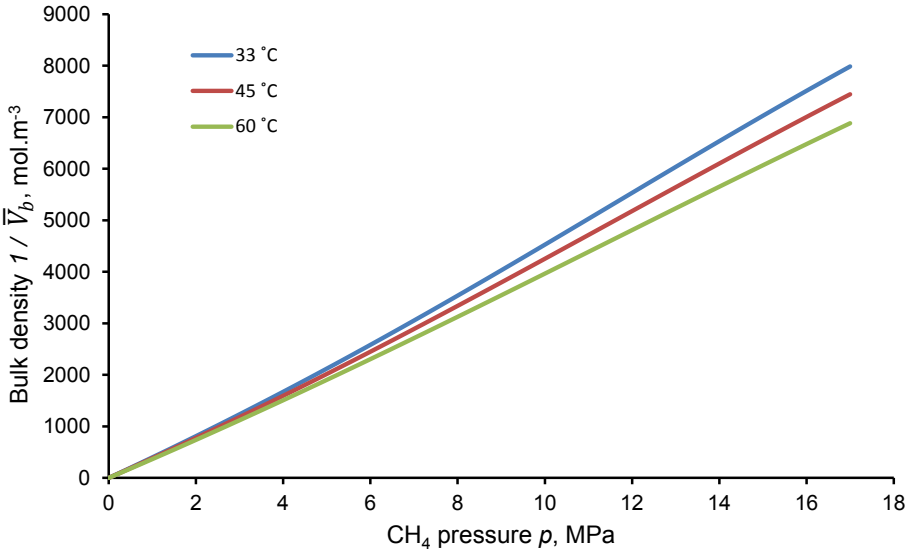

Figure 4.18 – Equation of state for CH_4 at various temperatures. The data is from NIST Chemistry WebBook (http://webbook.nist.gov/chemistry/).

Ribolla coal, 1D simulations are performed. We consider productions over a one-year period in a reservoir that initially contains methane at 4 MPa. The performed simulations are axisymmetric plane-strain one-dimensional. The radius of the reservoir is set to 500 m, the radius of the bore hole is 10 cm. Production pressures of 0.1 MPa are applied and kept constant over time. We impose zero displacement and no flow on the edge of the reservoir. We consider that the permeability in the reservoir is governed by Eq. (4.1).

Figure 4.19 shows the variations of production rate within a year for the three temperatures considered. The greater the temperature of the coal seam, the less pronounced the production rate of methane, which makes the process of producing methane less profitable. Such behavior is due to the facts that, with an increase of temperature, methane is less dense and adsorption of methane on coal decreases (see Table 4.4). The variations of fluid pressure in cleats with the distance from the wellbore after a year are displayed in Fig. 4.20. With an increase of temperature, the decrease of fluid pressure in the reservoir is less pronounced, as a consequence of the less pronounced adsorption of methane (see Table 4.4).

4.5 Injection of carbon dioxide in methane-free coal bed

In contrast to what was done in the previous section, in which we considered a production of methane from a coal bed reservoir, we now consider an injection of carbon dioxide into a coal bed reservoir. We restrict our numerical study to the hypothetical case in which all methane initially present in the reservoir would have been produced thanks to a former injection of carbon dioxide. Some CO_2 is therefore already present in the methane-free reservoir, and further injections of CO_2 are thus performed into a saturated medium. The aim of the numerical study is to investigate how adsorption and swelling

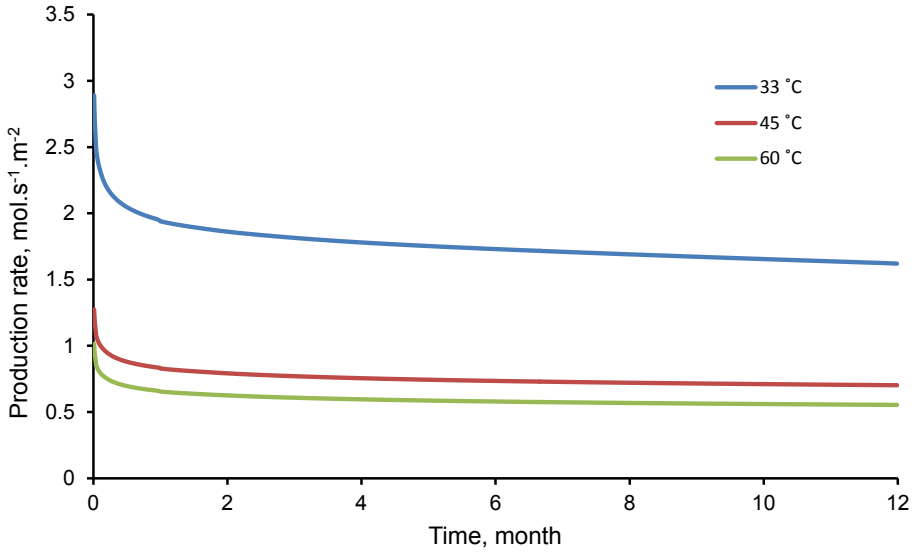

Figure 4.19 – Production rate of methane for coal bed reservoirs at various temperatures during a year of production.

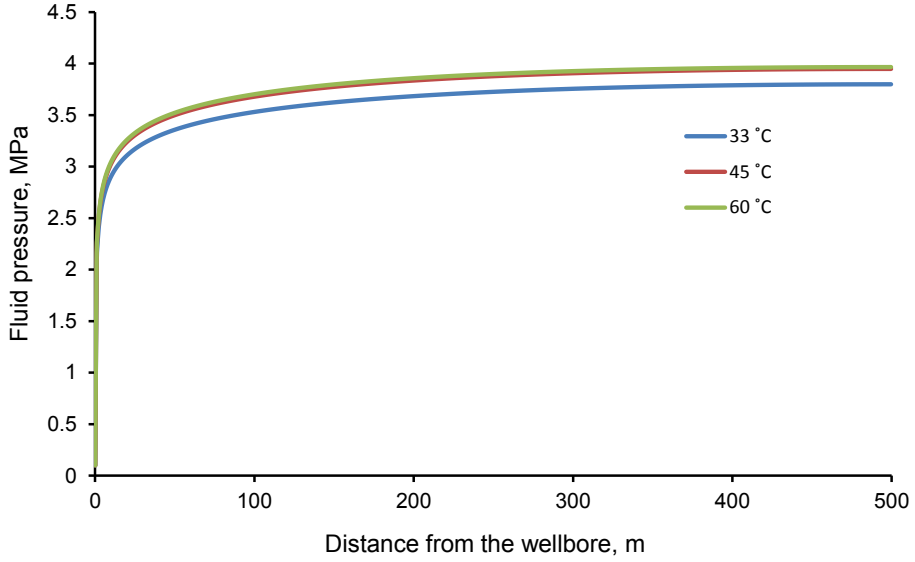

Figure 4.20 – Pressures of methane in coal bed reservoirs at various temperatures, after a year of production.

affect the variations of permeability and injectivity.

Using coal properties of Ribolla and Sulcis coals, 1D simulations are performed, again with the finite element and finite volume platform Bil. The material properties for Sulcis and Ribolla coal are given in Table 4.5, while their adsorptive properties (among which $C(p)$ and $b_m^{tan}(p)$) in presence of pure CO_2 are given in Sec. 3.3.

Table 4.5 – Model input parameters for simulation of methane-free coal seam injected with carbon dioxide.

Property	Definition	Value
T	Temperature, K	318.15
E	Young's modulus of coal seam, GPa	1.12
ν	Poisson's ratio of coal seam	0.26
ϕ_{c0}	Initial porosity of coal seam	0.032
k_0	Initial permeability of coal seam, mD	10
p_0	Initial pressure of CO_2, MPa	1
p_{inj}	Pressures of injection of CO_2, MPa	8, 10, 12
K	Bulk modulus of coal seam, GPa	0.78
b	Biot coefficient of coal seam	0.25
K_m	Bulk modulus of coal matrix, GPa	1.04
L	Radius of coal seam, m	500

We consider injections of CO_2 over a one-year period into a methane-free reservoir in which the initial pressure of CO_2 is equal to 1 MPa. The performed simulations are axisymmetric plane-strain one-dimensional. The radius of the reservoir is set to 500 m, and the radius of the bore hole is 10 cm. Injection pressures of 8, 10, and 12 MPa are applied and kept constant over time. We impose zero displacement and no flow on the edge of reservoir. We consider that the permeability in the reservoir is governed by the Kozeny-Carman equation (4.1), in which only the cleat porosity intervenes.

The rates of injection calculated for the two reservoirs at the three pressures of injection are displayed in Fig. 4.21. For both reservoirs, as expected, the higher the injection pressure, the higher the rate of injection. The decrease of the rate of injection over time is more significant for the reservoir made of Sulcis coal than for the reservoir made of Ribolla coal. Such a difference is due to the fact that Sulcis coal swells more than Ribolla coal in presence of carbon dioxide (see Fig. 3.5): the swelling of the coal matrix leads to a closure of the cleat system, which itself leads to a decrease of the injectivity of the reservoir. Figure 4.22 displays the volumetric strains in the two reservoirs at various times during the injection process. Close to the wellbore, as soon as the injection starts, a swelling is observed. Then, over the injection process, the region in which a swelling is observed extends from the wellbore toward the edge of the reservoir: this extension accompanies the penetration of carbon dioxide in the reservoir. Due to the boundary conditions used, the adsorption-induced swelling close to the wellbore leads to a compressed coal far from the wellbore, i.e., near the edge of the reservoir. Variations of volume are

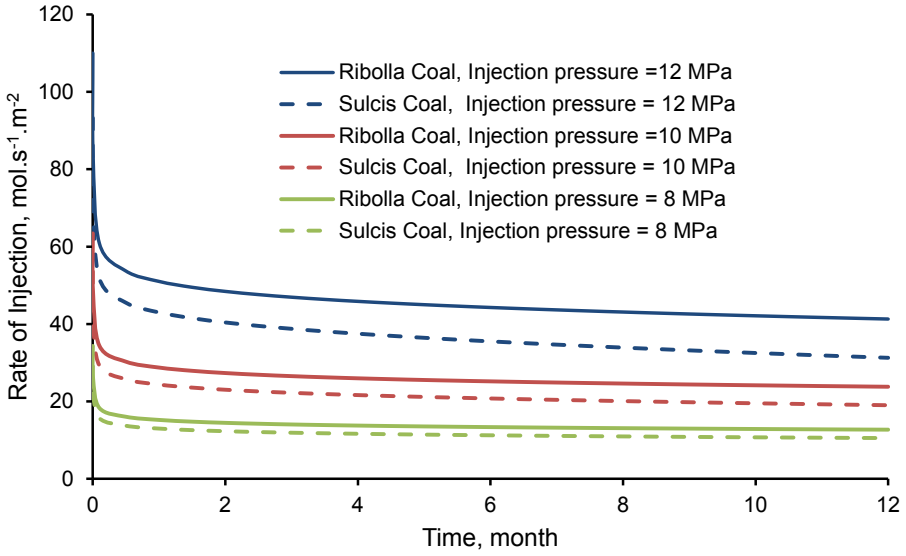

Figure 4.21 – Injectivity of reservoirs made of Ribolla coal and of Sulcis coal with pure CO_2 injected at three different pressures of injection.

more pronounced into the reservoir made of Sulcis coal than in the reservoir made of Ribolla coal, as a direct consequence of the fact that Sulcis coal swells more in presence of carbon dioxide than Ribolla coal.

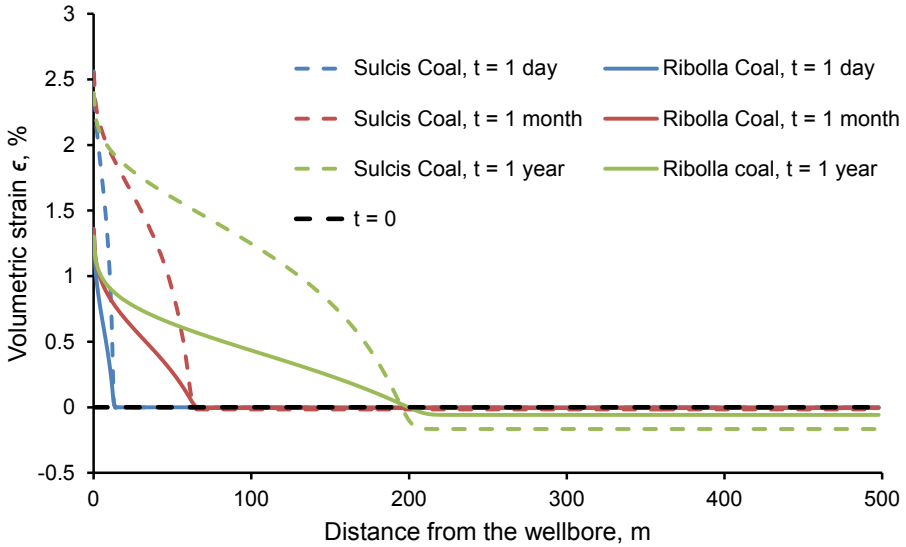

Figure 4.22 – Volumetric strains at various times over the injection process in reservoirs made of Sulcis and Ribolla coals.

Starting from this base case, in the next sections we will study the effect of various parameters on the behavior of the seam while injecting CO_2. Those parameters are the boundary conditions (Sec. 4.5.1), the compressibility of the coal matrix (Sec. 4.5.2), and

the kinetics of transfer of fluid between cleats and coal matrix (Sec. 4.5.3).

4.5.1 Effect of boundary conditions

Here we perform 2D simulations of a coal seam under various boundary conditions: a coal seam located between layers of deformable and permeable sandstones, a coal seam whose thickness is kept constant, and a coal seam to which constant confining vertical stresses are applied. The various types of boundary conditions are displayed in Fig. 4.23.

We only consider a coal seam made of Sulcis coal. The performed simulations of pure CO_2 injection are axisymmetric and two-dimensional. The material properties for Sulcis coal in presence of CO_2 are given in Tables 3.2 and 3.3 and in Sec. 3.3. The radius of the wellbore of injection of pure CO_2 is 0.1 m. The thickness of the simulated coal seam is 13 m, its radius is 200 m. The pressure at which the CO_2 is injected is kept at 6 MPa. The parameters of the coal seam and of the sandstone parameters are summarized in Table 4.6. We consider that the sandstone is less permeable than the coal seam (see Table 4.6).

Table 4.6 – Model input parameters of 2D simulations of a coal seam under various boundary conditions.

Property	Definition	Value
T	Temperature, K	318.15
E_{co}	Young's modulus of coal seam, GPa	1.12
E_{sa}	Young's modulus of sandstone, GPa	6.62
ν_{co}	Poisson's ratio of coal seam	0.26
ν_{sa}	Poisson's ratio of sandstone	0.33
ϕ_{c0}	Initial porosity of coal seam	0.032
ϕ_{s0}	Porosity of sandstone	0.02
k_{0co}	Initial permeability of coal seam, mD	10
k_{0sa}	Initial permeability of sandstone, mD	1
p_0	Initial pressure of CO_2, MPa	1
p_{inj}	Injection pressure of pure CO_2, MPa	6
K_{co}	Bulk modulus of coal seam, GPa	0.78
K_{sa}	Bulk modulus of sandstone, GPa	4.6
b_{co}	Biot coefficient of coal seam	0.25
b_{sa}	Biot coefficient of sandstone	0.69
K_m	Bulk modulus of coal matrix, GPa	1.04
L	Length of coal seam, m	200
D	Thickness of coal seam, m	13
Z	Depth of coal seam, m	500

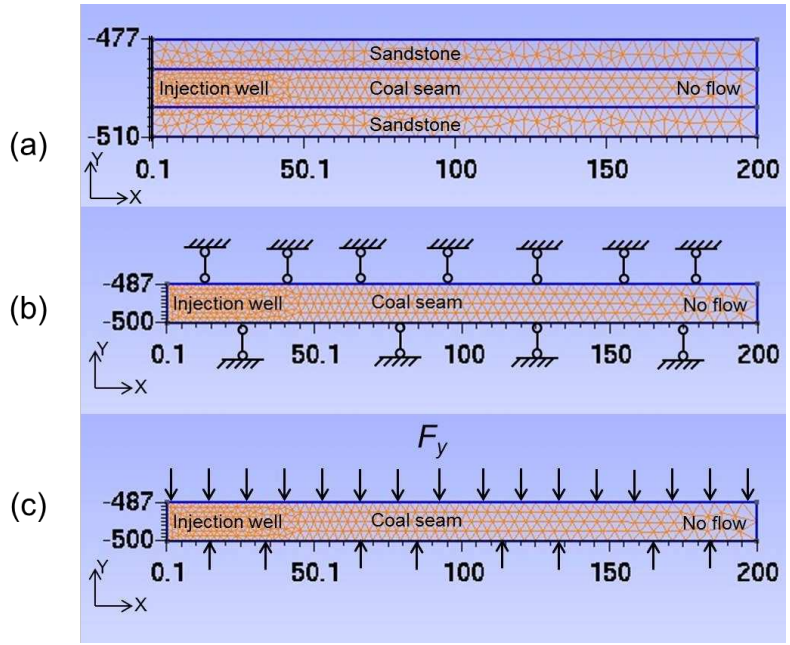

Figure 4.23 – Various types of boundary conditions used for simulating an injection of carbon dioxide into a methane-free coal bed reservoir: (a) coal seam located between sandstone layers, (b) coal seam with constant thickness, (c) coal seam under constant vertical confining stress.

Figure 4.24 shows the distribution of pressure of fluid in the coal seam and in the surrounding sandstone layers at various times of the injection process. We can see that the CO_2 front progresses initially more rapidly in the sandstones than in the coal seam. Such a behavior comes from the swelling of the coal matrix which in turn closes the apertures of cleats and reduces the permeability of coal. After about a year, the pressure of the fluid equilibrates in both the coal seam and the sandstone layers.

Figure 4.25 displays both the rate of injection of CO_2 in the seam (Fig. 4.25a) and the average amount of CO_2 in the seam per unit volume of the seam (Fig. 4.25b). One observes that, at equilibrium, the amount of CO_2 stored in the seam depends moderately on the boundary conditions (see Fig. 4.25b). Similarly, the rate of injection varies moderately with the type of boundary condition used. However, this rate of injection is the lowest when the thickness of the seam is imposed: indeed, as was observed for a Representative Elementary Volume in Sec. 4.3.1, in such a case, any swelling of the coal matrix translates into a decrease of the cleats porosity and thus of the permeability. In contrast, this rate is the highest when the vertical confining stress applied to the seam is kept constant: indeed, as was again observed on a Representative Elementary Volume in Sec. 4.3.1, in such a case any swelling of the coal matrix translates into an increase of the cleats porosity and thus of the permeability.

In conclusion, we observed in this section that the boundary conditions have moderate influence on the amount of CO_2 and on the kinetics of the process of injection.

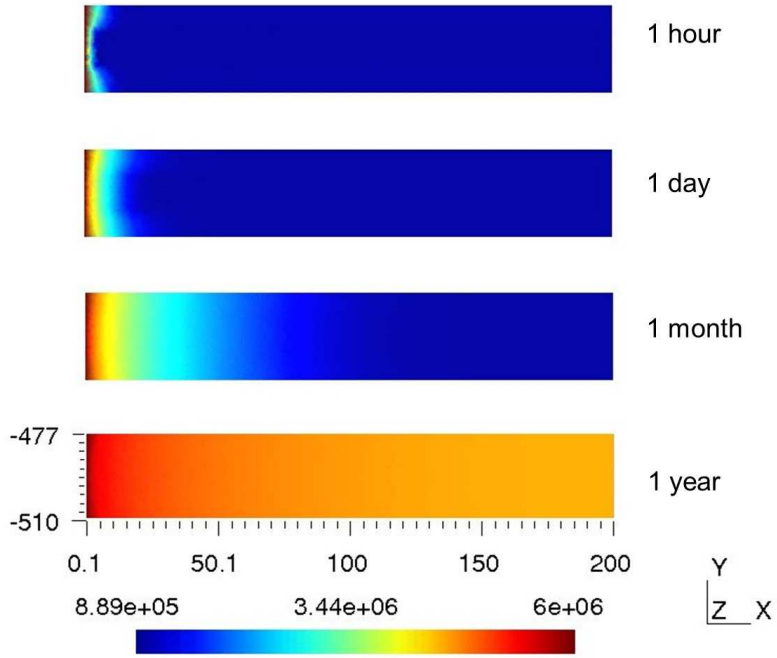

Figure 4.24 – Distribution of CO_2 pressure in a coal seam and in surrounding sandstone layers at various times of the injection process.

4.5.2 Effect of compressibility of coal matrix

In this section, we discuss the effect of the bulk modulus of the coal matrix on the injection rate. This discussion is restricted to the reservoir made of Sulcis coal, which is the coal that exhibits the larger swellings. During the calibration of the model, we needed to assume the Biot coefficient b of the reservoir. As already explained in Sec. 4.3.2, another choice for this Biot coefficient leads to a different coupling coefficient $C(p)$ and to a different calibration for the adsorption-induced pressure $p^a(p)$.

Figure 4.26 displays the dimensionless permeability k/k_0 along the reservoir at various times of the injection process, when the Biot coefficient b is set to 0.25 (and thus when $K/K_m = 0.75$), and when the Biot coefficient b is set to 0.8 (and thus when $K/K_m = 0.2$). We observe that the Biot coefficient has a significant effect on how the permeability evolves over time: in the reservoir with a larger Biot coefficient, the decrease of permeability is more pronounced than in the reservoir with a smaller Biot coefficient. Such a behavior comes from a phenomenon already explained at the scale of a Representative Elementary Volume in Sec. 4.3.2: if the Biot coefficient is high, most swelling of the coal matrix translates into a loss of pore volume while, if the Biot coefficient is low, only part of this swelling translates into a loss of pore volume. Therefore, variations of porosity and thus of permeability are more pronounced when the Biot coefficient is low than when it is high. In terms of rate of injection (see Fig. 4.27), such variations make the injection of CO_2 slower in the reservoir with a less compressible coal matrix than in the reservoir with a more compressible coal matrix.

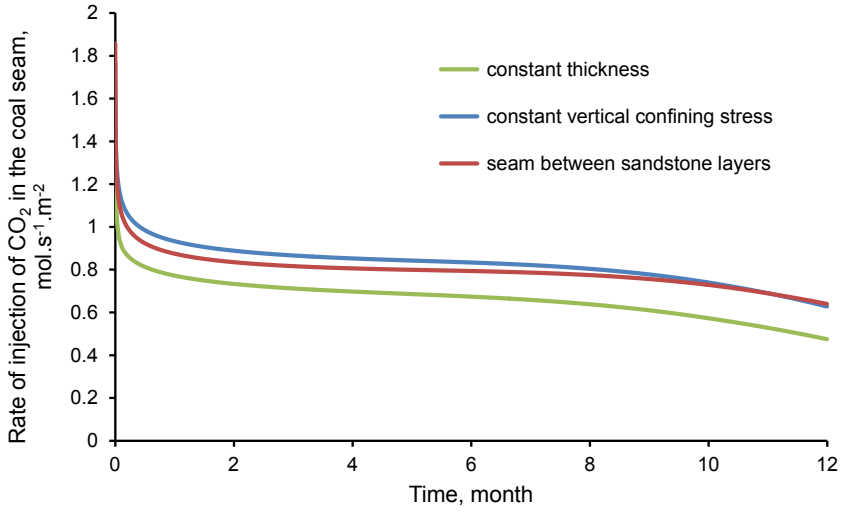

(a)

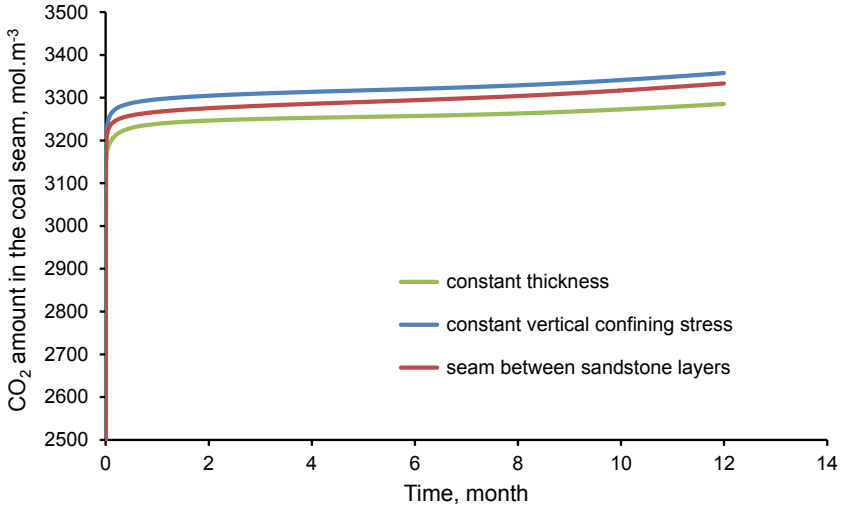

(b)

Figure 4.25 – (a) Rate of injection in the coal seam and (b) Average amount of CO_2 per unit volume of the seam for various boundary conditions: seam between two sandstone layers, seam to which a constant vertical confining stress is applied, and seam with a constant thickness.

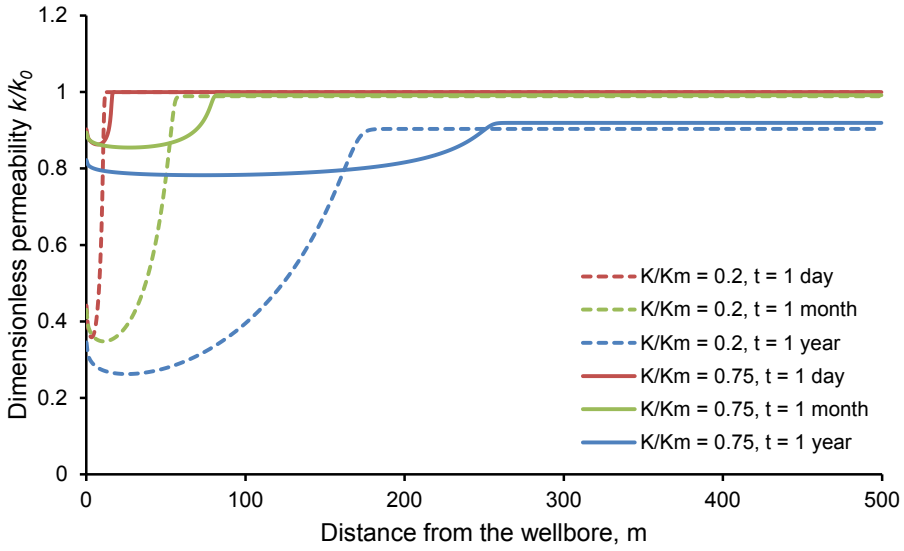

Figure 4.26 – Dimensionless permeability along the reservoir made of Sulcis coal for various ratios K/K_m of the bulk modulus K of the reservoir to the bulk modulus K_m of the coal matrix.

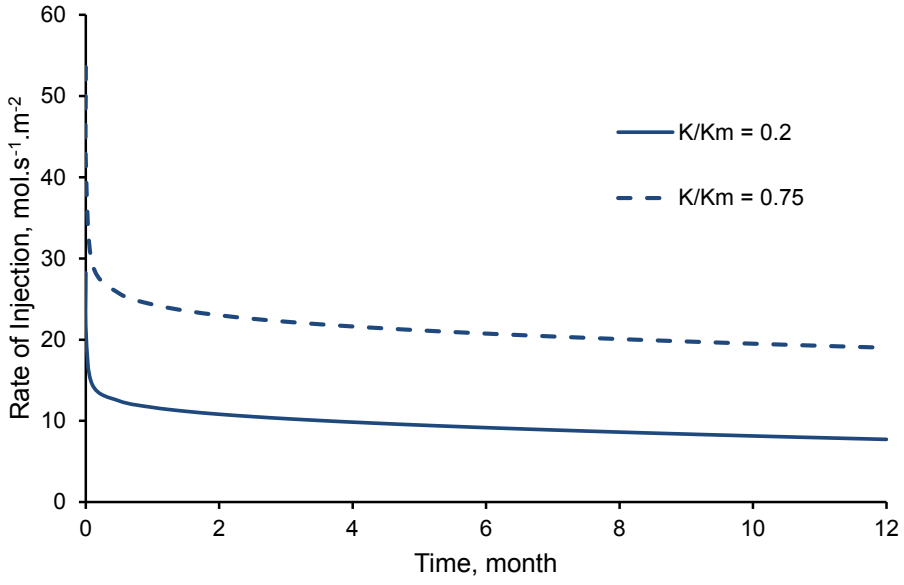

Figure 4.27 – Injection rates of CO_2 into the reservoir made of Sulcis coal for various ratios K/K_m of the bulk modulus K of the reservoir to the bulk modulus K_m of the coal matrix.

4.5.3 Effect of kinetics of transfer of fluid between cleats and coal matrix

Up to now, reservoir simulations were performed by considering that cleats and coal matrix were in thermodynamic equilibrium. In contrast, in this section, we aim at performing reservoir simulations by explicitly taking into account this transfer. In order to do so, we use the set of constitutive equations (4.2)-(4.5) derived in Sec. 4.3.3. Again we perform simulations of pure CO_2 injection at 10 MPa in a reservoir made of Sulcis coal, the parameters of which were given in Chapter 3 and recalled in Table 4.5. We consider injections over a one-year period in a reservoir that initially contained pure carbon dioxide only at a pressure of 1 MPa. The performed simulations are axisymmetric plane-strain one dimensional. The radius of the reservoir is set to 500 m, the radius of the bore hole is 10 cm. We impose zero displacement and no flow on the edge of reservoir. Permeability is given by Eq. (4.1).

Figure 4.28 displays the variations of fluid pressure p_c in the cleats of the reservoir versus the distance from the wellbore after a month of injection. Data is displayed for various characteristic times τ_d of diffusion: $\tau_d = 0$ s, which corresponds to the case where cleats and coal matrix are always in thermodynamic equilibrium (i.e., $p_c = p_m$); a characteristic time τ_d that tends toward infinity, which corresponds to the case $p_m = 0$; a characteristic time τ_d which, with the viscosity $\mu = 1.79 \times 10^{-5}$ Pa.s for CO_2 and a centimetric spacing of the cleats, corresponds to a permeability $k_m = 10^{-8}$ mD of the coal matrix.

On this figure 4.28, one observes that, the greater the characteristic time τ_d of diffusion, the faster the front progresses in the seam: indeed, for larger τ_d, swelling happens later, so that the fluid has more time to penetrate.

Figures 4.29 and 4.30 display the pressure p_m in the coal matrix and the amount n_m of fluid in the coal matrix after a month of injection for various characteristic times τ_d of diffusion, respectively. Close to the wellbore, the amount of fluid and the pressure in the coal matrix increase with a decreasing characteristic time τ_d of diffusion, since a smaller value of τ_d enables the fluid to penetrate faster in the coal matrix. In contrast, far from the wellbore (above 150 m from the wellbore on Fig. 4.30), there is more fluid in the matrix for an intermediate value of τ_d than for either very large or very small values of τ_d, since the characteristic time τ_d needs to be low enough in order to allow a penetration of fluid into the matrix, but needs to be not too low in order for the front of fluid to have penetrated far enough from the wellbore.

For the various cases, figure 4.31 shows nonmonotonic variations of the permeability of the seam with the distance from the wellbore. Such phenomenon is due to two competing effects: on one hand the increase of the pressure of fluid in the cleats increases the permeability (see Fig. 4.28), while on the other hand the increase of the pressure of fluid in the coal matrix leads to a swelling and to a decrease of permeability.

We finally show in Fig. 4.32 the variations of injectivity over a year for the various characteristic times τ_d of diffusion. The greater the characteristic time τ_d of diffusion, the more pronounced the loss of injectivity in the reservoir. Those variations of rate of injection result also from a competition: on one hand, for smaller values of τ_d, swelling happens faster and the permeability of the reservoir is smaller (see Fig. 4.31), which tends to lower the rate of injection; but on the the other hand, smaller values of τ_d lead to faster

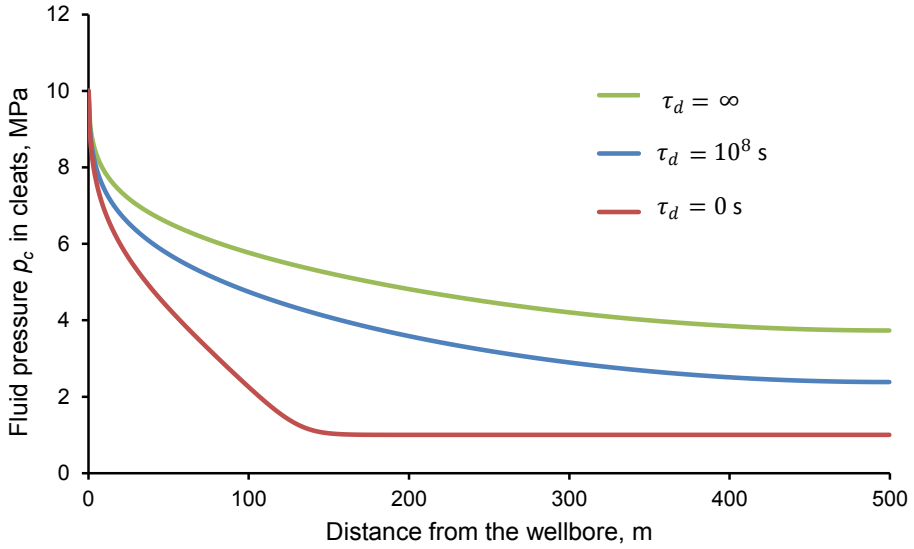

Figure 4.28 – Pressure of fluid in cleats after a month of injection for various characteristic times τ_d of diffusion.

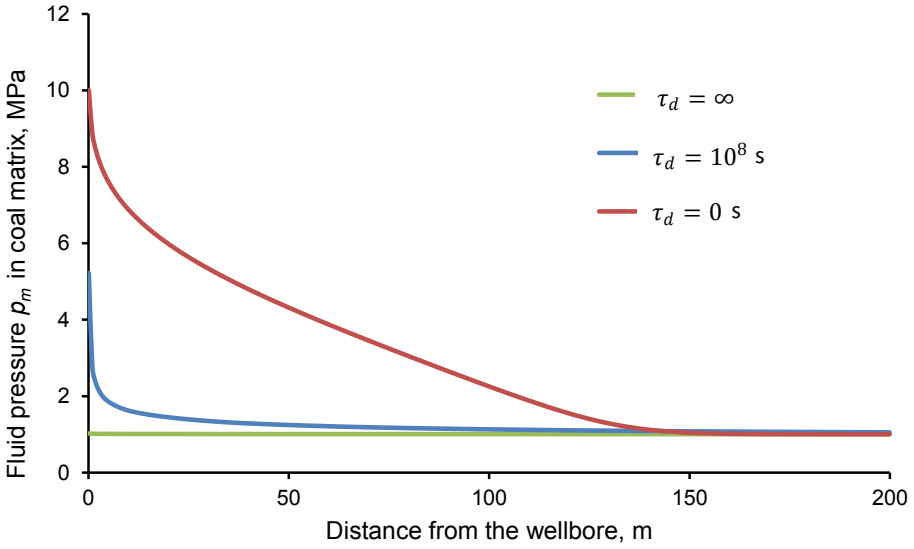

Figure 4.29 – Pressure of fluid in coal matrix after a month of injection for various characteristic times τ_d of diffusion.

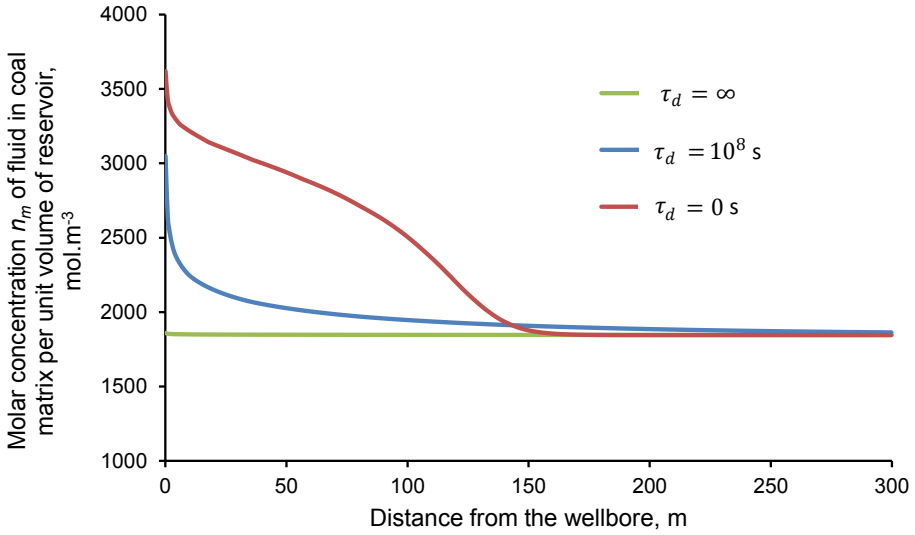

Figure 4.30 – Molar concentration n_m of fluid in coal matrix per unit volume of reservoir after a month of injection for various characteristic times τ_d of diffusion.

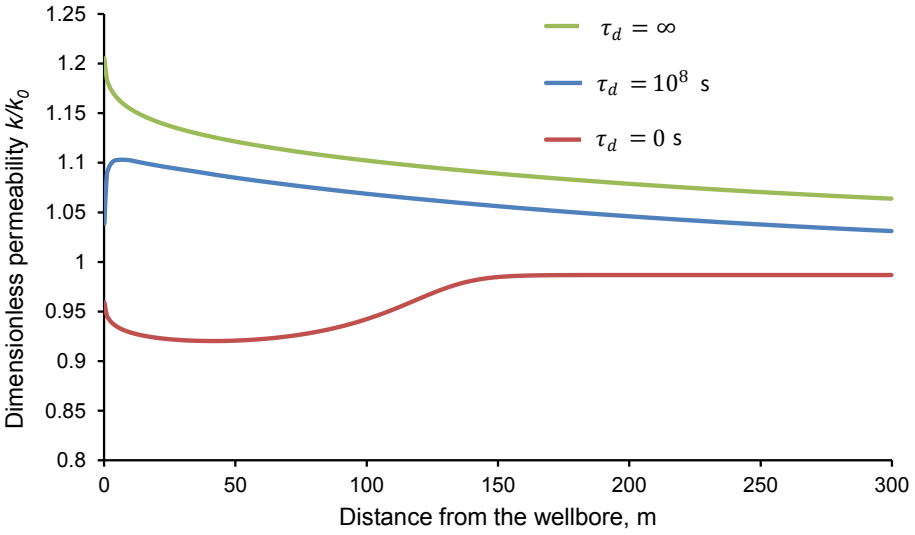

Figure 4.31 – Dimensionless permeability in the reservoir after a month of injection for various characteristic times τ_d of diffusion.

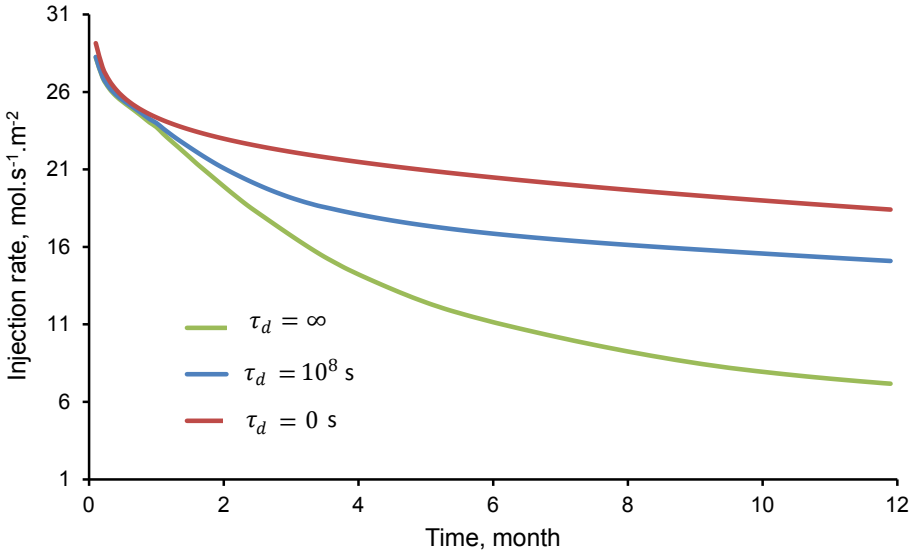

Figure 4.32 – Variations of injectivity of carbon dioxide over a year for various characteristic times τ_d of diffusion.

adsorption in the coal matrix, which provides additional accessible pore volume and tends to increase the amount of fluid that is injected in a given period of time.

In conclusions, the kinetics of transfer of fluid between cleats and coal matrix have a very significant impact on the kinetics of the injection process.

The simulations whose results are displayed on Figs. 4.28 to 4.32 were also performed for a characteristic time τ_d of diffusion equal to $\tau_d = 4.11 \times 10^3$ s:, for a spacing between cleats of 1 cm, this characteristic time corresponds to a permeability $k_m = 4.34 \times 10^{-4}$ mD of the coal matrix, which is the value back-calculated in Sec. 4.2 from the permeability experiments performed by Pini. Results obtained with such a value for τ_d coincide with results obtained with $\tau_d = 0$, i.e., when assuming thermodynamic equilibrium between cleats and coal matrix. Therefore, for the reservoir and the profile of injection of interest, it appears that assuming an infinitely fast transfer of fluid between cleats and coal matrix is a very reasonable assumption.

4.6 Conclusion

In this section, simulations at various scales (scale of a Representative Elementary Volume, scale of a coal sample, and scale of a reservoir) have been performed. As inputs to these simulations, we used the calibrated constitutive equations of the double porosity poromechanical model for a medium saturated with a pure fluid (see Chapter 3). We first validated our model by comparing numerical results with measured variations of permeability of a coal sample induced by adsorption. At the scale of a Representative Elementary Volume, variations of permeability in presence of CO_2 or of CH_4 were computed for various boundary conditions. We showed that boundary conditions play a significant role on adsorption-induced variations of permeability. At the same scale, we also studied the

effect of the kinetics of transfer of fluid between cleats and coal matrix and the effect of the compressibility of the coal matrix.

At the scale of a reservoir, we performed simulations of production of methane from the coal bed (a process known as CBM). The effects of the coal properties, of the compressibility of the coal matrix, and of the temperature on the rate of production of methane were discussed. Simulations of injection of carbon dioxide into a coal bed that would have previously been emptied from all its methane have also been performed. The effect of the boundary conditions, of the compressibility of the coal matrix, and of the kinetics of transfer of fluid between cleats and coal matrix on the rate of injection of carbon dioxide were discussed. In particular, we show that, for a typical reservoir and a typical profile of injection, considering that the transfer of fluid between cleats and coal matrix is infinitely fast is a very reasonable assumption.

All simulations performed in this chapter were for a coal bed filled with a pure fluid only. In order to simulate an ECBM process (Enhanced Coal Bed Methane recovery), in which the production of methane could be stimulated by an injection of carbon dioxide, mixtures of fluid must be considered. Extending our model to binary fluids is the aim of the next chapter.

Chapter 5

Toward enhanced coal bed methane recovery: extension of model to binary mixtures

---

This chapter is dedicated to the extension of the poromechanical dual-porosity model for a coal bed reservoir that contains two fluids. Indeed, as a prerequisite to any simulation of an Enhanced Coal Bed Methane recovery process (ECBM), we need constitutive equations to model variations of porosity and of permeability in presence of a mixture of CH_4 and CO_2. The two fluids are considered to be miscible. The mixture in the cleats is assumed to be in a bulk state. The derived equations are thermodynamically consistent. The model is fully calibrated: experimental data are still used to calibrate the behavior of coal in presence of a pure fluid, but we refer to available numerical data obtained by molecular simulations to calibrate the behavior in presence of a binary mixture. With the calibrated constitutive equations, we perform calculations to predict how porosity and permeability of a Representative Elementary Volume depend on the pressure and on the composition of the fluid in the cleats.

Ce chapitre est dédié à l'extension du modèle poromécanique à double porosité au cas d'une veine de charbon qui contient deux fluides. En effet, comme prérequis à toute simulation du processus de récupération assistée de coal bed methane (ECBM), nous avons besoin d'équations constitutives pour modéliser les variations de porosité et de perméabilité en présence d'un mélange de CH_4 et de CO_2. Les deux fluides sont considérés comme étant miscibles. Le mélange de fluides dans les fractures est supposé être dans un état bulk. Les équations dérivées sont cohérentes thermodynamiquement. Le modèle est entièrement calibré : des données expérimentales sont encore utilisées pour calibrer le comportement du charbon en présence de fluide pur, mais nous référons à des données numériques disponibles obtenues par simulations moléculaires pour calibrer le comportement en présence d'un mélange binaire. Avec les équations constitutives calibrées, nous effectuons des calculs pour prédire comment la porosité et la perméabilité d'un Volume Élémentaire Représentatif dépendent de la pression et de la composition du fluide dans les fractures.

Contents

5.1 Introduction 120

5.2 Assumptions of the model extended to binary mixtures 120

5.3 Derivation of constitutive equations 121

5.4 Simplification and calibration for coal 128

5.5 Simulation of a Representative Elementary Volume 134

5.6 Concluding remarks 134

5.1 Introduction

During Enhanced Coal Bed Methane recovery (ECBM), methane is produced while carbon dioxide is injected. An accurate description of the mixture of CO_2/CH_4 in the coal seam is essential for the development of reliable reservoir simulators used to history match field test data obtained from ECBM field tests [Mazzotti et al., 2009]. Recently, Wu et al. [2011] developed a dual poroelastic model for CO_2-enhanced coalbed methane recovery. In their work, models for variations of porosity and permeability were developed to explicitly quantify the interactions between binary gas mixtures (CO_2 and CH_4) and dual-porosity media (coal matrix and cleats).

Until now, the dual-porosity poromechanical models which we derived only hold for media saturated with a pure fluid. In this chapter, we develop a dual-porosity model for media exposed to binary mixtures of fluids. During ECBM, as the coal bed reservoirs initially contain methane, the injection of carbon dioxide induces a progressive replacement of CH_4 with CO_2. Here we aim at deriving poromechanical equations to model how this replacement leads to strains and variations of porosity. Molecular simulations performed by Brochard et al. [2012a] provide adsorption isotherms of mixtures of methane and carbon dioxide on coal matrix which can be used as inputs in the model.

5.2 Assumptions of the model extended to binary mixtures

We still consider that the reservoir is made of cleats and of a coal matrix which is potentially microporous (see Fig. 5.1). Molecules of fluid can be found in the cleats or in the

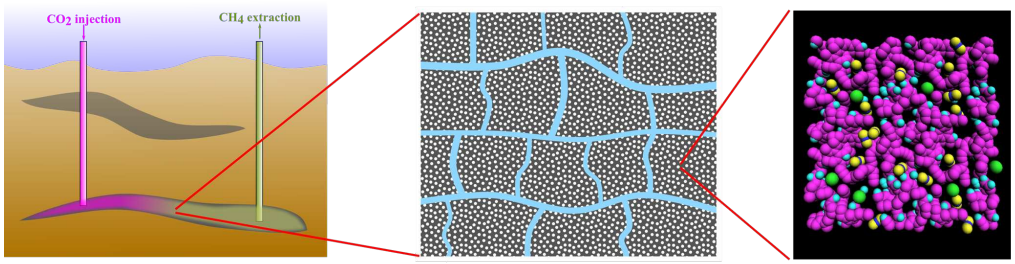

Figure 5.1 – Different scales considered for a coal bed reservoir which contains two fluids.

coal matrix. We assume that fluids in the cleats and in the coal matrix are in equilibrium at all times: the kinetics associated to a transfer of fluid from the cleats to the coal matrix is much faster than any other kinetics of the process. The elastic behavior of the reservoir is still considered to be linear and isotropic. The pore space is filled with carbon dioxide and methane, which are assumed to be miscible. The fluid in the cleats is considered to be in a bulk state.

The mixture of bulk fluid in the cleats is characterized by its pressure p and by its molar fraction $x^{\mathrm{CO_2}}$ of carbon dioxide. In addition, as was already showed in Chapter 2, amounts of fluid adsorbed in the coal matrix can significantly depend on the volumetric strain ϵ_m of the matrix. Therefore, the amounts $n_m^{\mathrm{CH_4}}$ of methane and $n_m^{\mathrm{CO_2}}$ of carbon dioxide adsorbed in the coal matrix depend on the following parameters: $n_m^{\mathrm{CH_4}} = n_m^{\mathrm{CH_4}}(\epsilon_m, p, x^{\mathrm{CO_2}})$ and $n_m^{\mathrm{CO_2}} = n_m^{\mathrm{CO_2}}(\epsilon_m, p, x^{\mathrm{CO_2}})$.

Alternatively, the state of the fluid in the cleats can be defined through the molar chemical potentials $\mu^{\mathrm{CH_4}}$ of methane and $\mu^{\mathrm{CO_2}}$ of carbon dioxide, i.e., $p = p(\mu^{\mathrm{CO_2}}, \mu^{\mathrm{CH_4}})$ and $x^{\mathrm{CO_2}} = x^{\mathrm{CO_2}}(\mu^{\mathrm{CO_2}}, \mu^{\mathrm{CH_4}})$. Such functions can for instance be obtained by molecular simulations, as can be observed on Fig. 5.2 adapted from results obtained by Brochard et al. [2012a]. In this figure, the molar chemical potential μ of a species (holds for CH_4 or CO_2) is linked to its fugacity f through: $\mu(T, f) = \alpha(T) + RT\ln(f/f_0)$, where $\alpha(T)$ is a function of temperature only and where f_0 is the fugacity in the state of reference.

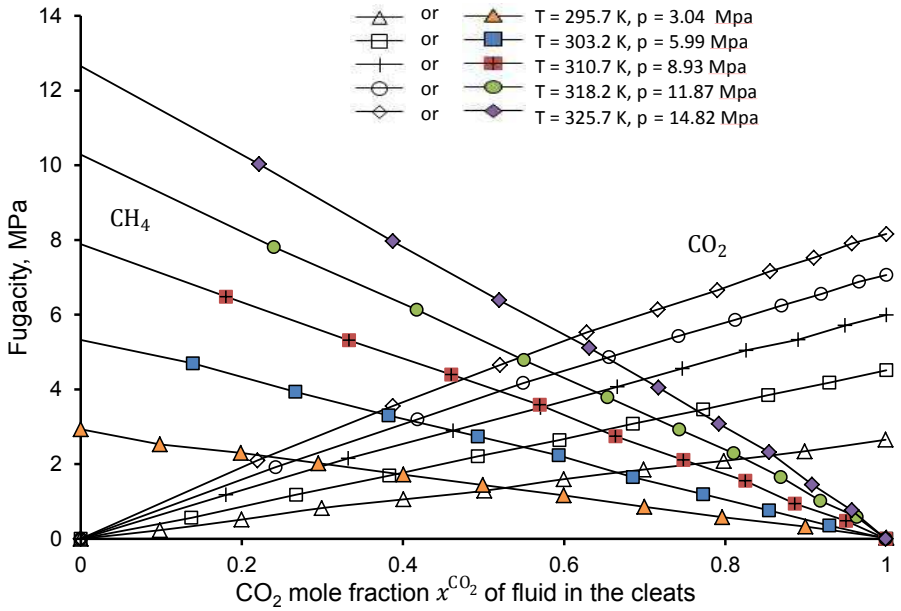

Figure 5.2 – Fugacity of CH_4 and CO_2 as a function of the mixture composition, adapted from Brochard et al. [2012a]. Open symbols are for CO_2 while filled symbols are for CH_4.

5.3 Derivation of constitutive equations

During the derivation, we consider that the pressure p_c of the fluid in the cleats and the thermodynamic pressure p_m of the fluid in the coal matrix differ from each other. Those two pressures will only be equated at the end of the derivation. Thus, for the derivation, the molar chemical potentials $\mu_m^{\mathrm{CH_4}}$ of methane and $\mu_m^{\mathrm{CO_2}}$ of carbon dioxide in the coal matrix are considered to differ from the molar chemical potentials $\mu_c^{\mathrm{CH_4}}$ of methane and $\mu_c^{\mathrm{CO_2}}$ of carbon dioxide in the cleats.

We consider the system made of the coal matrix only, i.e., the reservoir without the fluid in the cleats. Energy can be brought to this system either by straining it with a volumetric confining stress ('$\sigma d\epsilon$'), by straining it with a deviatoric confining stress ('$s_{ij}de_{ij}$'), by deforming the cleat porosity with the pressure of the fluid in the cleats ('$p_c d\Phi_c$'), by adding fluid methane in the coal matrix ('$\mu_m^{\mathrm{CH_4}} dn_r^{\mathrm{CH_4}}$'), or by adding fluid carbon dioxide in the coal matrix ('$\mu_m^{\mathrm{CO_2}} dn_r^{\mathrm{CO_2}}$'):

$$df = \sigma d\epsilon + s_{ij}de_{ij} + p_c d\Phi_c + \mu_m^{\mathrm{CH_4}} dn_r^{\mathrm{CH_4}} + \mu_m^{\mathrm{CO_2}} dn_r^{\mathrm{CO_2}} \tag{5.1}$$

Rewriting the above equation yields:

$$\begin{aligned} d(f - \mu_m^{\mathrm{CH_4}} n_r^{\mathrm{CH_4}} - \mu_m^{\mathrm{CO_2}} n_r^{\mathrm{CO_2}}) = \sigma d\epsilon + s_{ij}de_{ij} + p_c d\Phi_c \\ - n_r^{\mathrm{CH_4}} d\mu_m^{\mathrm{CH_4}} - n_r^{\mathrm{CO_2}} d\mu_m^{\mathrm{CO_2}} \end{aligned} \tag{5.2}$$

from which one concludes that the state equations can be five equations which link σ, s_{ij}, p_c, $n_m^{\mathrm{CH_4}}$, $n_m^{\mathrm{CO_2}}$ to ϵ, e_{ij}, φ_c, $\mu_m^{\mathrm{CH_4}}$, $\mu_m^{\mathrm{CO_2}}$. The rest of this section is dedicated to the derivation of those constitutive equations one after the other.

Equation governing the shear stresses s_{ij}

We first consider the state equation that governs s_{ij}. For symmetry reasons, under the hypotheses of isotropy and of small deformations, this state equation remains the same as in regular poroelasticity:

$$s_{ij}(\epsilon, e_{ij}, \varphi_c, \mu_m^{\mathrm{CH_4}}, \mu_m^{\mathrm{CO_2}}) = 2Ge_{ij} \tag{5.3}$$

Equations governing the amounts $n_r^{\mathrm{CH_4}}$ of methane and $n_r^{\mathrm{CO_2}}$ of carbon dioxide in the coal matrix

We now consider the state equations that govern $n_r^{\mathrm{CH_4}}$ and $n_r^{\mathrm{CO_2}}$, i.e., the amounts of carbon dioxide and methane in the coal matrix per unit volume of undeformed reservoir, respectively. $n_r^{\mathrm{CH_4}}$ and $n_r^{\mathrm{CO_2}}$ can be obtained geometrically from the amounts $n_m^{\mathrm{CH_4}}$ and $n_m^{\mathrm{CO_2}}$ of fluids in the coal matrix per unit volume of undeformed coal matrix with:

$$n_r^{\mathrm{CH_4}}(\epsilon, e_{ij}, \varphi_c, \mu_m^{\mathrm{CO_2}}, \mu_m^{\mathrm{CH_4}}) = [1 - \Phi_{c0}] n_m^{\mathrm{CH_4}}(\epsilon_m, p_m, x^{\mathrm{CO_2}}) \tag{5.4}$$

$$n_r^{\mathrm{CO_2}}(\epsilon, e_{ij}, \varphi_c, \mu_m^{\mathrm{CO_2}}, \mu_m^{\mathrm{CH_4}}) = [1 - \Phi_{c0}] n_m^{\mathrm{CO_2}}(\epsilon_m, p_m, x^{\mathrm{CO_2}}) \tag{5.5}$$

where $p_m(\mu_m^{\mathrm{CH_4}}, \mu_m^{\mathrm{CO_2}})$ is obtained from the equation of state of the fluid mixture considered, and where $x^{\mathrm{CO_2}}$ is the molar fraction of carbon dioxide in the reservoir in thermodynamic equilibrium with the coal matrix.

The volumetric strain ϵ_m of the coal matrix is still linked to the volumetric strain ϵ of a Representative Elementary Volume of the reservoir through Eq. (5.7):

$$\epsilon = (1 - \Phi_{c0})\epsilon_m + \varphi_c \tag{5.6}$$

$$\epsilon_m = \frac{\epsilon - \varphi_c}{1 - \Phi_{c0}} \tag{5.7}$$

Equation governing the volumetric confining stress σ

The derivation of the next state equation starts from the following two Maxwell relations based on Eq. (5.2):

$$\left.\frac{\partial \sigma}{\partial \mu_m^{\mathrm{CH_4}}}\right|_{\epsilon,e_{ij},\varphi_c,\mu_m^{\mathrm{CO_2}}} = -\left.\frac{\partial n_r^{\mathrm{CH_4}}}{\partial \epsilon}\right|_{e_{ij},\varphi_c,\mu_m^{\mathrm{CH_4}},\mu_m^{\mathrm{CO_2}}} \tag{5.8}$$

$$\left.\frac{\partial \sigma}{\partial \mu_m^{\mathrm{CO_2}}}\right|_{\epsilon,e_{ij},\varphi_c,\mu_m^{\mathrm{CH_4}}} = -\left.\frac{\partial n_r^{\mathrm{CO_2}}}{\partial \epsilon}\right|_{e_{ij},\varphi_c,\mu_m^{\mathrm{CH_4}},\mu_m^{\mathrm{CO_2}}} \tag{5.9}$$

for which the right-hand term can be rewritten with the help of Eqs. (5.5) and (5.6):

$$\begin{aligned}\left.\frac{\partial n_r^{\mathrm{X}}}{\partial \epsilon}\right|_{e_{ij},\varphi_c,\mu_m^{\mathrm{CH_4}},\mu_m^{\mathrm{CO_2}}} &= \frac{1}{1-\Phi_{c0}}\left.\frac{\partial n_r^{\mathrm{X}}}{\partial \epsilon_m}\right|_{e_{ij},\varphi_c,\mu_m^{\mathrm{CH_4}},\mu_m^{\mathrm{CO_2}}} \\ &= \frac{1}{1-\Phi_{c0}}\left.\frac{\partial n_r^{\mathrm{X}}}{\partial \epsilon_m}\right|_{\mu_m^{\mathrm{CH_4}},\mu_m^{\mathrm{CO_2}}} = \left.\frac{\partial n_m^{\mathrm{X}}}{\partial \epsilon_m}\right|_{\mu_m^{\mathrm{CH_4}},\mu_m^{\mathrm{CO_2}}}\end{aligned} \tag{5.10}$$

where X stands for CH_4 or CO_2. Eqs (5.8) and (5.9) can therefore be rewritten:

$$\left.\frac{\partial \sigma}{\partial \mu_m^{\mathrm{CH_4}}}\right|_{\epsilon,e_{ij},\varphi_c,\mu_m^{\mathrm{CO_2}}} = -\left.\frac{\partial n_m^{\mathrm{CH_4}}}{\partial \epsilon_m}\right|_{\mu_m^{\mathrm{CH_4}},\mu_m^{\mathrm{CO_2}}} \tag{5.11}$$

$$\left.\frac{\partial \sigma}{\partial \mu_m^{\mathrm{CO_2}}}\right|_{\epsilon,e_{ij},\varphi_c,\mu_m^{\mathrm{CH_4}}} = -\left.\frac{\partial n_m^{\mathrm{CO_2}}}{\partial \epsilon_m}\right|_{\mu_m^{\mathrm{CH_4}},\mu_m^{\mathrm{CO_2}}} \tag{5.12}$$

Further differentation of Eq. (5.11) with respect to $\mu_m^{\mathrm{CO_2}}$ and of Eq. (5.12) with respect to $\mu_m^{\mathrm{CH_4}}$ enables to find the following equality:

$$\left.\frac{\partial^2 n_m^{\mathrm{CH_4}}}{\partial \mu_m^{\mathrm{CO_2}} \partial \epsilon_m}\right|_{\mu_m^{\mathrm{CH_4}}} = \left.\frac{\partial^2 n_m^{\mathrm{CO_2}}}{\partial \mu_m^{\mathrm{CH_4}} \partial \epsilon_m}\right|_{\mu_m^{\mathrm{CO_2}}} \tag{5.13}$$

An integration of Eq. (5.12) yields:

$$\begin{aligned}\sigma(\epsilon, e_{ij}, \varphi_c, \mu_m^{\mathrm{CH_4}}, \mu_m^{\mathrm{CO_2}}) = f_1(\epsilon, e_{ij}, \varphi_c, \mu_m^{\mathrm{CH_4}}) \\ - \int_{\tilde{\mu}_m^{\mathrm{CO_2}}=-\infty}^{\mu_m^{\mathrm{CO_2}}} \left.\frac{\partial n_m^{\mathrm{CO_2}}}{\partial \epsilon_m}\right|_{\mu_m^{\mathrm{CH_4}},\tilde{\mu}_m^{\mathrm{CO_2}}} d\tilde{\mu}_m^{\mathrm{CO_2}}\end{aligned} \tag{5.14}$$

where f_1 is a dummy function.

A differentiation of this equation with respect to $\mu_m^{\mathrm{CH_4}}$ yields:

$$\left.\frac{\partial \sigma}{\partial \mu_m^{\mathrm{CH_4}}}\right|_{\epsilon, e_{ij}, \varphi_c, \mu_m^{\mathrm{CO_2}}} = \left.\frac{\partial f_1}{\partial \mu_m^{\mathrm{CH_4}}}\right|_{\epsilon, e_{ij}, \varphi_c} - \int_{\tilde{\mu}_m^{\mathrm{CO_2}}=-\infty}^{\mu_m^{\mathrm{CO_2}}} \left.\frac{\partial^2 n_m^{\mathrm{CO_2}}}{\partial \mu_m^{\mathrm{CH_4}} \partial \epsilon_m}\right|_{\tilde{\mu}_m^{\mathrm{CO_2}}} d\tilde{\mu}_m^{\mathrm{CO_2}} \tag{5.15}$$

which, with the help of Eq. (5.13), can be rewritten as:

$$\begin{aligned}\left.\frac{\partial \sigma}{\partial \mu_m^{\mathrm{CH_4}}}\right|_{\epsilon, e_{ij}, \varphi_c, \mu_m^{\mathrm{CO_2}}} &= \left.\frac{\partial f_1}{\partial \mu_m^{\mathrm{CH_4}}}\right|_{\epsilon, e_{ij}, \varphi_c} - \int_{\tilde{\mu}_m^{\mathrm{CO_2}}=-\infty}^{\mu_m^{\mathrm{CO_2}}} \left.\frac{\partial^2 n_m^{\mathrm{CH_4}}}{\partial \tilde{\mu}_m^{\mathrm{CO_2}} \partial \epsilon_m}\right|_{\mu_m^{\mathrm{CH_4}}} d\tilde{\mu}_m^{\mathrm{CO_2}} \\ &= \left.\frac{\partial f_1}{\partial \mu_m^{\mathrm{CH_4}}}\right|_{\epsilon, e_{ij}, \varphi_c} - \left.\frac{\partial n_m^{\mathrm{CH_4}}}{\partial \epsilon_m}\right|_{\mu_m^{\mathrm{CH_4}}, \mu_m^{\mathrm{CO_2}}} + \left.\frac{\partial n_m^{\mathrm{CH_4}}}{\partial \epsilon_m}\right|_{\mu_m^{\mathrm{CH_4}}, \mu_m^{\mathrm{CO_2}}=-\infty}\end{aligned} \tag{5.16}$$

A combination of the above equation with Eq. (5.11) yields a differential equation on f_1:

$$\left.\frac{\partial f_1}{\partial \mu_m^{\mathrm{CH_4}}}\right|_{\epsilon, e_{ij}, \varphi_c} = - \left.\frac{\partial n_m^{\mathrm{CH_4}}}{\partial \epsilon_m}\right|_{\mu_m^{\mathrm{CH_4}}, \mu_m^{\mathrm{CO_2}}=-\infty} \tag{5.17}$$

which, after integration, yields:

$$f_1(\epsilon, e_{ij}, \varphi_c, \mu_m^{\mathrm{CH_4}}) = f_2(\epsilon, e_{ij}, \varphi_c) - \int_{\tilde{\mu}_m^{\mathrm{CH_4}}=-\infty}^{\mu_m^{\mathrm{CH_4}}} \left.\frac{\partial n_m^{\mathrm{CH_4}}}{\partial \epsilon_m}\right|_{\tilde{\mu}_m^{\mathrm{CH_4}}, \mu_m^{\mathrm{CO_2}}=-\infty} d\tilde{\mu}_m^{\mathrm{CH_4}} \tag{5.18}$$

where f_2 is a dummy function, so that Eq. (5.14) can be rewritten:

$$\begin{aligned}\sigma(\epsilon, e_{ij}, \varphi_c, \mu_m^{\mathrm{CH_4}}, \mu_m^{\mathrm{CO_2}}) = f_2(\epsilon, e_{ij}, \varphi_c) &\\ - \int_{\tilde{\mu}_m^{\mathrm{CO_2}}=-\infty}^{\mu_m^{\mathrm{CO_2}}} \left.\frac{\partial n_m^{\mathrm{CO_2}}}{\partial \epsilon_m}\right|_{\mu_m^{\mathrm{CH_4}}, \tilde{\mu}_m^{\mathrm{CO_2}}} d\tilde{\mu}_m^{\mathrm{CO_2}} &\\ - \int_{\tilde{\mu}_m^{\mathrm{CH_4}}=-\infty}^{\mu_m^{\mathrm{CH_4}}} \left.\frac{\partial n_m^{\mathrm{CH_4}}}{\partial \epsilon_m}\right|_{\tilde{\mu}_m^{\mathrm{CH_4}}, \mu_m^{\mathrm{CO_2}}=-\infty} d\tilde{\mu}_m^{\mathrm{CH_4}} &\end{aligned} \tag{5.19}$$

The function f_2 is determined by soliciting the material while preventing any penetration of fluid in the coal matrix (i.e., by setting $\mu_m^{\mathrm{CH_4}} = -\infty$ and $\mu_m^{\mathrm{CO_2}} = -\infty$). In such a case, for which $\sigma = f_2(\epsilon, e_{ij}, \varphi_c)$, we must recover regular poroelasticity, from what follows that:

$$f_2(\epsilon, e_{ij}, \varphi_c) = (K + b^2 N)\epsilon - bN\varphi_c \tag{5.20}$$

where K is the bulk modulus of reservoir, b is the Biot coefficient, N is the Biot modulus of the reservoir associated to the cleat system and φ_c is the variation of Lagrangian cleat

porosity. These poroelastic coefficients verify the classical relations:

$$b = 1 - K/K_m \tag{5.21}$$

$$\frac{1}{N} = \frac{b - \Phi_{c0}}{K_m} \tag{5.22}$$

The fourth state equation can therefore be written:

$$\begin{aligned}\sigma(\epsilon, e_{ij}, \varphi_c, \mu_m^{\mathrm{CH_4}}, \mu_m^{\mathrm{CO_2}}) = {} & [K + b^2 N]\epsilon - bN\varphi_c \\ & - \int_{\tilde{\mu}_m^{\mathrm{CO_2}}=-\infty}^{\mu_m^{\mathrm{CO_2}}} \left.\frac{\partial n_m^{\mathrm{CO_2}}}{\partial \epsilon_m}\right|_{\mu_m^{\mathrm{CH_4}}, \tilde{\mu}_m^{\mathrm{CO_2}}} d\tilde{\mu}_m^{\mathrm{CO_2}} \\ & - \int_{\tilde{\mu}_m^{\mathrm{CH_4}}=-\infty}^{\mu_m^{\mathrm{CH_4}}} \left.\frac{\partial n_m^{\mathrm{CH_4}}}{\partial \epsilon_m}\right|_{\tilde{\mu}_m^{\mathrm{CH_4}}, \mu_m^{\mathrm{CO_2}}=-\infty} d\tilde{\mu}_m^{\mathrm{CH_4}}\end{aligned} \tag{5.23}$$

Equation governing the pressure p_c of the fluid in the cleats

The derivation of the last state equation starts from the following two Maxwell relations based on Eq. (5.2):

$$\left.\frac{\partial p_c}{\partial \mu_m^{\mathrm{CH_4}}}\right|_{\epsilon, e_{ij}, \varphi_c, \mu_m^{\mathrm{CO_2}}} = \left.\frac{\partial n_r^{\mathrm{CH_4}}}{\partial \epsilon}\right|_{e_{ij}, \varphi_c, \mu_m^{\mathrm{CH_4}}, \mu_m^{\mathrm{CO_2}}} \tag{5.24}$$

$$\left.\frac{\partial p_c}{\partial \mu_m^{\mathrm{CO_2}}}\right|_{\epsilon, e_{ij}, \varphi_c, \mu_m^{\mathrm{CH_4}}} = \left.\frac{\partial n_r^{\mathrm{CO_2}}}{\partial \epsilon}\right|_{e_{ij}, \varphi_c, \mu_m^{\mathrm{CH_4}}, \mu_m^{\mathrm{CO_2}}} \tag{5.25}$$

which, with the help of Eq. (5.10), can be rewritten as:

$$\left.\frac{\partial p_c}{\partial \mu_m^{\mathrm{CH_4}}}\right|_{\epsilon, e_{ij}, \varphi_c, \mu_m^{\mathrm{CO_2}}} = \left.\frac{\partial n_m^{\mathrm{CH_4}}}{\partial \epsilon_m}\right|_{\mu_m^{\mathrm{CH_4}}, \mu_m^{\mathrm{CO_2}}} \tag{5.26}$$

$$\left.\frac{\partial p_c}{\partial \mu_m^{\mathrm{CO_2}}}\right|_{\epsilon, e_{ij}, \varphi_c, \mu_m^{\mathrm{CH_4}}} = \left.\frac{\partial n_m^{\mathrm{CO_2}}}{\partial \epsilon_m}\right|_{\mu_m^{\mathrm{CH_4}}, \mu_m^{\mathrm{CO_2}}} \tag{5.27}$$

An integration of Eq. (5.27) yields:

$$\begin{aligned}p_c(\epsilon, e_{ij}, \varphi_c, \mu_m^{\mathrm{CH_4}}, \mu_m^{\mathrm{CO_2}}) = {} & f_3(\epsilon, e_{ij}, \varphi_c, \mu_m^{\mathrm{CH_4}}) \\ & - \int_{\tilde{\mu}_m^{\mathrm{CO_2}}=-\infty}^{\mu_m^{\mathrm{CO_2}}} \left.\frac{\partial n_m^{\mathrm{CO_2}}}{\partial \epsilon_m}\right|_{\mu_m^{\mathrm{CH_4}}, \tilde{\mu}_m^{\mathrm{CO_2}}} d\tilde{\mu}_m^{\mathrm{CO_2}}\end{aligned} \tag{5.28}$$

where f_3 is a dummy function.

A differentiation of this equation with respect to $\mu_m^{\mathrm{CH_4}}$ yields:

$$\left.\frac{\partial p_c}{\partial \mu_m^{\mathrm{CH_4}}}\right|_{\epsilon,e_{ij},\varphi_c,\mu_m^{\mathrm{CO_2}}} = \left.\frac{\partial f_3}{\partial \mu_m^{\mathrm{CH_4}}}\right|_{\epsilon,e_{ij},\varphi_c} - \int_{\tilde{\mu}_m^{\mathrm{CO_2}}=-\infty}^{\mu_m^{\mathrm{CO_2}}} \left.\frac{\partial^2 n_m^{\mathrm{CO_2}}}{\partial \mu_m^{\mathrm{CH_4}} \partial \epsilon_m}\right|_{\tilde{\mu}_m^{\mathrm{CO_2}}} d\tilde{\mu}_m^{\mathrm{CO_2}} \tag{5.29}$$

which, with the help of Eq. (5.13), can be rewritten as:

$$\begin{aligned}\left.\frac{\partial p_c}{\partial \mu_m^{\mathrm{CH_4}}}\right|_{\epsilon,e_{ij},\varphi_c,\mu_m^{\mathrm{CO_2}}} &= \left.\frac{\partial f_3}{\partial \mu_m^{\mathrm{CH_4}}}\right|_{\epsilon,e_{ij},\varphi_c} - \int_{\tilde{\mu}_m^{\mathrm{CO_2}}=-\infty}^{\mu_m^{\mathrm{CO_2}}} \left.\frac{\partial^2 n_m^{\mathrm{CH_4}}}{\partial \tilde{\mu}_m^{\mathrm{CO_2}} \partial \epsilon_m}\right|_{\mu_m^{\mathrm{CH_4}}} d\tilde{\mu}_m^{\mathrm{CO_2}} \\ &= \left.\frac{\partial f_3}{\partial \mu_m^{\mathrm{CH_4}}}\right|_{\epsilon,e_{ij},\varphi_c} - \left.\frac{\partial n_m^{\mathrm{CH_4}}}{\partial \epsilon_m}\right|_{\mu_m^{\mathrm{CH_4}},\mu_m^{\mathrm{CO_2}}} + \left.\frac{\partial n_m^{\mathrm{CH_4}}}{\partial \epsilon_m}\right|_{\mu_m^{\mathrm{CH_4}},\mu_m^{\mathrm{CO_2}}=-\infty}\end{aligned} \tag{5.30}$$

A combination of the above equation with Eq. (5.11) yields a differential equation on f_3:

$$\left.\frac{\partial f_3}{\partial \mu_m^{\mathrm{CH_4}}}\right|_{\epsilon,e_{ij},\varphi_c} = - \left.\frac{\partial n_m^{\mathrm{CH_4}}}{\partial \epsilon_m}\right|_{\mu_m^{\mathrm{CH_4}},\mu_m^{\mathrm{CO_2}}=-\infty} \tag{5.31}$$

which, after integration, yields:

$$f_3(\epsilon, e_{ij}, \varphi_c, \mu_m^{\mathrm{CH_4}}) = f_4(\epsilon, e_{ij}, \varphi_c) - \int_{\tilde{\mu}_m^{\mathrm{CH_4}}=-\infty}^{\mu_m^{\mathrm{CH_4}}} \left.\frac{\partial n_m^{\mathrm{CH_4}}}{\partial \epsilon_m}\right|_{\tilde{\mu}_m^{\mathrm{CH_4}},\mu_m^{\mathrm{CO_2}}=-\infty} d\tilde{\mu}_m^{\mathrm{CH_4}} \tag{5.32}$$

where f_4 is a dummy function, so that Eq. (5.28) can be rewritten:

$$\begin{aligned}p_c(\epsilon, e_{ij}, \varphi_c, \mu_m^{\mathrm{CH_4}}, \mu_m^{\mathrm{CO_2}}) = f_4(\epsilon, e_{ij}, \varphi_c) &+ \int_{\tilde{\mu}_m^{\mathrm{CO_2}}=-\infty}^{\mu_m^{\mathrm{CO_2}}} \left.\frac{\partial n_m^{\mathrm{CO_2}}}{\partial \epsilon_m}\right|_{\mu_m^{\mathrm{CH_4}},\tilde{\mu}_m^{\mathrm{CO_2}}} d\tilde{\mu}_m^{\mathrm{CO_2}} \\ &+ \int_{\tilde{\mu}_m^{\mathrm{CH_4}}=-\infty}^{\mu_m^{\mathrm{CH_4}}} \left.\frac{\partial n_m^{\mathrm{CH_4}}}{\partial \epsilon_m}\right|_{\tilde{\mu}_m^{\mathrm{CH_4}},\mu_m^{\mathrm{CO_2}}=-\infty} d\tilde{\mu}_m^{\mathrm{CH_4}}\end{aligned} \tag{5.33}$$

The function f_4 is determined by soliciting the material while preventing any penetration of fluid in the coal matrix (i.e., by setting $\mu_m^{\mathrm{CH_4}} = -\infty$ and $\mu_m^{\mathrm{CO_2}} = -\infty$). In such a case, for which $p_c = f_4(\epsilon, e_{ij}, \varphi_c)$, we must recover regular poroelasticity, from what follows that:

$$f_4(\epsilon, e_{ij}, \varphi_c) = -Nb\epsilon + N\varphi_c \tag{5.34}$$

The last state equation can therefore be written:

$$p_c(\epsilon, e_{ij}, \varphi_c, \mu_m^{\mathrm{CH_4}}, \mu_m^{\mathrm{CO_2}}) = -Nb\epsilon + N\varphi_c + \int_{\tilde{\mu}_m^{\mathrm{CO_2}}=-\infty}^{\mu_m^{\mathrm{CO_2}}} \left.\frac{\partial n_m^{\mathrm{CO_2}}}{\partial \epsilon_m}\right|_{\mu_m^{\mathrm{CH_4}}, \tilde{\mu}_m^{\mathrm{CO_2}}} d\tilde{\mu}_m^{\mathrm{CO_2}} + \int_{\tilde{\mu}_m^{\mathrm{CH_4}}=-\infty}^{\mu_m^{\mathrm{CH_4}}} \left.\frac{\partial n_m^{\mathrm{CH_4}}}{\partial \epsilon_m}\right|_{\tilde{\mu}_m^{\mathrm{CH_4}}, \mu_m^{\mathrm{CO_2}}=-\infty} d\tilde{\mu}_m^{\mathrm{CH_4}} \tag{5.35}$$

Summary

In summary, the state equations are:

$$\sigma = [K + b^2 N]\epsilon - bN\varphi_c - p^a(\epsilon_m, p_m, x^{\mathrm{CO_2}}) \tag{5.36}$$

$$p_c = -Nb\epsilon + N\varphi_c + p^a(\epsilon_m, p_m, x^{\mathrm{CO_2}}) \tag{5.37}$$

$$n_r^{\mathrm{CH_4}} = [1 - \Phi_{c0}] n_m^{\mathrm{CH_4}}(\epsilon_m, p_m, x^{\mathrm{CO_2}}) \tag{5.38}$$

$$n_r^{\mathrm{CO_2}} = [1 - \Phi_{c0}] n_{m0}^{\mathrm{CO_2}}(\epsilon_m, p_m, x^{\mathrm{CO_2}}) \tag{5.39}$$

$$s_{ij} = 2Ge_{ij} \tag{5.40}$$

where:

$$p^a(\epsilon_m, p_m, x^{\mathrm{CO_2}}) = \int_{\tilde{\mu}_m^{\mathrm{CH_4}}=-\infty}^{\mu_m^{\mathrm{CH_4}}} \left.\frac{\partial n_m^{\mathrm{CH_4}}}{\partial \epsilon_m}\right|_{\tilde{\mu}_m^{\mathrm{CH_4}}, \mu_m^{\mathrm{CO_2}}=-\infty} d\tilde{\mu}_m^{\mathrm{CH_4}} + \int_{\tilde{\mu}_m^{\mathrm{CO_2}}=-\infty}^{\mu_m^{\mathrm{CO_2}}} \left.\frac{\partial n_m^{\mathrm{CO_2}}}{\partial \epsilon_m}\right|_{\mu_m^{\mathrm{CH_4}}, \tilde{\mu}_m^{\mathrm{CO_2}}} d\tilde{\mu}_m^{\mathrm{CO_2}} \tag{5.41}$$

is a pressure induced by adsorption in the coal matrix, and where:

$$p_m = p_m(\mu_m^{\mathrm{CO_2}}, \mu_m^{\mathrm{CH_4}}) \tag{5.42}$$

$$\epsilon_m = \frac{\epsilon - \varphi_c}{1 - \Phi_{c0}} \tag{5.43}$$

$$b = 1 - K/K_m \tag{5.44}$$

$$\frac{1}{N} = \frac{b - \Phi_{c0}}{K_m} \tag{5.45}$$

If we now set $p_m = p_c = p$, we obtain the state equations that govern the behavior of the reservoir:

$$\sigma = [K + b^2 N]\epsilon - bN\varphi_c - p^a(\epsilon_m, p, x^{\mathrm{CO_2}}) \tag{5.46}$$
$$p = -Nb\epsilon + N\varphi_c + p^a(\epsilon_m, p, x^{\mathrm{CO_2}}) \tag{5.47}$$
$$n_r^{\mathrm{CH_4}} = [1 - \Phi_{c0}] n_m^{\mathrm{CH_4}}(\epsilon_m, p, x^{\mathrm{CO_2}}) \tag{5.48}$$
$$n_r^{\mathrm{CO_2}} = [1 - \Phi_{c0}] n_m^{\mathrm{CO_2}}(\epsilon_m, p, x^{\mathrm{CO_2}}) \tag{5.49}$$
$$s_{ij} = 2Ge_{ij} \tag{5.50}$$

or, likewise:

$$\sigma = K\epsilon - b[p - p^a] - p^a \tag{5.51}$$
$$\varphi_c = b\epsilon + [p - p^a]/N \tag{5.52}$$
$$n_r^{\mathrm{CH_4}} = [1 - \Phi_{c0}] n_m^{\mathrm{CH_4}}(\epsilon_m, p, x^{\mathrm{CO_2}}) \tag{5.53}$$
$$n_r^{\mathrm{CO_2}} = [1 - \Phi_{c0}] n_m^{\mathrm{CO_2}}(\epsilon_m, p, x^{\mathrm{CO_2}}) \tag{5.54}$$
$$s_{ij} = 2Ge_{ij} \tag{5.55}$$

5.4 Simplification and calibration for coal

As was shown in the previous chapters, the adsorptive behavior of coal in presence of a pure fluid can be characterized experimentally. Such did Pini et al. [2010a] for Ribolla coal for which they measured the adsorbed amounts of pure CO_2 or of pure CH_4 (the data is recalled in Fig. 5.3a). From their measurements of adsorption-induced swellings (see Sec. 3.3), it is also possible to calibrate the coefficient $C(p)$ for pure CO_2 or for pure CH_4, which characterizes the coupling between adsorption and strain (the data is recalled in Fig. 5.3b). In contrast, data of adsorption of mixtures are difficult to obtain experimentally, not only because of the complexity of the required experimental setup, but also because of the duration of such experiments. For our specific problem we aim at using numerical adsorption isotherms obtained by molecular simulations by Brochard et al. [2012a]. In particular, Brochard et al. [2012a] obtained data of adsorbed amounts of both CO_2 and CH_4 when coal is exposed to a mixture of CO_2 and CH_4 at various mole fractions $x^{\mathrm{CO_2}}$ of carbon dioxide (see Fig. 5.4). In our case, the bulk fluid in thermodynamical equilibrium with the coal matrix is the fluid in the cleats, so that $x^{\mathrm{CO_2}}$ is also the mole fraction of carbon dioxide in the binary mixture in the cleats. Our goal is to use the numerical results of Brochard et al. [2012a] in order to simplify enough the constitutive equations (5.51)-(5.55), so that those equations can be fully calibrated with available data. We aim at doing so while keeping the thermodynamical consistency of the model.

For coal, Brochard et al. [2012b] showed that the adsorption isotherm of methane is well approximated by a first-order expansion with respect to the strain ϵ_m of the coal matrix. We will assume that such a dependence remains valid for adsorption of mixtures:

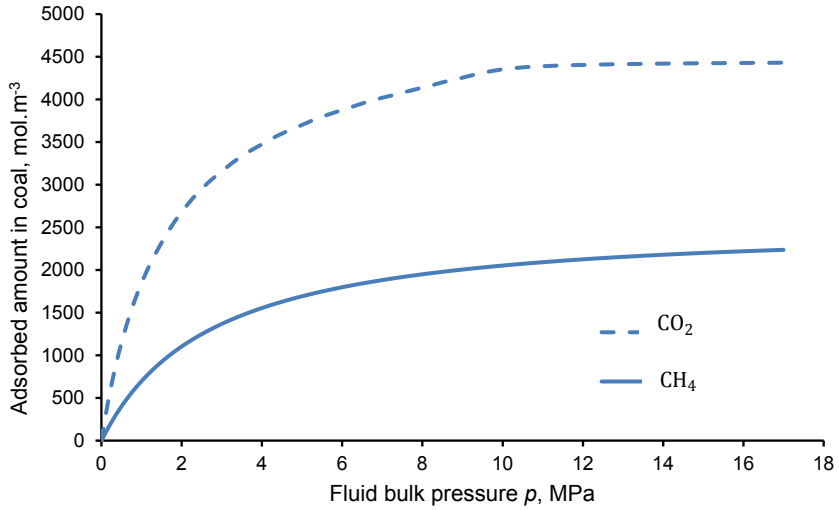

(a)

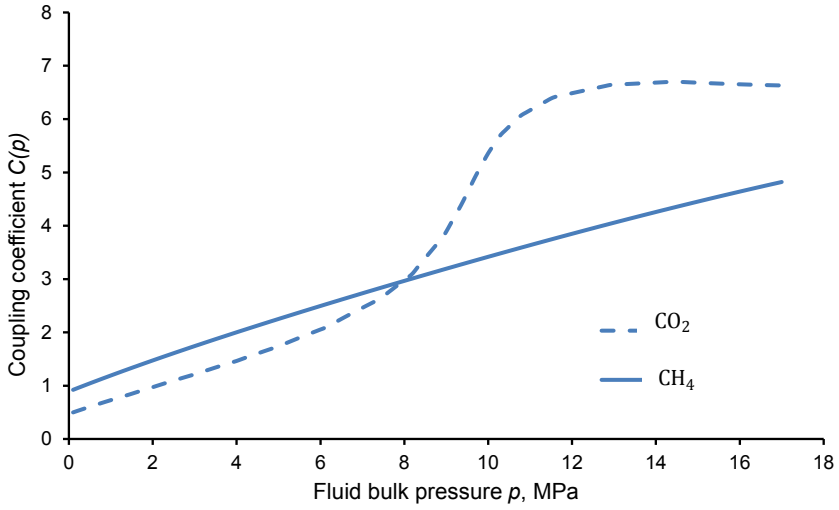

(b)

Figure 5.3 – (a) Adsorbed amounts of pure fluids in Ribolla coal, adapted from Pini et al. [2010a] and (b) coupling coefficients $C(p)$ for pure fluids and Ribolla coal.

$$n_m^{\mathrm{CH_4}}(\epsilon_m, p, x^{\mathrm{CO_2}}) = n_{m0}^{\mathrm{CH_4}}(p, x^{\mathrm{CO_2}}) + A^{\mathrm{CH_4}}(p, x^{\mathrm{CH_4}})\epsilon_m \tag{5.56}$$

$$n_m^{\mathrm{CO_2}}(\epsilon_m, p, x^{\mathrm{CO_2}}) = n_{m0}^{\mathrm{CO_2}}(p, x^{\mathrm{CO_2}}) + A^{\mathrm{CO_2}}(p, x^{\mathrm{CO_2}})\epsilon_m \tag{5.57}$$

where $A^{\mathrm{CH_4}}$ and $A^{\mathrm{CO_2}}$ are functions, and where $n_{m0}^{\mathrm{CH_4}}$ and $n_{m0}^{\mathrm{CO_2}}$ are the adsorption isotherms of methane and of carbon dioxide on a rigid coal matrix, respectively. Under the assumption that the first-order expansions (5.56) and (5.57) are valid, we find out with Eq. (5.67) that:

$$p^a(\epsilon_m, p, x^{\mathrm{CO_2}}) = p^a(p, x^{\mathrm{CO_2}}) \tag{5.58}$$

In other words, the adsorption-induced pressure p^a depends no more on the strain ϵ_m of the coal matrix.

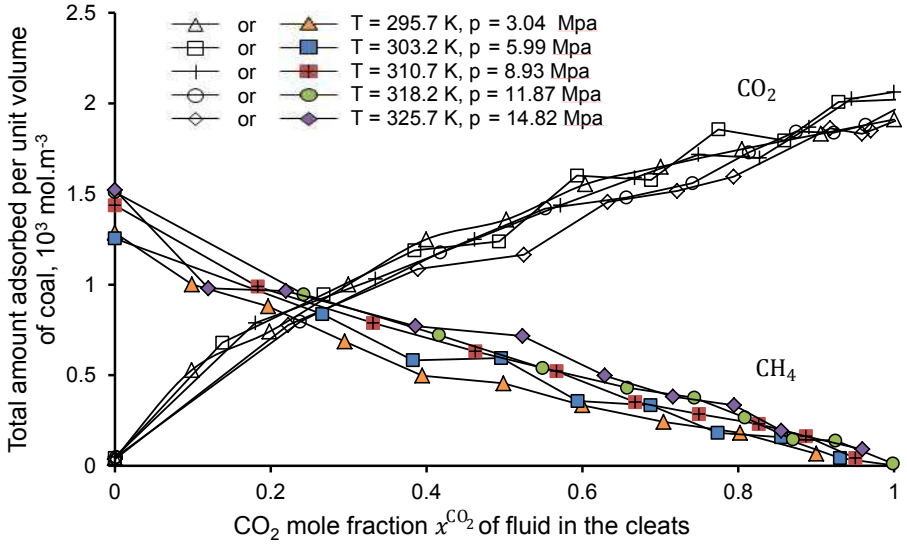

Figure 5.4 – Total amounts of CO_2 and CH_4 adsorbed in a coal sample exposed to a mixture of CO_2 and CH_4 for, adapted from Brochard et al. [2012a]. Open symbols are for CO_2 while filled symbols are for CH_4. The CO_2 mole fraction is that in a reservoir in thermodynamic equilibrium with the sample (i.e., in our case, of the fluid in the cleats).

From Fig. 5.4 it appears that the relative amounts of CO_2 and CH_4 in the coal matrix depend mostly on the composition of the fluid in thermodynamical equilibrium with the coal matrix, which, in our case, is the fluid in the cleats, but are mostly independent of the bulk pressure. Therefore, we will approximate the mixed adsorption isotherms $n_{m0}^{\mathrm{CH_4}}(p, x^{\mathrm{CO_2}})$ and $n_{m0}^{\mathrm{CO_2}}(p, x^{\mathrm{CO_2}})$ by:

$$n_{m0}^{\mathrm{CH_4}}(p, x^{\mathrm{CO_2}}) = n_{m0}^{\mathrm{CH_4}}(p, x^{\mathrm{CO_2}} = 0) g^{\mathrm{CH_4}}(x^{\mathrm{CO_2}}) \tag{5.59}$$

$$n_{m0}^{\mathrm{CO_2}}(p, x^{\mathrm{CO_2}}) = n_{m0}^{\mathrm{CO_2}}(p, x^{\mathrm{CO_2}} = 1) g^{\mathrm{CO_2}}(x^{\mathrm{CO_2}}) \tag{5.60}$$

where $n_{m0}^{\mathrm{CH_4}}(p, x^{\mathrm{CO_2}} = 0)$ and $n_{m0}^{\mathrm{CO_2}}(p, x^{\mathrm{CO_2}} = 1)$ are the adsorption isotherms of pure CH_4 and pure CO_2, respectively, and where $g^{\mathrm{CH_4}}(x^{\mathrm{CO_2}})$ and $g^{\mathrm{CO_2}}(x^{\mathrm{CO_2}})$ are functions. Those functions can readily be obtained from Fig. 5.4 and the adsorption isotherms of pure methane and pure carbon dioxide on coal have been obtained by Pini et al. [2010a], as displayed in Fig. 5.3a.

From the lack of knowledge, we will assume that the coefficients $A^{\mathrm{CH_4}}$ and $A^{\mathrm{CO_2}}$ are of the form:

$$A^{\mathrm{CH_4}}(p, x^{\mathrm{CH_4}}) = A^{\mathrm{CH_4}}(f^{\mathrm{CH_4}}) \tag{5.61}$$
$$A^{\mathrm{CO_2}}(p, x^{\mathrm{CO_2}}) = A^{\mathrm{CO_2}}(f^{\mathrm{CO_2}}) \tag{5.62}$$

where $f^{\mathrm{CH_4}}$ and $f^{\mathrm{CO_2}}$ are the fugacities of methane and carbon dioxide in the mixture, respectively. From molecular simulations of bulk binary mixtures of CO_2 and CH_4 (see Fig. 5.2), one observes that, in first-order approximation, those fugacities are assumed to be linked to the fugacity $f_*^{\mathrm{CO_2}}$ of pure carbon dioxide and $f_*^{\mathrm{CH_4}}$ of pure methane through:

$$f^{\mathrm{CO_2}} = f_*^{\mathrm{CO_2}} x^{\mathrm{CO_2}} \tag{5.63}$$
$$f^{\mathrm{CH_4}} = f_*^{\mathrm{CH_4}} \left(1 - x^{\mathrm{CO_2}}\right) \tag{5.64}$$

where fugacity $f_*^{\mathrm{CO_2}}(p)$ of pure carbon dioxide and $f_*^{\mathrm{CH_4}}(p)$ of pure methane are calculated from the state equations developed by Span and Wagner [2003a, b] (see Fig. 5.5).

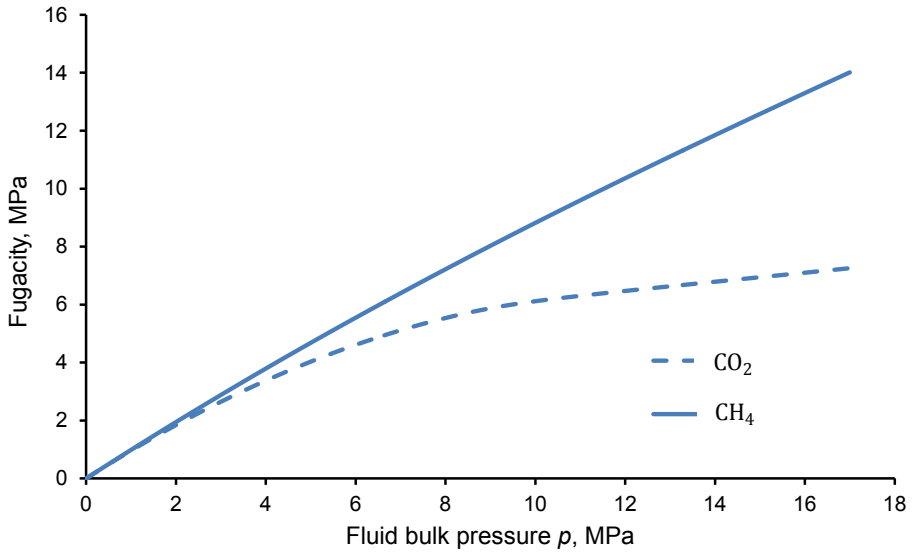

Figure 5.5 – Fugacity $f_*^{\mathrm{CO_2}}(p)$ of pure carbon dioxide and $f_*^{\mathrm{CH_4}}(p)$ of pure methane at $T = 318.15$ K, adapted from Span and Wagner [2003a, b].

Moreover, the functions $A^{\mathrm{CH_4}}$ and $A^{\mathrm{CO_2}}$ can be identified with the equations derived

in Sec. 2.4.2 for pure fluids:

$$A^{\mathrm{CH_4}}\left(f_*^{\mathrm{CH_4}}(p)\right) = n_{m0}^{\mathrm{CH_4}}(p, x^{\mathrm{CO_2}}=0)C^{\mathrm{CH_4}}(p) \tag{5.65}$$
$$A^{\mathrm{CO_2}}\left(f_*^{\mathrm{CO_2}}(p)\right) = n_{m0}^{\mathrm{CO_2}}(p, x^{\mathrm{CO_2}}=1)C^{\mathrm{CO_2}}(p) \tag{5.66}$$

where $C^{\mathrm{CH_4}}(p)$ and $C^{\mathrm{CO_2}}(p)$ are the coupling coefficients between adsorption and strain for pure methane and pure carbon dioxide, respectively. Those coupling coefficients have been back-calculated from experimental data obtained by Pini et al. [2010a], as displayed in Fig. 5.3b.

The functions $A^{\mathrm{CH_4}}$ and $A^{\mathrm{CO_2}}$ being now known, the adsorption-induced pressure p^a can be calculated with the help of Eq. (5.67):

$$\begin{aligned} p^a(p, x^{\mathrm{CO_2}}) &= \int_{\tilde{\mu}^{\mathrm{CH_4}}=-\infty}^{\mu^{\mathrm{CH_4}}} A^{\mathrm{CH_4}} d\tilde{\mu}^{\mathrm{CH_4}} + \int_{\tilde{\mu}^{\mathrm{CO_2}}=-\infty}^{\mu^{\mathrm{CO_2}}} A^{\mathrm{CO_2}} d\tilde{\mu}^{\mathrm{CO_2}} \\ &= RT\left[\int_0^{f^{\mathrm{CH_4}}} \frac{A^{\mathrm{CH_4}}(\tilde{f}^{\mathrm{CH_4}})}{\tilde{f}^{\mathrm{CH_4}}} d\tilde{f}^{\mathrm{CH_4}} + \int_0^{f^{\mathrm{CO_2}}} \frac{A^{\mathrm{CO_2}}(\tilde{f}^{\mathrm{CO_2}})}{\tilde{f}^{\mathrm{CO_2}}} d\tilde{f}^{\mathrm{CO_2}}\right] \\ &= RT\left[\int_0^{f_*^{\mathrm{CH_4}} x^{\mathrm{CH_4}}} \frac{A^{\mathrm{CH_4}}(\tilde{f}^{\mathrm{CH_4}})}{\tilde{f}^{\mathrm{CH_4}}} d\tilde{f}^{\mathrm{CH_4}} + \int_0^{f_*^{\mathrm{CO_2}} x^{\mathrm{CO_2}}} \frac{A^{\mathrm{CO_2}}(\tilde{f}^{\mathrm{CO_2}})}{\tilde{f}^{\mathrm{CO_2}}} d\tilde{f}^{\mathrm{CO_2}}\right] \end{aligned} \tag{5.67}$$

Combining Eqs. (5.53)-(5.54) with Eqs. (5.56)-(5.57), Eqs. (5.59)-(5.60) and Eqs. (5.61)-(5.62) enables to rewrite the adsorption isotherms as:

$$\begin{aligned} n_r^{\mathrm{CH_4}}(\epsilon, p, x^{\mathrm{CO_2}}) &= [1-\phi_{c0}]\, n_{m0}^{\mathrm{CH_4}}(p, x^{\mathrm{CO_2}}=0) g^{\mathrm{CH_4}}(x^{\mathrm{CO_2}}) \\ &\quad + A^{\mathrm{CH_4}}(f^{\mathrm{CH_4}})(\epsilon - \varphi_c) \end{aligned} \tag{5.68}$$
$$\begin{aligned} n_r^{\mathrm{CO_2}}(\epsilon, p, x^{\mathrm{CO_2}}) &= [1-\phi_{c0}]\, n_{m0}^{\mathrm{CO_2}}(p, x^{\mathrm{CO_2}}=1) g^{\mathrm{CO_2}}(x^{\mathrm{CO_2}}) \\ &\quad + A^{\mathrm{CO_2}}(f^{\mathrm{CO_2}})(\epsilon - \varphi_c) \end{aligned} \tag{5.69}$$

Finally, it is now possible to modify the constitutive equations (5.51)-(5.55) in order to express σ, φ_c, $n_r^{\mathrm{CH_4}}$, $n_r^{\mathrm{CH_4}}$, and s_{ij} as functions of ϵ, e_{ij} and p:

$$\sigma(\epsilon, p, x^{\mathrm{CO_2}}) = K\epsilon - b[p - p^a] - p^a \tag{5.70}$$
$$\varphi_c(\epsilon, p, x^{\mathrm{CO_2}}) = b\epsilon + [p - p^a]/N \tag{5.71}$$
$$\begin{aligned} n_r^{\mathrm{CH_4}}(\epsilon, p, x^{\mathrm{CO_2}}) &= (1-\phi_{c0})\, n_{m0}^{\mathrm{CH_4}}(p, x^{\mathrm{CO_2}}=0) g^{\mathrm{CH_4}}(x^{\mathrm{CO_2}}) \\ &\quad + A^{\mathrm{CH_4}}(f^{\mathrm{CH_4}})(\epsilon - \varphi_c) \end{aligned} \tag{5.72}$$
$$\begin{aligned} n_r^{\mathrm{CO_2}}(\epsilon, p, x^{\mathrm{CO_2}}) &= (1-\phi_{c0})\, n_{m0}^{\mathrm{CO_2}}(p, x^{\mathrm{CO_2}}=1) g^{\mathrm{CO_2}}(x^{\mathrm{CO_2}}) \\ &\quad + A^{\mathrm{CO_2}}(f^{\mathrm{CO_2}})(\epsilon - \varphi_c) \end{aligned} \tag{5.73}$$
$$s_{ij}(e_{ij}) = 2Ge_{ij} \tag{5.74}$$

where the fugacities f^{CH_4} of methane and f^{CO_2} of carbon dioxide are given by Eqs. (5.63)-(5.64), where the functions A^{CH_4} and A^{CO_2} are given by Eqs. (5.65)-(5.66), where x^{CO_2} is the CO_2 mole fraction of the fluid in the cleats, and where the adsorption-induced pressure p^a is given by Eq. (5.67).

The constitutive equations (5.70)-(**??**) are thermodynamically consistent and can be calibrated on available data. This calibration can be performed with experimental data obtained for the pure fluids (see Fig. 5.3) and with numerical data obtained by molecular simulations needed to characterize the adsorption of the binary mixture (see Fig. 5.4). Here, in order to calibrate our model, the adsorption-induced pressure $p^a(p, x^{CO_2})$ is calculated based on the experimental data obtained for pure CO_2 and pure CH_4 on Ribolla coal at $T = 318.15$ K (see Fig. 5.3) and the fugacities of pure CO_2 and pure CH_4 at $T = 318.15$ K obtained by molecular simulations (see Fig. 5.5).

Figure 5.6 displays the adsorption-induced pressure $p^a(p, x^{CO_2})$ for various values of the CO_2 mole fraction x^{CO_2} of the fluid in the cleats and the fluid pressure p_c in the cleats. Fig. 5.6 shows that the adsorption-induced pressure $p^a(p, x^{CO_2})$ increases both with the the fluid pressure p_c and the CO_2 mole fraction x^{CO_2}.

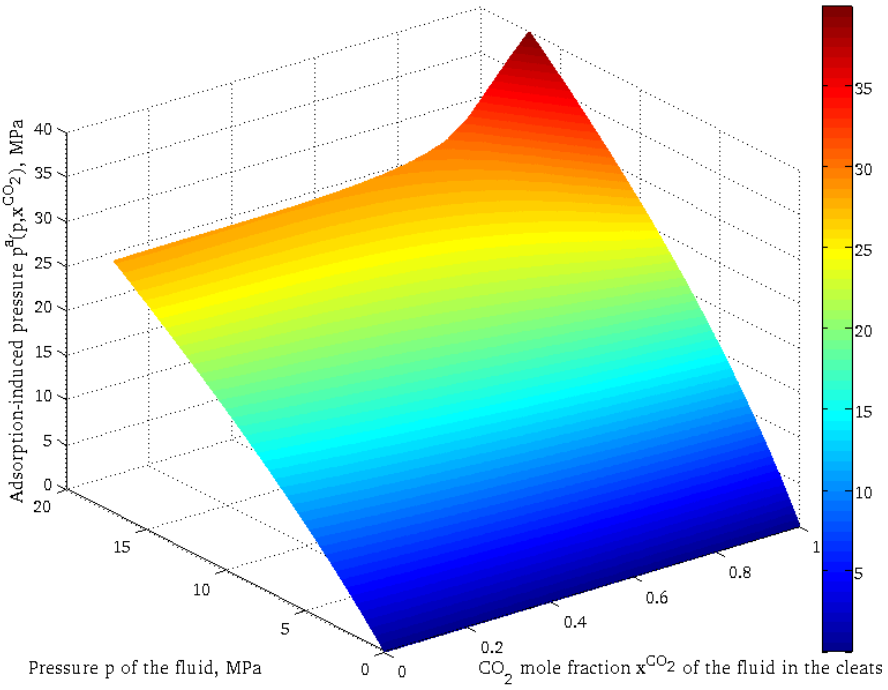

Figure 5.6 – Adsorption-induced pressure $p^a(p, x^{CO_2})$ versus the pressure p of the fluid and the CO_2 mole fraction x^{CO_2} of the fluid in the cleats for Ribolla coal sample exposed to a mixture of CO_2 and CH_4 at $T = 318.15$ K.

Calculating the adsorption-induced pressure $p^a(p, x^{CO_2})$ is a prerequisite to perform simulations at the scale of a Representative Elementary Volume and the scale of a coal bed reservoir (ECBM). In the next section, simulations at the scale of a Representative Elementary Volume for Ribolla coal are performed.

5.5 Simulation of a Representative Elementary Volume

In this section, we use the constitutive equations derived and calibrated in Sec. 5.4 in order to simulate the evolutions of cleat porosity of a Representative Elementary Volume of Ribolla coal kept at constant volume ($\epsilon = 0$). We consider that the permeability k of the volume still depends on the cleat porosity only, according to the Kozeny-Carman equation (4.1). The mechanical properties of Ribolla coal are given in Table 4.1.

Figure 5.7 displays those evolutions of cleat porosity ϕ_c and of permeability k versus the pressure p of the fluid and the CO_2 mole fraction x^{CO_2} of the fluid in the cleats. This figure shows that, with an increasing pressure p of the fluid at a given composition, the cleat porosity and thus the permeability decrease, as a consequence of the swelling of the coal matrix. Results obtained with the model for a reservoir saturated with a pure fluid (see Sec. 4.3) are recalled in Fig. 5.7 with dashed lines: as expected, those results are exactly retrieved with the model extended to binary mixtures, for the limit cases $x^{CO_2} = 1$ (which corresponds to an injection with pure carbon dioxide) and $x^{CO_2} = 0$ (which corresponds to an injection with pure methane).

Figure 5.8 displays the same results, but as a function of the CO_2 mole fraction x^{CO_2} of the fluid in the cleats, for various pressures p of the fluid. Each curve corresponds to the case for which, at a given pressure, the methane naturally present in the coal would be progressively replaced with carbon dioxide. As expected, this gradual replacement translates into a gradual decrease of permeability of the sample. At the lowest pressure considered for the fluid (i.e., $p = 2$ MPa), the cleat porosity ϕ_c varies linearly with the CO_2 mole fraction x^{CO_2} of the fluid in the cleats. In contrast, at the largest pressure considered (i.e., $p = 12$ MPa), the variations of cleat porosity ϕ_c with the CO_2 mole fraction x^{CO_2} of the fluid in the cleats become significantly nonlinear.

5.6 Concluding remarks

In this chapter, the poromechanical model derived in Chapter 2 for coal exposed to a pure fluid was extended to coal exposed to a binary mixture. Some assumptions needed to be made in order to obtain a thermodynamically consistent model that could be fully calibrated with available data. Those assumptions were on the shape of the adsorption isotherms of mixtures (see Eqs. (5.59)-(5.60)), on their dependency on strain (see Eqs. (5.56)-(5.57)), and on the dependency of the introduced functions A^{CH_4} and A^{CO_2} (see Eqs. (5.61)-(5.62)). The model was fully calibrated with experimental data in combination with numerical data obtained by molecular simulations (see Figs. 5.5 and 5.3).

This calibrated model was then used in order to perform calculations at the scale of a Representative Elementary Volume kept at constant volume case and exposed to a binary mixture such as the one formed by methane and carbon dioxide.

Deriving the constitutive equations (5.70)-(5.74) in a thermodynamically consistent manner and making sure that those equations could be fully calibrated was a first step toward an implementation in a finite-element code and the numerical modelling of a full CO_2-enhanced coal bed methane (CO_2-ECBM) recovery process.

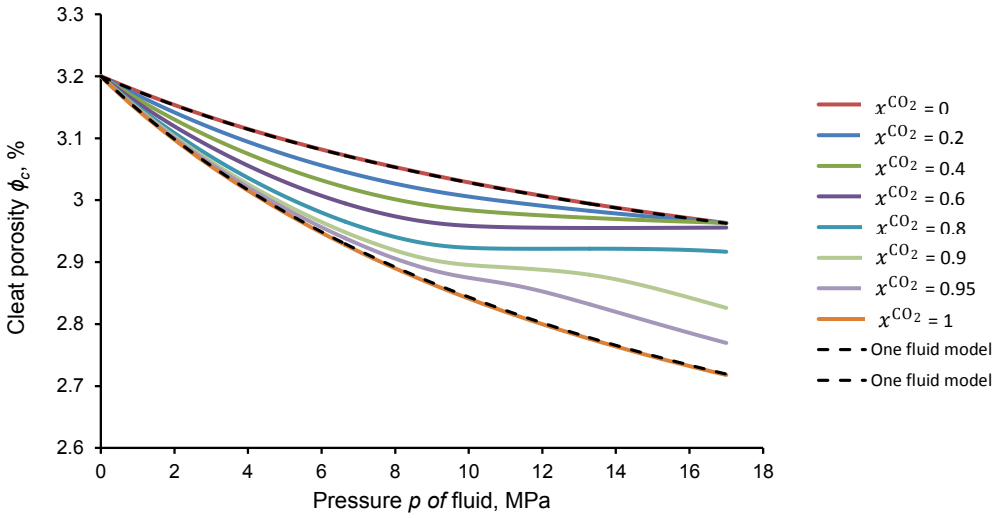

(a)

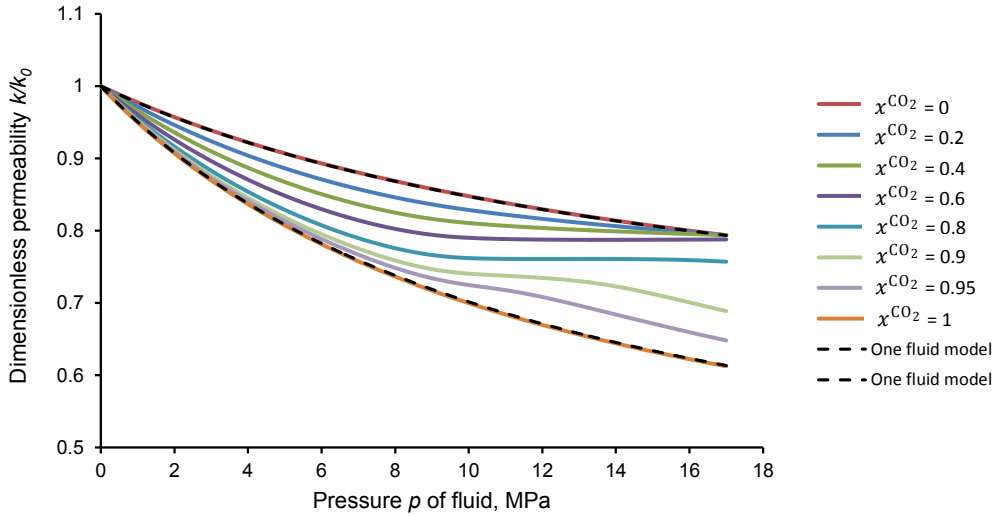

(b)

Figure 5.7 – (a) Cleat porosity ϕ_c and (b) permeability of a Representative Elementary Volume versus the pressure p of fluid for various values of CO_2 mole fraction x^{CO_2} of the fluid in the cleats for Ribolla coal sample kept at constant volume.

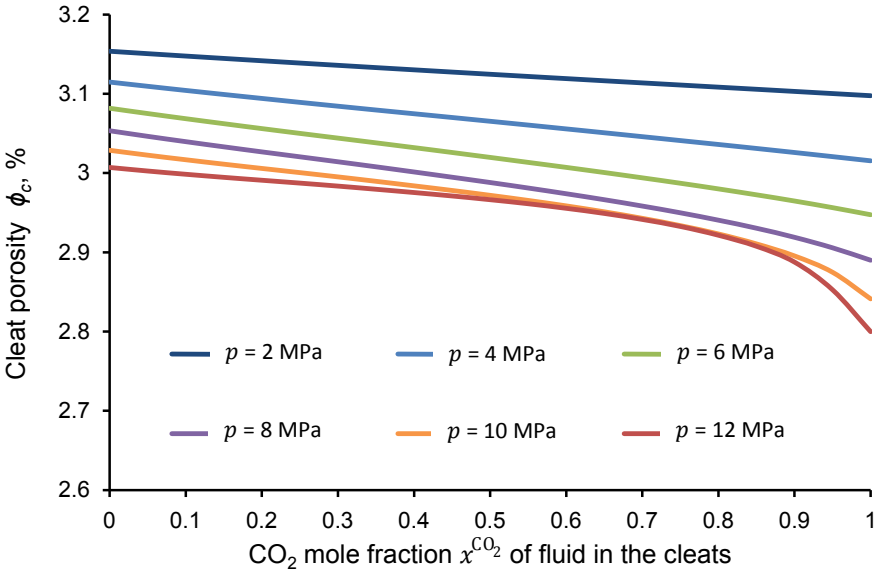

(a)

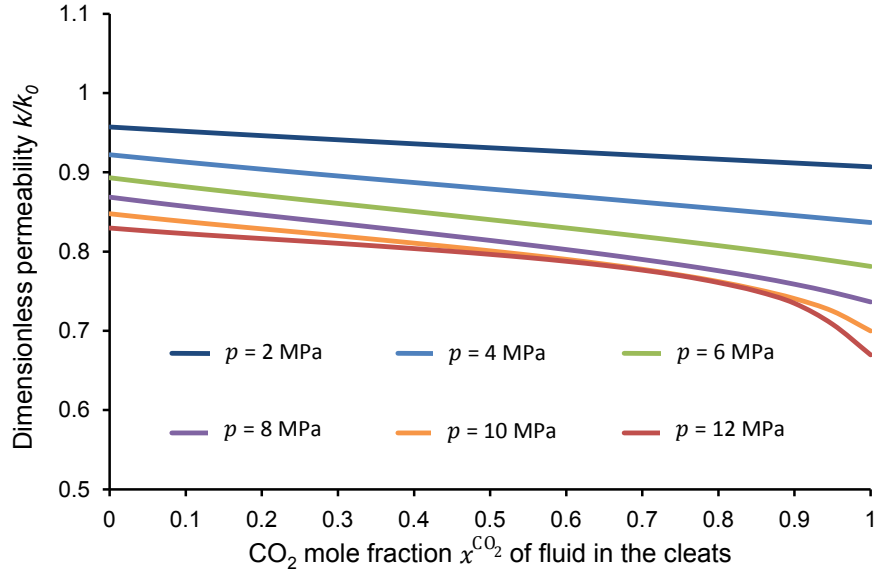

(b)

Figure 5.8 – (a) Cleat porosity ϕ_c and (b) permeability of a Representative Elementary Volume versus the CO_2 mole fraction x^{CO_2} of the fluid in the cleats for various pressures p of the fluid for Ribolla coal sample kept at constant volume.

Chapter 6

Conclusion and perspectives

Contents

6.1 Conclusion 138

6.2 Perspectives 140

6.1 Conclusion

Underground coal bed reservoirs naturally contain methane which can be produced. In parallel of the production of this methane, carbon dioxide can be injected, either to enhance the production of methane, or to have this carbon dioxide stored over geological periods of time. While injecting CO_2, a swelling of the coal matrix is observed, which hinders further injection of CO_2. We studied such phenomenon analytically with poromechanical modeling using the Biot-Coussy framework. The derived models exhibit a dual porosity, since the pore space of a coal bed reservoir can be divided into the cleats and the porosity of the coal matrix. All derived models are isotropic and linear elastic. Transport properties were assumed to be governed by the cleat system only. In those cleats, fluid molecules were assumed to be in a bulk state.

In a first step, we considered a reservoir saturated with a pure fluid. A first model (see Sec. 2.3) was derived by considering that adsorption in the coal matrix was a surface phenomenon occurring at the surface of the pores, while a second model (see Sec. 2.4) was derived for a generic coal matrix. In particular, this model is valid for a microporous coal matrix, in which adsorption occurs by pore filling more than by surface covering. This latter model has a wider range of validity than the former one. Adsorption induces stresses and pressures that can strain the solid. In the generic case, adsorption and strain can be coupled (in the sense that the adsorption isotherm depends on the strain of the adsorbent). For the specific case of coal, this coupling can be captured by a pressure-dependent coefficient.

In order to calibrate the derived constitutive equations, adsorption isotherms and experimental data of swelling upon adsorption are required. We considered two sets of experimental data obtained by Pini et al. [2010b] on two coals with different sorption and swelling properties, subjected to adsorption of pure carbon dioxide and of pure methane (see Chapter 3). The coefficient that couples adsorption and strain was calibrated. For both carbon dioxide and methane, we observed that this coefficient varied significantly with the pressure of the fluid. From the calibration of the model on coal samples for the fluids of interest, we could identify additional parameters of the microporous coal matrix. The tangent Biot coefficient of the coal matrix was identified as a function of the fluid bulk pressure: interestingly this Biot coefficient was out of the usual range for regular macroporous media. This unconventional value is a direct consequence of the intermolecular forces between the molecules of fluid and the atoms of the microporous matrix. Also, we investigated how the choice of the compressibility of the coal matrix impacted the calibration of the parameters.

We then performed simulations at various scales (scale of a Representative Elementary Volume, scale of a coal sample, and scale of reservoir) in Chapter 4. At the scale of a Representative Elementary Volume, using the calibration parameters for adsorption of CO_2 and CH_4, variations of permeability under various boundary conditions were simulated. With our model, if the volumetric confining stress on the REV is kept constant, the porosity and thus the permeability increase with the pore pressure; if the volume of the REV is kept constant, the porosity and thus the permeability start decreasing with an increasing pore pressure. We also studied the effect of the kinetics of transfer of fluid between cleats and coal matrix. The whole model was validated with permeability experiments of coal to CO_2 under various boundary conditions. At the scale of a reservoir,

simulations of injection of carbon dioxide into the reservoir or of production of methane from the reservoir (to simulate CBM) were performed with various boundary conditions. The effect of the compressibility of the coal matrix and the effect of the kinetics of transfer of fluid between cleats and coal matrix were discussed. On a Representative Elementary Volume of coal exposed to a binary mixture of methane and carbon dioxide, we calculated how the porosity and the permeability depended on the pressure and on the composition of the fluid in the cleats.

In Chapter 5, the model was extended to a reservoir containing a binary mixture, in order for it to be usable for simulations of a CO_2-ECBM (CO_2- Enhanced Coal Bed Methane recovery) process. Special care was dedicated to keep the model thermodynamically consistent. The model was fully calibrated with a mix of experimental data and numerical data from molecular simulations. With the calibrated constitutive equations, we performed calculations to predict how the porosity and the permeability of a Representative Elementary Volume depend on the pressure and on the composition of the fluid in the cleats.

We hope that this work will be useful for those aiming at modelling, simulating and developing methane production from and carbon storage in coal bed reservoirs and facing geomechanical issues.

6.2 Perspectives

The dual-porosity model developed in this thesis is restricted to linear isotropic reservoirs, while the presence of cleats (i.e., of fractures) induces mechanical nonlinearities. Therefore, the poromechanical parameters of the model such as the bulk modulus K of, the Biot coefficient b of, and the Biot modulus N of the reservoir will depend on the effective stress in practice. Moreover, the cleats being vertical, and because of the history of loading, coal is anisotropic, both in terms of mechanical properties and permeability. For example, the permeability perpendicular to the bedding plane can be 4 times as small as (or even one order of magnitude smaller than) the permeability parallel to the bedding plane [Massarotto et al., 2006] [Li et al., 2004]. This anisotropy, as well as the mechanical one, is expected to play a significant role on the CBM and ECBM processes. At least transverse isotropy should be considered.

Although we know that adsorption and strain can be significantly coupled in the general case, in this work a simplified form of the dependency of the adsorption isotherm on the strains of the coal matrix was considered: following results shown with molecular simulations by Brochard et al. [2012b] for adsorption of methane on coal, we assumed that adsorption isotherms of pure fluids (and of their mixtures) could be well captured by a first-order expansion with respect to the strain of the coal matrix. The validity of such an assumption should be explored experimentally.

The most complex model derived in this work was limited to mixture of two fluids, in order to make it possible to consider mixtures of methane and of carbon dioxide. But, in practice, more fluids are involved. We know that liquid water is commonly present in coal seams and affects the injection process [Jahediesfanjani and Civan, 2005]. Indeed, at the scale of the coal matrix, water molecules are adsorbed in hydrophilic sites in the micropores [White et al., 2005]. Therefore, in practice, water contributes to the adsorption-induced swelling of coal. Moreover, the access to the micropores and the amount of stored carbon dioxide are reduced in presence of water [Busch and Gensterblum, 2011]. At the scale of the cleat network, water reduces the apparent permeability of the coal reservoir to carbon dioxide [Jahediesfanjani and Civan, 2005]. Indeed, liquid water is not miscible with pure carbon dioxide and thus restrains the flow of carbon dioxide inside the cleats. In addition, carbon dioxide molecules can dissolve in liquid water, thus increasing its acidity and inducing chemical reactions with the mineral matter in coal [Massarotto et al., 2010]. Moreover, the dissolved CO_2 can be transported away from the coal seam, which is a potential leakage route [White et al., 2005]. We also disregarded the presence of nitrogen. Nitrogen can indeed be injected into coal seams along with carbon dioxide, as is the case for flue gas-ECBM. Nitrogen is adsorbed in coal, although its affinity for coal is lower than those of carbon dioxide and methane [Fitzgerald et al., 2005]. Therefore, the competitive adsorption of a CO_2-CH_4-N_2 mixture (or of a CO_2-CH_4-N_2-H_2O mixture) is likely to induce a swelling which differs from the swelling induced by a mere CO_2-CH_4 mixture. In the perspective of flue gas-ECBM, mixtures more complex than binary ones should be studied.

All the limitations here described should be addressed in the future in order to increase the range of validity of our model.

Conclusion(fr)

Les veines de charbon souterraines contiennent naturellement du méthane qui peut être produit. En parallèle de la production de ce méthane, du dioxyde de carbone peut être injecté, soit pour augmenter la production de méthane, soit pour stocker ce dioxyde de carbone pour de longues périodes. Au cours de l'injection de CO_2, un gonflement de la matrice de charbon est observé, qui gêne l'injection ultérieure de CO_2. Nous avons étudié ce phénomène analytiquement avec un modèle poromécanique basé sur le formalisme de Biot-Coussy. Les modèles dérivés exhibent une double porosité, puisque l'espace poreux d'une veine de charbon peut être divisé en les cleats et la porosité de la matrice de charbon. Tous les modèles dérivés sont isotropes et linéaires élastiques. Nous avons supposé que les propriétés de transport étaient gouvernées par le système de cleats seulement. Dans ces cleats, nous avons supposé que les molécules de fluides étaient dans un état bulk.

Dans une premier temps, nous avons considéré un réservoir saturé par un fluide pur. Un premier modèle (voir la Section 2.3) a été dérivé en considérant que l'adsorption dans la matrice de charbon était un phénomène de surface se déroulant à la surface des pores, tandis qu'un deuxième modèle (voir la Section 2.4) a été dérivé pour une matrice de charbon générique. En particulier, ce modèle est valide pour une matrice de charbon microporeuse, dans laquelle l'adsorption se déroule par remplissage de pores plus que par adsorption de surface. L'adsorption induit des contraintes et des pressions qui peuvent déformer le solide. Dans le cas générique, adsorption et déformation peuvent être couplées (dans le sens que l'isotherme d'adsorption dépend de la déformation de l'adsorbant). Pour le cas spécifique du charbon, ce couplage peut être capturé par un coefficient dépendant de la pression.

Pour calibrer les équations constitutives dérivées, des isothermes d'adsorption et des données expérimentales de gonflement induit par adsorption sont requis. Nous avons considéré deux ensembles de données expérimentales obtenues par Pini et al. [2010b] sur deux charbons ayant des propriétés de sorption et de gonflement différentes, soumis à une adsorption de dioxyde de carbone pur et de méthane pur (voir le Chapitre 3). Le coefficient qui couple adsorption et déformation a été calibré. Tant pour le dioxyde de carbone que pour le méthane, nous avons observé que ce coefficient variait significativement avec la pression du fluide. De la calibration du modèle sur des échantillons de charbon pour les fluides d'intérêt, nous avons pu identifier des paramètres supplémentaires de la matrice microporeuse de charbon. Le coefficient de Biot tangentiel de la matrice de charbon a été identifié comme une fonction de la pression thermodynamique du fluide : de manière intéressante, ce coefficient de Biot était en dehors de la gamme habituellement observée pour les milieux macroporeux réguliers. Cette valeur non conventionnelle est une conséquence directe des forces intermoléculaires entre les molécules de fluide et les atomes de la matrice microporeuse. Nous avons également examiné comment le choix de la compressibilité de la matrice de charbon impactait la calibration des paramètres.

Nous avons ensuite effectué des simulations à diverses échelles (d'un Volume Élémentaire Représentatif, d'un échantillon de charbon, de la veine) dans le Chapitre 4. À l'échelle d'un Volume Élémentaire Représentatif, utilisant les paramètres de calibration pour l'adsorption de CO_2 et CH_4, les variations de perméabilité sous diverses conditions aux limites ont été simulées. Avec notre modèle, si la contrainte volumique de confinement sur le Volume Élémentaire Représentatif est gardée constante, la porosité et donc

la perméabilité augmentent avec la pression de pore; si le volume du Volume Élémentaire Représentatif est gardé constant, la porosité et donc la perméabilité commencent par diminuer avec une pression de pore croissante. Nous avons aussi étudié l'effet de la cinétique de transfert de fluide entre les cleats et la matrice de charbon. Le modèle complet a été validé avec des expériences de perméabilité de charbon au CO_2 sous diverses conditions aux limites. À l'échelle d'une veine, des simulations d'injection de dioxyde de carbone dans la veine ou de production de méthane de la veine (pour simuler du CBM) ont été réalisées, sous diverses conditions aux limites. L'effet de la compressibilité de la matrice de charbon et l'effet de la cinétique de transfert de fluide entre les cleats et la matrice de charbon ont aussi été discutés.

Dans le Chapitre 5, le modèle a été étendu à un réservoir contenant un mélange binaire, afin qu'il puisse être utilisé pour des simulations de CO_2-ECBM (récupération de méthane assistée par injection de CO_2). Un soin spécial a été consacré à la conservation de la cohérence thermodynamique du modèle. Le modèle a été entièrement calibré avec un mélange de données expérimentales et de données numériques obtenues par simulations moléculaires. Avec les équations constitutives calibrées, nous avons effectué des calculs pour prédire comment la porosité et la perméabilité d'un Volume Élémentaire Représentatif dépendaient de la pression et de la composition du fluide dans les cleats.

Nous espérons que ce travail sera utile pour ceux cherchant à modéliser, simuler, ou développer la production de méthane et le stockage de dioxyde de carbone dans les veines de charbon et qui feraient face à des problèmes d'ordre géomécanique.

List of Notations

Symbol	Description
	Latin letters
b	Biot coefficient (-)
b_c	Biot coefficient of reservoir associated to cleat system (-)
b_m	Biot coefficient of coal matrix (-)
C	Coupling coefficient (-)
$C^{\mathrm{CO_2}}$	Coupling coefficient for carbon dioxide (-)
$C^{\mathrm{CH_4}}$	Coupling coefficient for methane (-)
c_{Φ_m}	Material parameter (m^{-1})
c_{Φ_c}	Material parameter (m^{-1})
e_{ij}	Deviatoric strains (-)
f	Helmholtz free energy of microporous coal per unit volume of undeformed reservoir ($\mathrm{J.mol}^{-1}$)
f_{skel}	Helmholtz free energy of solid skeleton per unit volume of undeformed medium ($\mathrm{J.mol}^{-1}$)
f_{surf}	Helmholtz free energy of coal matrix pore surface per unit volume of undeformed porous medium ($\mathrm{J.mol}^{-1}$)
G	Shear modulus of reservoir (Pa)
K	Bulk modulus of reservoir (Pa)
K_m	Bulk modulus of coal matrix (Pa)
K_s	Bulk modulus of solid skeleton (Pa)
k_m	Intrinsic permeability of coal matrix (m^2)
M_1^0	Mass of coal sample at measuring point under vacuum (g)
M_1	Mass of coal sample at measuring point (g)
M_m	Molar mass of adsorbed fluid (g/mol)
m^{ads}	Mass of adsorbed fluid (g)
m_0^{coal}	Initial mass of coal sample (g)
m^{met}	Weight of lifted metal parts (g)
N	Biot modulus of reservoir (Pa)
N_{cm}	Biot modulus of coal matrix (Pa)
N_c	Biot modulus of reservoir associated to cleat system (Pa)
N_m	Biot modulus of reservoir (Pa)
n_m^a	Molar density of fluid molecules adsorbed at surface of coal matrix pores per unit volume of undeformed porous medium ($\mathrm{mol.m}^{-3}$)

n_m^b	Molar density of fluid molecules in their bulk state in coal matrix pores per unit volume of undeformed porous medium (mol.m^{-3})
n^{ads}	Molar concentration of fluid in coal matrix per unit volume of undeformed coal matrix, i.e., adsorption isotherm (mol.m^{-3})
n_0^{ads}	Adsorption isotherm of fluid in coal matrix kept at constant volume (mol.m^{-3})
n^{excess}	Molar amount of fluid adsorbed in excess of the bulk density per unit volume of coal (mol/m^3)
n_c	Molar density of fluid molecules in the cleats per unit volume of undeformed porous medium (mol.m^{-3})
n_m	Molar concentration of fluid in coal matrix per unit volume of undeformed reservoir (mol.m^{-3})
$n_m^{\mathrm{CH_4}}$	Molar concentration of methane in coal matrix per unit volume of undeformed coal matrix (mol/m^3)
$n_m^{\mathrm{CO_2}}$	Molar concentration of carbon dioxide in coal matrix per unit volume of undeformed coal matrix (mol/m^3)
$n_{m0}^{\mathrm{CH_4}}$	Molar concentration of methane in coal matrix kept at constant volume per unit volume of coal matrix (mol/m^3)
$n_{m0}^{\mathrm{CO_2}}$	Molar concentration of carbon dioxide in coal matrix kept at constant volume per unit volume of coal matrix (mol/m^3)
$n_r^{\mathrm{CH_4}}$	Molar concentration of methane in coal matrix per unit volume of undeformed reservoir (mol/m^3)
$n_r^{\mathrm{CO_2}}$	Molar concentration of carbon dioxide in coal matrix per unit volume of undeformed reservoir (mol/m^3)
$\mathring{n}_{c\to m}$	Rate of molar flow of fluid per unit volume which flow from the cleats into coal matrix (mol.m^{-3}.s^{-1})
$\mathring{n}_{m\to c}$	Rate of molar flow of fluid per unit volume which flow from the coal matrix into cleats (mol.m^{-3}.s^{-1})
p	Thermodynamic pressure of fluid (Pa)
p_m^a	Pre-pore pressure acting in coal matrix pore system (Pa)
p_c^a	Pre-pore pressure acting in cleat system (Pa)
p_c	Pressure of fluid in cleats (Pa)
p_m	Thermodynamic pressure of fluid in coal matrix (Pa)
s_{ij}	Deviatoric confining stresses (Pa)
s_m	Surface of coal matrix pores per unit volume of undeformed porous medium (m^{-1})
T	Temperature (K)
V^{ads}	Volume of adsorbed fluid (cm^3)
V_0^{coal}	Initial volume of coal sample (cm^3)
V^{met}	Volume of lifted metal parts (cm^3)
$\bar{V_b}$	Molar volume of bulk fluid (m^3.mol^{-1})
$\bar{V_b}^{\mathrm{CH_4}}$	Molar volume of bulk methane (m^3/mol)

$\bar{V_b}^{CO_2}$	Molar volume of bulk carbon dioxide (m^3/mol)
$\bar{W}_c$	Relative vector of fluid mass flow with respect to cleats ($mol.m^{-3}.s^{-1}$)
$\bar{W}_m$	Relative vector of fluid mass flow with respect to coal matrix ($mol.m^{-3}.s^{-1}$)
x^{CH_4}	Molar fraction of methane in the fluid in the cleats (-)
x^{CO_2}	Molar fraction of carbon dioxide in the fluid in the cleats (-)
	Greek letters
ϵ	Volumetric strain (-)
ϵ_m	Volumetric strain of coal matrix (-)
ϵ_T	Surface strain of the surface of the pore (-)
Γ	Molar amount of adsorbed molecules of fluid in excess of the bulk density per unit area of interface ($mol.m^{-2}$)
Γ^L	Molar amount of adsorbed molecules of fluid in excess of the bulk density per unit area of the surface in the reference state ($mol.m^{-2}$)
ϕ_{c0}	Porosity associated to cleat system in state of reference (-)
ϕ_c	Lagrangian porosity associated to cleat system (-)
ϕ_m	Lagrangian porosity of coal matrix (-)
φ_c	Variation of Lagrangian porosity associated to cleat system (-)
μ	Molar chemical potential of fluid ($J.mol^{-1}$)
μ_c	Molar chemical potential of fluid in cleats ($J.mol^{-1}$)
μ_m	Molar chemical potential of fluid in coal matrix ($J.mol^{-1}$)
$\mu_m^{CO_2}$	Molar chemical potential of carbon dioxide in coal matrix ($J.mol^{-1}$)
$\mu_m^{CH_4}$	Molar chemical potential of methane in coal matrix ($J.mol^{-1}$)
σ	Volumetric confining stress (Pa)
σ^s	Surface stress (Pa.m)
τ_d	Characteristic time of diffusion in the coal matrix (s)
τ_l	Characteristic time of loading (s)

Bibliography

Beaton, A. (2003). Coal-bearing formations and coal bed methane potential in the alberta plains and foothills. *Alberta Energy and Utilities Board/Alberta Geological Survey; Edmonton, Alberta*, pages 22–29.

Berkowitz, N. (1985). The chemistry of coal. *Elsevier Science*, 86.

Bernstein, L., Bosch, P., Canziani, O., Chen, Z.and Christ, R. a. D. O., Hare, W., Huq, S., Karoly, D., Stott, P., Stouffer, R., Sugiyama, T., S. R., Tirpak, D., Vogel, C., and Yohe, G. (2007). *IPCC Fourth Assessment Report: Climate Change 2007 Synthesis Report. IPCC*, pages 431–442.

Brochard, L., Vandamme, M., J.-M. Pellenq, R., and Fen-Chong, T. (2012a). Adsorption-induced deformation of microporous materials: Coal swelling induced by CO_2-CH_4 competitive adsorption. *Langmuir*, 28(5):2659–2670.

Brochard, L., Vandamme, M., and Pellenq, R.-M. (2012b). Poromechanics of microporous media. *Journal of the Mechanics and Physics of Solids*, 60(4):606–622.

Busch, A. and Gensterblum, Y. (2011). Cbm and CO_2-ECBM related sorption processes in coal: A review. *International Journal of Coal Geology*, 87(2):49–71.

Cantucci, B., Montegrossi, G., Vaselli, O., Tassi, F., Quattrocchi, F., and Perkins, E. H. (2009). Geochemical modeling of CO_2 storage in deep reservoirs: The weyburn project (canada) case study. *Chemical Geology*, 265(1-2):181–197.

Carman, P. (1937). Fluid flow through granular beds. *Transactions, Institution of Chemical Engineers, London*, 15:150–166.

Christensen, N. P. and Holloway, S. (2004). Assessing european potential for geological storage of CO_2 from fossil fuel combustion. *Technical report, The GESTCO project*.

Clarkson, C. (2008). Case study: production data and pressure transient analysis of horseshoe canyon cbm wells. *CIPC/SPE Gas Technology Symposium 2008 Joint Conference, Calgary, Alberta, Canada.*

Connell, L. D., Lu, M., and Pan, Z. (2010). An analytical coal permeability model for tri-axial strain and stress conditions. *International Journal of Coal Geology*, 84(2):103–114.

Coudert, F.-X., Jeffroy, M., Fuchs, A. H., Boutin, A., and Mellot-Draznieks, C. (2008). Thermodynamics of guest-induced structural transitions in hybrid organic-inorganic frameworks. *Journal of the American Chemical Society*, 130(43):14294–302.

Coussy, O. (2004). *Poromechanics*. John Wiley & Sons, Ltd.

Coussy, O. (2010). *Mechanics and Physics of Porous Solids*. John Wiley & Sons, Ltd.

Cui, X. and Bustin, R. (2005). Volumetric strain associated with methane desorption and its impact on coalbed gas production from deep coal seams. *AAPG Bulletin*, 89(9):1181–1202.

Darcy, H. (1856). Les fontaines publiques de la ville de dijon, dalmont, paris.

Day, S., Fry, R., and Sakurovs, R. (2008). Swelling of australian coals in supercritical CO_2. *International Journal of Coal Geology*, 74(1):41–52.

De Laplace, P. (1806). Traité de mécanique céleste. *Paris: Gauthier-Villars.*

Dolino, G., Bellet, D., and Faivre, C. (1996). Adsorption strains in porous silicon. *Phys. Rev. B*, 54(24):17919.

Esterle, J., Williams, R., Sliwa, R., and Malone, M. (2006). Variability in coal seam gas parameters that impact on fugitive gas emissions estimations for australian black coals. *36th Sydney Basin Symposium 2006: Advances in the Study of the Sydney Basin*.

Feron, P. and Hendriks., C. (2005). CO_2 capture process principles and costs. *Oil & Gas Science and Technology - Rev. IFP*, 60(3):451–459.

Fitzgerald, J., Pan, Z., Sudibandriyo, M., Robinsonjr, R., Gasem, K., and Reeves, S. (2005). Adsorption of methane, nitrogen, carbon dioxide and their mixtures on wet tiffany coal. *Fuel*, 84(18):2351–2363.

Gaus, I. (2010). Role and impact of CO_2-rock interactions during CO_2 storage in sedimentary rocks. *International Journal of Greenhouse Gas Control*, 4(1):73–89.

Gentzis, T. (2000). Subsurface sequestration of carbon dioxide - an overview from an alberta (canada) perspective. *Int J. Coal Geol.*, 43(1-4):287–305.

Gibbs, J. (1928). *The Collected Works of J. Willard Gibbs*. New York: Longmans, Green and Co.

Gilman, A. and Beckie, R. (2000). Flow of coal bed methane to a gallery. *Transport in Porous Media*, 41(1):1–16.

Gor, G. Y. and Neimark, A. V. (2010). Adsorption-induced deformation of mesoporous solids. *Langmuir*, 26(16):13021–13027.

Gor, G. Y. and Neimark, A. V. (2011). Adsorption-induced deformation of mesoporous solids: Macroscopic approach and density functional theory. *Langmuir*, 27(11):6926–6931.

Grosman, A. and Ortega, C. (2005). Nature of capillary condensation and evaporation processes in ordered porous materials. *Langmuir*, 21(23):10515–10521.

Grosman, A. and Ortega, C. (2008a). Capillary condensation in porous materials. hysteresis and interaction mechanism without pore blocking/percolation process. *Langmuir*, 24(8):3977–86.

Grosman, A. and Ortega, C. (2008b). Influence of elastic deformation of porous materials in adsorption-desorption process: A thermodynamic approach. *Phys. Rev. B*, 78(8):085433.

Grosman, A. and Ortega, C. (2009). Influence of elastic strains on the adsorption process in porous materials: An experimental approach. *Langmuir*, 25(14):8083–8093.

Gu, F. and Chalaturnyk, R. (2006). Numerical simulation of stress and strain due to gas sorption/desorption and their effects on in-situ permeability of coalbeds. *Journal of Canadian Petroleum Technology*, 45(10):52–62.

Gu, F. and Chalaturnyk, R. (2010). Permeability and porosity models considering anisotropy and discontinuity of coalbeds and application in coupled simulation. *Journal of Petroleum Science and Engineering*, 74(3-4):113–131.

Gu, F. and Chalaturnyk, R. J. (2005a). Analysis of coalbed methane production by reservoir and geomechanical coupling simulation. *Journal of Canadian Petroleum Technology*, 44(10):33–42.

Gu, F. and Chalaturnyk, R. J. (2005b). Sensitivity study of coalbed methane production with reservoir and geomechanic coupling simulation. *Journal of Canadian Petroleum Technology*, 44(10):23–32.

Gunter, W. D., Mavor, M. J., and Robinson, J. R. (2004). CO_2 storage and enhanced methane production: field testing at the fenn-big valley, alberta, canada, with application. *Proceedings of the 7th International Conference on Greenhouse Gas Control Technologies. Vancouver, Canada,*.

Gunther, G., Prass, J., Paris, O., and Schoen, M. (2008). Novel insights into nanopore deformation caused by capillary condensation. *Phys. Rev. Lett.*, 101(8):086104.

Harpalani, S. and Chen, G. (1997). Influence of gas production induced volumetric strain on permeability of coal. *Geotechnical and Geological Engineering*, 15(4):303–325.

Harpalani, S. and Schraufnagel, A. (1990). Measurement of parameters impacting methane recovery from coal seams. *International Journal of Mining and Geological Engineering*, 8(4):369–384.

Herman, T., Day, J., and Beamish, J. (2006). Deformation of silica aerogel during fluid adsorption. *Phys. Rev. B*, 73(9):094127.

IEA (2010). *World energy statistics*.

Inkpen, A. and Moffett, M. (2011). *The global oil and gas industry: management, strategy, and finance*. PennWell Corporation.

Izadi, G., Wang, S., Elsworth, D., Liu, J., Wu, Y., and Pone, D. (2011). Permeability evolution of fluid-infiltrated coal containing discrete fractures. *International Journal of Coal Geology*, 85(2):202–211.

Jahediesfanjani, H. and Civan, F. (2005). Damage tolerance of well-completion and stimulation techniques in coalbed methane reservoirs. *Journal of Energy Resources Technology*, 127(3):248–256.

Karaeusel, J., Wanner, B., and Kesicki, F. (2010). World energy outlook 2010 edition. *Executive Summary, IEA*, pages 431–442.

Keller, J. U. and Staudt, R. (2005). Gas adsorption equilibria: experimental methods and adsorption isotherms. *Springer Science+Business Media*.

Kowalczyk, P., C. A. and Neimark, A. V. (2008). Adsorption-induced deformation of microporous carbons: pore size distribution effect. *Lanmuir : the ACS journal of surfaces and colloids*, 24(13):6603–8.

Kroeger, K. F., Di Primio, R., and Horsfield, B. (2011). Atmospheric methane from organic carbon mobilization in sedimentary basins - the sleeping giant. *Earth-Science Reviews*, 107(3-4):423–442.

Levine, J. R. (1993). Coalification: The evolution of coal as source rock and reservoir rock for oil and gas. *Law, B., Rice, D. (Eds.), Hydrocarbons from Coal*, (38):39–77.

Levine, J. R. (1996). Model study of the influence of matrix shrinkage on absolute permeability of coal bed reservoirs. *Geological Society Special Publication*, 109(1):197–212.

Li, H., Shimada, S., and Zhang, M. (2004). Anisotropy of gas permeability associated with cleat pattern in a coal seam of the kushiro coalfield in japan. *Environmental Geology*, 47:45–50.

Litynski, J., Plasynski, S., Spangler, L., Finley, R., Steadman, E., Ball, D., Nemeth, J. K., McPherson, B., and Myer, L. (2008). U. s. department of energy's regional carbon sequestration partnership program: overview. *Proceedings of the 9th International Conference on Greenhouse Gas Control Technologies. Washington DC, USA*.

Liu, H.-H. and Rutqvist, J. (2009). A new coal-permeability model: Internal swelling stress and fracture–matrix interaction. *Transport in Porous Media*, 82(1):157–171.

Liu, J., Chen, Z., Elsworth, D., Miao, X., and Mao, X. (2010). Linking gas-sorption induced changes in coal permeability to directional strains through a modulus reduction ratio. *International Journal of Coal Geology*, 83(1):21–30.

Liu, J., Chen, Z., Elsworth, D., Qu, H., and Chen, D. (2011a). Interactions of multiple processes during cbm extraction: a critical review. *International Journal of Coal Geology*.

Liu, J., Wang, J., Chen, Z., Wang, S., Elsworth, D., and Jiang, Y. (2011b). Impact of transition from local swelling to macro swelling on the evolution of coal permeability. *International Journal of Coal Geology*, 88(1):31–40.

Loeser, J. and Treede, R. (2008). The kyoto protocol of iasp basic pain terminology. 137(3):473–477.

Lokhorst, A. and Wildenborg, T. (2005). Introduction au stockage geologique du CO_2 - classification des options de stockage. *Oil & Gas Science and Technology - Rev. IFP*, 60(3):513–515.

Luppens, J. A., Rohrbacher, T. J., Osmonson, L. M., and Carter, M. D. (2009). Coal resource availability, recoverability, and economic evaluations in the united states: A summary. *U.S. Department of the Interior, U.S. Geological Survey*.

Ma, Q., Harpalani, S., and Liu, S. (2011). A simplified permeability model for coalbed methane reservoirs based on matchstick strain and constant volume theory. *International Journal of Coal Geology*, 85(1):43–48.

Manancourt, A. and Gale, J. (2004). Alternative geological storage options. *In, E.S.Rubin, D.W.Keith and C.F. Gilboy (Eds.),Proceedings of 7th International Conference on Greenhouse Gas Control Technologies, IEA Greenhouse Gas Programme, Cheltenham, UK.*

Massarotto, P., Golding, S., Bae, J.-S., Iyer, R., and Rudolph, V. (2010). Changes in reservoir properties from injection of supercritical CO_2 into coal seams - a laboratory study. *International Journal of Coal Geology*, 82(3-4):269–279.

Massarotto, P., Golding, S., and Rudolph, V. (2006). Preliminary feasibility economics and risk of CO_2 geosequestration in coal seams of the bowen basin, australia. *Proceedings of the 8th International Conference of GHG Technologies, Trondheim, Norway*.

Massarotto, P., Golding, S., and Rudolph, V. (2009). Constant volume cbm reservoirs: an important principle. *International Coalbed Methane Symposium, Tuscaloosa, Alabama.*

Mazzotti, M., Pini, R., and Storti, G. (2009). Enhanced coalbed methane recovery. *The Journal of Supercritical Fluids*, 47(3):619–627.

Meinshausen, M., Meinshausen, N., Hare, W., Raper, S. C. B., Frieler, K., Knutti, R., Frame, D. J., and Allen, M. R. (2009). Greenhouse-gas emission targets for limiting global warming to 2 c. *Nature*, 458(7242):1158–1162.

Metz, B., O. Davidson, H. C., Coninck, M.Loos, and (eds.), L. A. M. (2005). *IPCC Special Report on Carbon Dioxide Capture and Storage*.

Murata, K., El-Merraoui, M., and Kaneko, K. (2001). A new determination method of absolute adsorption isotherm of supercritical gases under high pressure with a special relevance to density-functional theory study. *Journal of Chemical Physics*, 114:4196–4205.

Neimark, A. V., Coudert, F.-X., Boutin, A., and Fuchs, A. H. (2010). Stress-based model for the breathing of metal-organic frameworks. *The Journal of Physical Chemistry Letters*, 1(1):445–449.

Neimark, A. V., Coudert, F. X., Triguero, C., Boutin, A., Fuchs, A. H., Beurroies, I., and Denoyel, R. (2011). Structural transitions in mil-53 (cr): View from outside and inside. *The Journal of Physical Chemistry Letters*, 27(8):4734–4741.

Ottiger, S., Pini, R., Storti, G., and Mazzotti, M. (2008). Competitive adsorption equilibria of CO_2 and CH_4 on a dry coal. *Adsorption Journal Of The International Adsorption Society*, 14(4-5):539–556.

Ottiger, S., Pini, R., Storti, G., Mazzotti, M., Bencini, R., Quattrocchi, F., Sardu, G., and Deriu, G. (2006). Adsorption of pure carbon dioxide and methane on dry coal from the sulcis coal province (sw sardinia, italy). *Environmental Progress*, 25(4):355–364.

Pachauri, R. and Reisinger, A. e. (2007). *Climate Change 2007: Synthesis Report*.

Palmer, I. and Mansoori, J. (1996). How permeability depends on stress and pore pressure in coalbeds: a new model. *Copyright 1996 SPE Annual Technical Conference and Exhibition. Society of Petroleum Engineers, Inc., Denver, Colorado.*

Palmer, I., Mavor, M., and Gunter, B. (2007). Permeability changes in coal seams during production and injection. *International Coalbed Methane Symposium, University of Alabama, Tuscaloosa, Alabama.*, (0713).

Pan, Z. and Connell, L. (2007). A theoretical model for gas adsorption-induced coal swelling. *International Journal of Coal Geology*, 69(4):243–252.

Pan, Z., Connell, L. D., and Camilleri, M. (2010). Laboratory characterisation of coal reservoir permeability for primary and enhanced coalbed methane recovery. *International Journal of Coal Geology*, 82(3-4):252–261.

Pekot, L. J. and Reeves, S. R. (2002). Modeling coal matrix shrinkage and differential swelling with CO_2 injection for enhanced coalbed methane recovery and carbon sequestration applications. *Topical report, U.S. Department of Energy*.

Pijaudier-Cabot, G., Vermorel, R., Miqueu, C., and Mendiboure, B. (2011). Revisiting poromechanics in the context of microporous materials. *Comptes Rendus Mécanique*, 339(12):770–778.

Pini, R. (2009). Phd thesis: Enhanced coal bed methane recovery finalized to carbon dioxide storage.

Pini, R., Ottiger, S., Burlini, L., Storti, G., and Mazzotti, M. (2009). Role of adsorption and swelling on the dynamics of gas injection in coal. *Journal of Geophysical ResearchSolid Earth*, 114.

Pini, R., Ottiger, S., Burlini, L., Storti, G., and Mazzotti, M. (2010a). Sorption of carbon dioxide, methane and nitrogen in dry coals at high pressure and moderate temperature. *International Journal of Greenhouse Gas Control*, 4(1):90–101.

Pini, R., Ottiger, S., Burlini, L., Storti, G., and Mazzotti, M. (2010b). Sorption of carbon dioxide, methane and nitrogen in dry coals at high pressure and moderate temperature. *International Journal of Greenhouse Gas Control*, 4(1):90 – 101.

Raaness, O. (1990). The role of reactivity in the production of silicon, silicon carbide and silicon rich ferroalloys. *Lecture notes. Trondheim, Norway*, (STF34 A90092).

Rajendran, A., Bonavoglia, B., Forrer, N., Storti, G., Mazzotti, M., and Morbidelli, M. (2005). Simultaneous measurement of swelling and sorption in a supercritical CO_2-poly(methyl methacrylate) system. *Industrial and Engineering Chemistry Research*, 44(8):2549–2560.

Ravikovitch, P. I. and Neimark, A. V. (2006). Density functional theory model of adsorption deformation. *Lanmuir : the ACS journal of surfaces and colloids*, 22(26):10864–8.

Reeves, S., Taillefert, A., Pekot, L., and Clarkson, C. (2003). The allison unit CO_2-ecbm pilot: A reservoir modeling study. *Topical report, U.S. Department of Energy*.

Reeves, S. R. (2004). The coal-seq project: results from field, laboratory, and modeling studies. *Proceedings of the 7th International Conference on Greenhouse Gas Control Technologies. Vancouver, Canada*.

Reichenauer, G. and Scherer, G. W. (2000). Nitrogen adsorption in compliant materials. *Journal of Non-Crystalline Solids*, 277(2-3):162–172.

Reiss, L. (1980). The reservoir engineering aspects of fractured formations. *Gulf Publishing Co., Houston.*

Robertson, E. and Christiansen, R. (2008). A permeability model for coal and other fractured, sorptive-elastic media. *SPE Journal*, 13(3):314–424.

Schepers, K., Oudinot, A., and Ripepi, N. (2010). Enhanced gas recovery and CO_2 storage in coalbed-methane reservoirs: Optimized injected-gas composition for mature basins of various coal rank. *SPE International Conference on CO_2 Capture, Storage, and Utilization, 10-12 November 2010, New Orleans, Louisiana, USA*, (139723-MS).

Scherer, G. W. (1986). Dilatation of porous glass. *Journal of the American Ceramic Society*, 69(6):473–480.

Seidle, J. and Huitt, L. (1995). Experimental measurement of coal matrix shrinkage due to gas desorption and implications for cleat permeability increases. *nternational Meeting on Petroleum Engineering. Society of Petroleum Engineers, Inc., Beijing, China.*

Shi, J. Q. and Durucan, S. (2004a). Drawdown induced changes in permeability of coalbeds: A new interpretation of the reservoir response to primary recovery. *Transport in Porous Media*, 56(1):1–16.

Shi, J.-Q. and Durucan, S. (2004b). A numerical simulation study of the allison unit CO_2-ecbm pilot: the effect of matrix shrinkage and swelling on ecbm production and CO_2 injectivity. *In Proceedings of the 7th International Conference on Greenhouse Gas Control Technologies (GHGT-7)*, pages 431–442.

Shuttleworth, R. (1950). The surface tension of solids. *Proceedings of the Physical Society. Section A*, 63(5):444.

Sing, K. S. W., Everett, D. H., Haul, R. A. W., Moscou, L., Pierotti, R. A., Rouquerol, J., and Siemieniewska, T. (1985). Reporting physisorption data for gas/solid systems. *Pure and Applied Chemistry*, 57(4):603–619.

Sircar, S. (2001). Measurement of gibbsian surface excess. *AlChE J.*, 47(5):1169–1176.

Span, R. and Wagner, W. (2003a). Equations of state for technical applications. ii. results for nonpolar fluids. *International Journal of Thermophysics*, 24(1):41–109.

Span, R. and Wagner, W. (2003b). Equations of state for technical applications. iii. results for polar fluids. *International Journal of Thermophysics*, 24(1):111–162.

Steiner, A. (2007). United nations environment programme.

Tajnik, T., Bogataj, L. K., Jurac, E., Lasnik, C. R., Likar, J., and Debelak, B. (2012). Investigation of adsorption properties of geological materials for CO_2 storage. *International Journal of Energy Research*, pages n/a–n/a.

Tollefsen, E., Perry, A., Kok, J., Alford, J., Han, S. Y., Malpani, R., Baihly, J., and Vauter, E. (2010). Spe 139007 unlocking the secrets for viable and sustainable shale gas development. *Most*, pages 1–21.

Van Bergen, F., Pagnier, H., and Krzystolik, P. (2006). Field experiment of CO_2-ECBM in the upper silesian basin of poland. *Proceedings of the 8th International Conference on Greenhouse Gas Control Technologies, Trondheim, Norway*.

Vandamme, M., Brochard, L., Lecampion, B., and Coussy, O. (2010). Adsorption and strain: The CO_2-induced swelling of coal. *Journal of the Mechanics and Physics of Solids*, 58(10):1489–1505.

Vassilev, S. V., Kitano, K., and Vassileva, C. G. (1996). Some relationships between coal rank and chemical and mineral composition. *Fuel*, 75(13):1537–1542.

Washburn, E. W. (1933). International critical tables of numerical data, physics, chemistry and technology. *Published for the National Research Council by McGraw-Hill.*

White, C. M., Smith, D. H., Jones, K. L., Goodman, A. L., Jikich, S. A., LaCount, R. B., DuBose, S. B., Ozdemir, E., Morsi, B. I., and Schroeder, K. T. (2005). Sequestration of carbon dioxide in coal with enhanced coalbed methane recovery: A review. *Energy and Fuels*, 19(3):659–724.

Wong, S., Law, D., Deng, X., Robinson, J., Kadatz, B., Gunter, W. D., Ye, J., Feng, S., and Fan, Z. (2006). Enhanced coalbed methane, micropilot test at south qinshui, shanxi, china. *Proceedings of the 8th International Conference on Greenhouse Gas Control Technologies, Trondheim, Norway*.

Wood, G., Jr., Kehn, T., Carter, M., and Culbertson, W. (1983). Coal resource classification system of the u.s. *Geological Survey: U.S. Geological Survey Circular 891*.

Wu, Y., Liu, J., Chen, Z., Elsworth, D., and Pone, D. (2011). A dual poroelastic model for CO_2-enhanced coalbed methane recovery. *International Journal of Coal Geology*, 86(2-3):177–189.

Yamaguchi, S., Ohga, K., Fujioka, M., Nako, M., and Muto, S. (2006). Field experiment of japan CO_2 geosequestration in coal seams project. *Proceedings of the 8th International Conference on Greenhouse Gas Control Technologies, Trondheim, Norway*.

Young, T. (1805). An essay on the cohesion of fluids. *Philos. T. R. Soc. Lon.*, 95:65–87.

Zhang, H., Liu, J., and Elsworth, D. (2008). How sorption-induced matrix deformation affects gas flow in coal seams: A new FE model. *International Journal of Rock Mechanics and Mining Sciences*, 45(8):1226–1236.